CR-196603

Ionizing Radiation Measurements on LDEF: A0015 Free Flyer Biostack Experiment

Final Report

E. V. Benton, A. L. Frank, E. R. Benton,
I. Csige and L. A. Frigo

(NASA-CR-196603) IONIZING RADIATION MEASUREMENTS ON LDEF: A0015 FREE FLYER BIOSTACK EXPERIMENT Final Report, Sep. 1991 - Mar. 1995 (Eril Research) 127 p

N95-27168

Unclas

G3/25 0049663

Contract No. NAS8-38610
George C. Marshall Space Flight Center
National Aeronautics and Space Administration
Marhsall Space Flight Center, AL 35812

30 March 1995

ERIL RESEARCH, INC.
P.O. BOX 150788 - SAN RAFAEL, CA 94915-0788

NASA National Aeronautics and Space Administration

Report Documentation Page

1. Report No.	2. Government Accession No.	3. Recipient's Catalog No.

4. Title and Subtitle

Ionizing Radiation Measurements on LDEF: A0015 Free Flyer Biostack Experiment Final Report

5. Report Date

30 March 1995

6. Performing Organization Code

7. Author(s)

E. V. Benton, A. L. Frank, E. R. Benton, I. Csige, and L. A. Frigo

8. Performing Organization Report No.

9. Performing Organization Name and Address

10. Work Unit No.

11. Contract or Grant No.

NAS8-38610

12. Sponsoring Agency Name and Address

13. Type of Report and Period Covered

September 1991 thru March 1994

14. Sponsoring Agency Code

15. Supplementary Notes

16. Abstract

This report covers the analysis of passive radiation detectors flown as part of the A0015 Free Flyer Biostack on LDEF. LET spectra and track density measurements were made with CR-39 and Polycarbonate plastic nuclear track detectors. Measurements of total absorbed dose were carried out using Thermoluminescent Detectors. Thermal and resonance neutron dose equivalents were measured with LiF/CF-39 detectors. High energy neutron and proton dose equivalents were measured with fission foil/CR-39 detectors.

17. Key Words (Suggested by Author(s))	18. Distribution Statement
LET Spectra, Dose, Dose Equivalent, Ionizing Radiation	Unclassified - Unlimited

19. Security Classif. (of this report)	20. Security Classif. (of this page)	21. No. of pages	22. Price
Unclassified	Unclassified	127	

NASA FORM 1626 OCT 86

Ionizing Radiation Measurements on LDEF: A0015 Free Flyer Biostack Experiment

Final Report

Abstract

This report covers the analysis of passive radiation detectors flown as part of the A0015 Free Flyer Biostack on LDEF. LET spectra and track density measurements were made with CR-39 and Polycarbonate plastic nuclear track detectors (PNTDs). Measurements of total absorbed dose were carried out using Thermoluminescent Detectors (TLDs). Thermal and resonance neutron dose equivalents were measured with LiF/CR-39 detectors. High energy neutron and proton dose equivalents were measured with fission foil/CR-39 detectors.

LET spectra were measured in CR-39 PNTDs as functions of spacecraft location and experiment shielding. At high LETs ($>$100 keV/μm), short-range inelastic secondary particles produced by trapped proton interactions with the CR-39 were found to be the principal contributor to the LET spectra. At lower LETs, the spectrum appeared to be made up of short-range inelastic secondaries and stopping primary protons. LET spectra were greater on the West-side of LDEF than on either the Earth-side or East-side, showing the effect of the East/West trapped proton anisotropy in the South Atlantic Anomaly (SAA).

Measurements of track density in CR-39 on the West-side of LDEF showed an increase with shielding depth. A similar measurement made in a thick stack of CR-39 interspersed with layers of Al and exposed to 154 MeV protons show a similar result, indicated that a significant fraction of the particle events counted were from secondaries and that the total cross section for the production of proton-induced secondaries increases as the energy of primary protons is attenuated. Little change was seen in either differential or integral LET spectra as a function of shielding depth, indicating that the increase in cross-section with decreasing proton energy affects mostly the shorter range secondary component. Similarity in the slopes of LET spectra from ground-based proton exposures and the A0015 LET spectra showed that modeling of a monoenergetic proton beam transported through a 1-D geometry is a useful first step in modeling the production of secondary particles by trapped protons in the SAA.

Measurement of charge, energy and azimuthal angle distributions from energetic secondary particles were carried out in the A0015 Earth-side stack. Charge and energy distribution measurements can be used in validation of computational models. Comparison of angular distributions with similar measurements made in CR-39 detectors exposed to accelerator based protons illustrated the anisotropic nature of the production of secondary particles.

Total absorbed dose was measured through the use of TLDs located in the A0015 experiment containers. Doses measured on the West side of LDEF exceed those measured on the East side by nearly a factor of 2, demonstrating the East/West trapped proton anisotropy. Comparison of measured doses from TLDs with two sets of model calculations showed that the models consistently under-predicted dose on the LDEF's West and Earth sides.

Thermal and resonance neutron dose equivalent rates measured from ^{6}LiF/CR-39 detectors were 0.0017 and 0.113 mrem/d on the Earth side and 0.0021 and 0.078 mrem/d on the West side of LDEF. Higher energy proton and neutron doses measured in fission foil/CR-39 detectors were 171 rad and 82 rem on the Earth side and 315 rad and 33 rem on the West side of LDEF, respectively.

Analysis of polycarbonate PNTDs from the West-side of LDEF have revealed a very high fluence of tracks ($>1 \times 10^{7}$ tracks/cm^{2} under 2 gm/cm^{2} shielding). Fluence drops off rapidly as shielding depth increases. Tracks only form in the region of the detector closest to the surface, not in the bulk of the detector. To date no adequate explanation for this observation has been found.

Contents

1 Introduction

The Long Duration Exposure Facility (LDEF) was a passive, free-flying cylindrical satellite which carried a total of 57 experiments in 86 experiment trays (72 around the perimeter and 14 on the two ends). The satellite was 30 feet long, 14 feet in diameter and weighed 21,500 lbs. when fully configured with experiments. The LDEF mission began on 6 April 1984 with the launch of STS-41C and the deployment of LDEF into a 28.5°, 480×474 km orbit. LDEF was returned to Earth by STS-32 on 20 January 1990 after a mission lasting 5.787 years (2114 days). The satellite completed 32,322 orbits and travelled a total of 741,928,837 miles. The LDEF mission encompassed a significant portion of the solar cycle. Altitude of the satellite slowly decreased as the mission progressed. The LDEF spacecraft was gravity gradient stabilized so that it orbited the Earth in a fixed orientation. This means the one end of LDEF always faced the Earth, while the other end always faced away from Earth. Since the spacecraft traveled from West to East, the leading edge of LDEF faced the East, while the trailing edge faced the West. The A0015 experiment was contained in two trays: G1 on the Earth-facing end of LDEF, and C2, close to the trailing edge of the spacecraft. Figure 1 shows the two locations of the A0015 experiment on LDEF as well as the locations of several other LDEF experiments which carried passive radiation detectors. Figure 1 also shows the orientation of LDEF as it passed through the South Atlantic Anomaly.

The LDEF mission provided a unique and unprecedented opportunity to monitor the space radiation environment in low Earth orbit (LEO). A number of features of the LDEF mission enhanced the ability of experiments on LDEF to measure the space radiation environment. These included the length of the mission and the fixed orientation of LDEF relative to the Earth. The ~5.8 year length of the LDEF mission permitted the radiation environment to be monitored for a significant fraction of the solar cycle. LDEF's fixed orientation relative to the Earth allowed for the measurement of the trapped proton anisotropy in the South Atlantic Anomaly and the directionality of galactic cosmic rays. Subsequent 3-D mass modeling of LDEF allowed the effects of spacecraft and experiment shielding on radiation measurements to be taken into account. LDEF carried a number of experiments designed to measure ionizing radiation, including the A0015 Free Flyer Biostack Experiment.

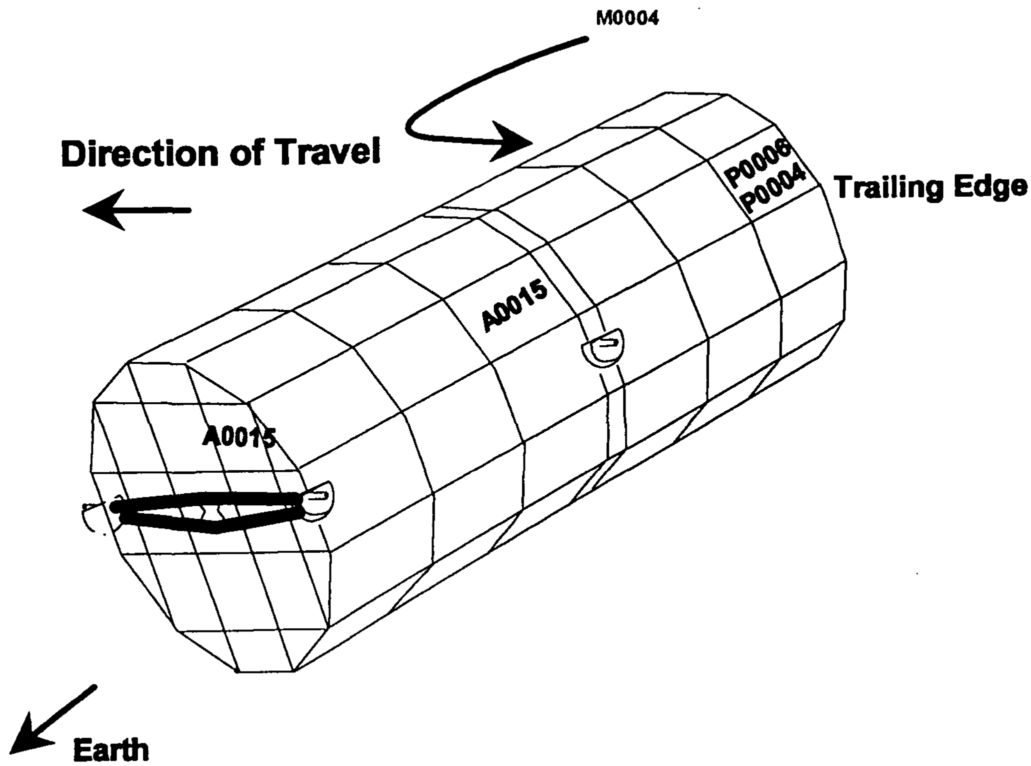

Figure 1: Location of experiments containing passive radiation detectors on LDEF.

The primary objectives of the A0015 experiment were the:

1. Measurement of Linear Energy Transfer (LET) spectra produced by ionizing radiation of $LET_{\infty} \cdot H_2O \geq 5$ keV/μm on the Earth-side and West-side (Trailing Edge) of LDEF. This included:

   (a) Measurement of the high LET tail ($LET_{\infty} \cdot H_2O \geq 100$ keV/μm) produced by HZE (high atomic number Z and energy) galactic cosmic rays (GCR) and proton-induced high-LET secondaries;

   (b) Measurement of Charge and Energy Spectrum of short-range secondaries;

   (c) Effects of spacecraft shielding on LET spectrum;

(d) Effects of directionality of particle fluxes on LET spectra;

2. Measurement of Total Absorbed Dose:

   (a) As a function of spacecraft shielding;

   (b) As a function of the orientation of the spacecraft in the SAA; and

   (c) In comparison with model calculations.

3. Measurement of high energy neutron and proton fluxes; and

4. Measurement of thermal and resonance neutron dose equivalents.

1.1 Experiment Description

The A0015 experiment was divided into three parts. One full stack of detectors was located on the Earth-facing end of LDEF in Tray G1 (Earth-side stack). Another full stack of detectors and one partial stack were located near the trailing edge of LDEF in Tray C2 (West-side stack). Each full detector stack occupied a Biostack container that was sealed from the outside environment with an O-ring. The partial stack was left open to vacuum. The inner wall of each Al Biostack canister consisted of an acrylic layer.

To achieve the objectives of the A0015 experiment, a variety of passive radiation detectors were employed. Measurements of LET, Charge and Energy spectra of trapped protons, GCR and high-LET secondaries were carried out using several types of plastic nuclear track detector (PNTD). These included CR-39 which is sensitive to ionizing radiation of $LET_\infty \cdot H_2O \geq 5$ keV/μm, Sheffield and Tuffak polycarbonate sensitive to radiation of $LET_\infty \cdot H_2O \geq 250$ keV/μm, and Melinex polyester sensitive to radiation of $LET_\infty \cdot H_2O \geq 350$ keV/μm. Total absorbed dose measurements were carried out using thermoluminescent detectors TLD-700 (^{7}LiF). Fission foil/mica nuclear track detectors were used to measure fluxes of high energy protons and neutrons. Thermal ($E_n < 0.2$ eV) and resonance (0.2 eV $\leq E_n \leq$ 1 MeV) neutron doses were measured using ^{6}LiF/CR-39 PNTD detectors. Tables 1 and 2 lists the contents, order and shielding of radiation detectors in the Earth-side and West-side stacks.

Table 1: Contents and Shielding of A0015 Earth-side Stack.

Assembly Code	Material	No. of Layers	Shielding (g/cm^2)
	Al	1	0.819
	Acrylic	1	0.939
1R168–1R165	Tuffak	4	1.061
1G164–1G151	Sheffield	14	1.483
No. 1	TLD	1	1.684
	Al	1	2.118
1C150–1C149	CR-39	2	2.378
1R148–1R145	Tuffak	4	2.499
1G144–1G120	Sheffield	15	2.952
1M129–1M128	Mica	2	2.996
	Al	1	3.430
1C127–1C126	CR-39	2	3.690
1R125–1R122	Tuffak	4	3.811
1G121–1G107	Sheffield	15	4.264
	Al	1	4.698
1C106–1C105	CR-39	2	4.957
1R104–1R100	Tuffak	4	5.079
1G99–1G85	Sheffield	15	5.531
No. 2	TLD	1	5.732
	Al	1	6.166
1R84–1R81	Tuffak	4	6.288
1G80–1G66	Sheffield	15	6.740
	Al	1	7.175
1C65–1C64	CR-39	2	7.434
1R63–1R60	Tuffak	4	7.555
1G59–1G45	Sheffield	15	8.008
1M44–1M43	Mica	2	8.052
	Al	1	8.487
1C42–1C41	CR-39	2	8.746
1R40–1R37	Tuffak	4	8.867
1G36–1G22	Sheffield	15	9.320
No. 3	TLD	1	9.521
	Al	1	9.955

continued on next page

continued from previous page

Assembly Code	Material	No. of Layers	Shielding (g/cm^2)
1C21–1C20	CR-39	2	10.215
1R19–1R16	Tuffak	4	10.336
1G15–1G01	Sheffield	15	10.788
	LiF/CR-39	1	11.226
	FFD	1	12.032

Table 2: Contents and Shielding of A0015 West-side Stack.

Assembly Code	Material	No. of Layers	Shielding (g/cm^2)
	Al	1	0.410
	Acrylic	1	0.530
	FFD	1	1.336
	LiF/CR-39	1	1.773
2G01–2G15	Sheffield	15	2.225
2R16–2R19	Tuffak	4	2.347
2C20–2C21	CR-39	2	2.606
	Si wafer	1	2.879
	Al	1	3.313
No. 1	TLD	1	3.515
2G22–2G36	Sheffield	15	3.967
2R37–2R40	Tuffak	4	4.089
2C41–2C42	CR-39	2	4.348
	Al	1	4.782
2M43–2M44	Mica	2	4.827
2G45–2G59	Sheffield	15	5.279
2R60–2R63	Tuffak	4	5.401
2C64–2C65	CR-39	2	5.660
	Al	1	6.094
2G66–2G80	Sheffield	15	6.546
2R81–2R84	Tuffak	4	6.668
	Al	1	7.102
No. 2	TLD	1	7.304
2G85–2G99	Sheffield	15	7.756
2C100–2C101	CR-39	2	8.015

continued on next page

continued from previous page

Assembly Code	Material	No. of Layers	Shielding (g/cm^2)
	Al	1	8.449
2C102–2G117	Sheffield	15	8.902
2R118–2R119	Tuffak	2	8.962
2C120–2C121	CR-39	2	9.222
	Al	1	6.656
2M122–2M123	Mica	2	9.700
2G124–2G139	Sheffield	15	10.153
2R140–2R141	Tuffak	2	20.214
2C142–2C143	CR-39	2	10.473
	Al	1	10.907
No. 3	TLD	1	11.108
2G144–2G156	Sheffield	13	11.500
2R157–2R159	Tuffak	3	11.592
2C160–2C161	CR-39	2	11.851
2G162–2G164	Sheffield	3	11.941

The detector assembly was 7.0 cm square and 8.6 cm in height. The sealed stacks consisted of eight detector modules stacked atop one another and separated by Al plates. Figure 2 shows the Earth-side stack while Figure 3 shows the contents of the West-side stack. Figure 4 shows the contents of the partial stack exposed to vacuum and the A0015 control detector stack.

2 Radiation Environment in Space

2.1 Radiation Measurements

PNTDs measure the ionizing radiation environment in terms of its Linear Energy Transfer (LET) spectrum. The LET of a particle of ionizing radiation is a measure of the change in the energy of the particle per unit path length and varies inversely with the kinetic energy of the particle. Measurements of LET are reported in units of keV/μm. From a radiobiological standpoint and from the point of view of effects on electronics, the LET of a charged particle is believed to be of greater relevance than its energy since LET is a measure of energy transferred to the surrounding medium through which the particle is traveling. This transferred energy is responsible for biological damage if the particle is passing through tissue. Similarly this transfer of energy can cause single event upsets (SEU) and damage of a more permanent nature in electronic circuit elements. CR-39 PNTDs measure the fluence (particle density per unit area, solid angle) and the LET of ionizing radiation of $\mathrm{LET}_\infty \cdot \mathrm{H_2O} \geq 5$ keV/μm. Less sensitive polycarbonate PNTDs like Tuffak and Sheffield measure fluence and LET of ionizing radiation of $\mathrm{LET}_\infty \cdot \mathrm{H_2O} \geq 250$ keV/μm. Fluence and LET measurements can be combined to produce integral fluence, flux (fluence per unit time) and LET dose spectra. The fluence, flux, or dose greater than a given LET on the y-axis is plotted as a function of LET on the x-axis. Most of the LET spectra included in this report are plotted in terms of flux or fluence since these quantities are of greatest use in comparing measurements with model calculations.

Ionizing radiation is measured in units of Gray (Gy) or rads and TLDs directly measure total absorbed dose. One Gy is equal to one joule absorbed by one kilogram of material. One rad is equal to 100 ergs absorbed by one gram of material (1 Gy = 100 rads). This

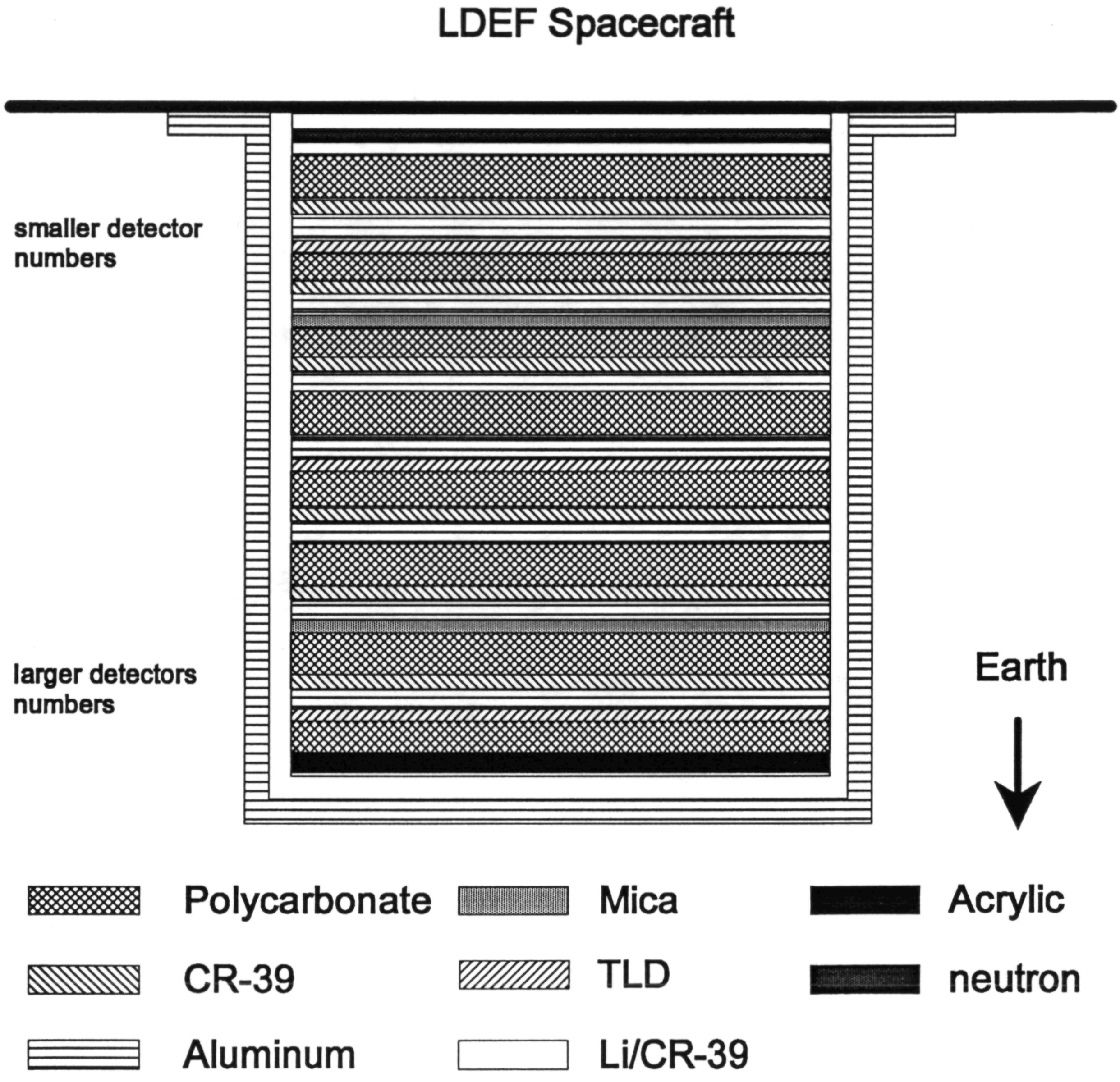

Figure 2: Cross-sectional diagram of A0015 Earth-side stack.

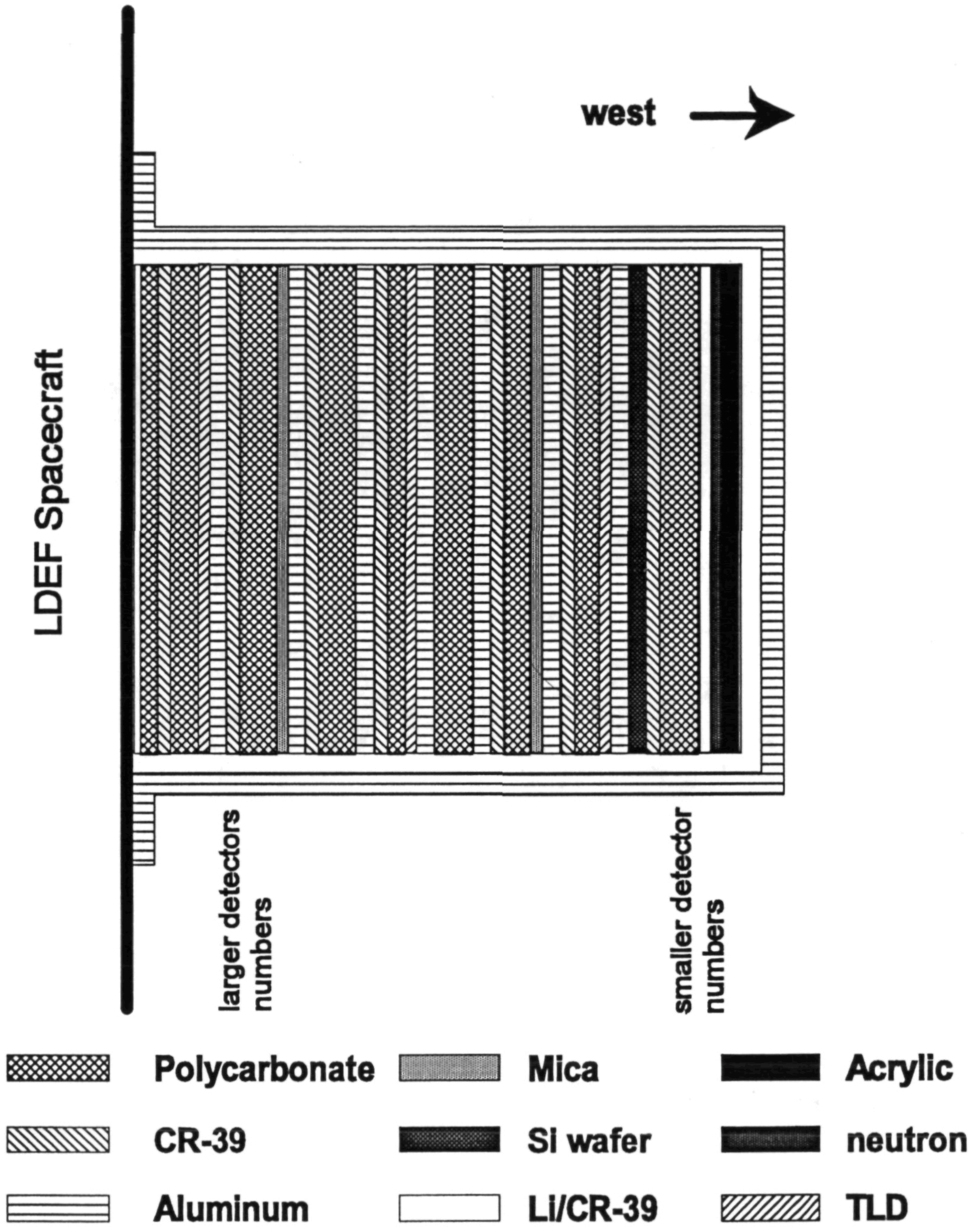

Figure 3: Cross-sectional diagram of A0015 West-side (trailing edge) stack.

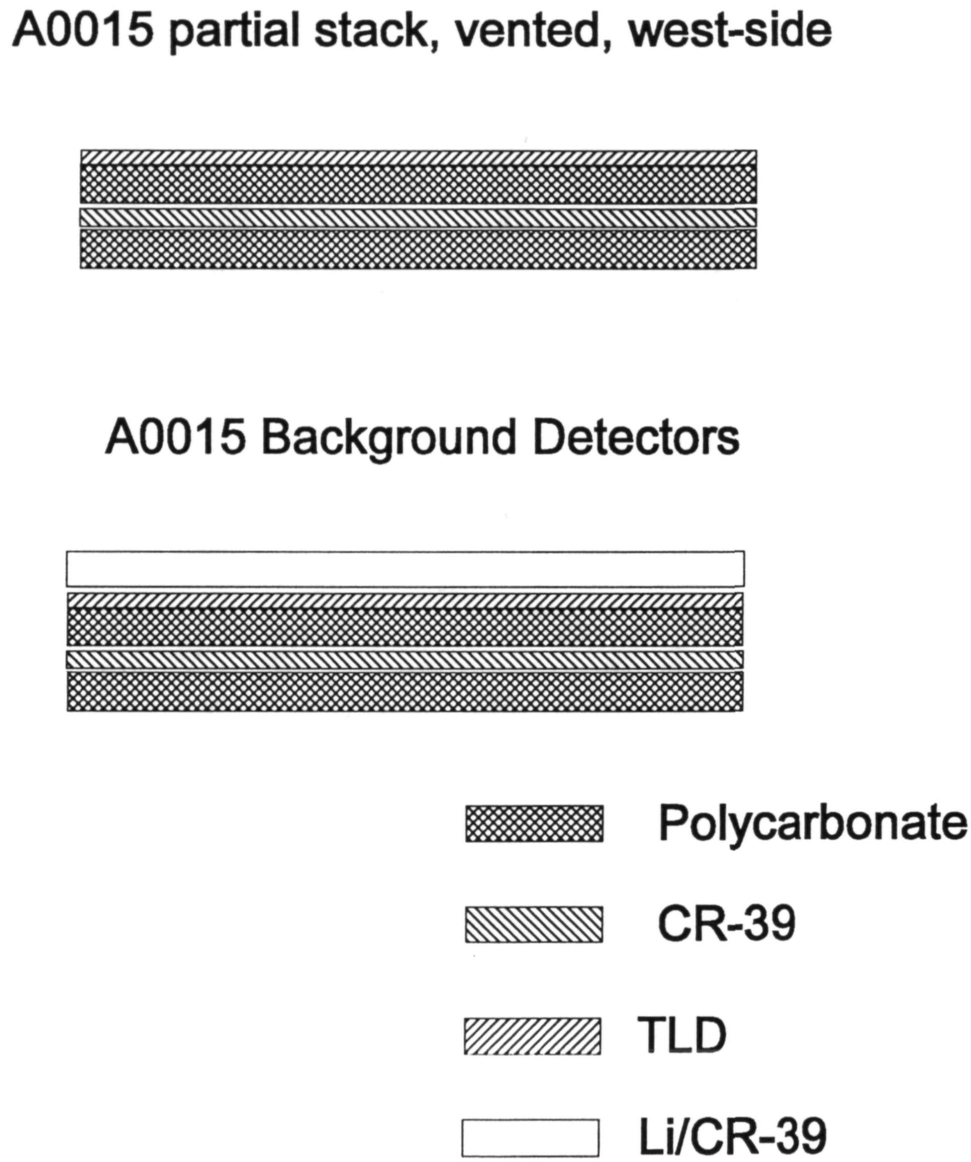

Figure 4: Cross-sectional diagram of A0015 West-side partial stack (vented to vacuum) and ground control stack.

measurement is referred to as total absorbed dose. Different particles of ionizing radiation produce different radiobiological effect (RBE), based on the LET of the radiation. Another measurement, dose equivalent, is used in radiobiology to scale the dose by a quality factor Q which is a function of LET. Dose equivalent is measured in units of Sievert (Sv) or rem (rad equivalent man, 1 Sv = 100 rem). Since it was not possible to obtain LET information from TLDs, dose measurements could not be converted to dose equivalent.

2.2 Radiation Components

The ionizing radiation environment in space consists of a variety of charged particles—electrons, protons, helium nuclei, and heavy ions—at a wide range of energies. The space radiation environment can be roughly divided into three distinct components: (a) trapped particle radiation, (b) galactic cosmic radiation, and (c) solar particle events.

(a) **Trapped Particle Radiation:** The trapped particle radiation component can be divided into three parts: (*i*) trapped electrons, and (*ii*) trapped protons, and (*iii*) trapped anomalous particles (which are of less significance in dosimetry).

(*i*) Trapped Electrons: Electrons are trapped in regions which follow the contours of the earth's geomagnetic field, drifting toward and away from the earth's magnetic poles. They are reflected at mirror points which lie toward the more northern and southern latitudes. There are two regions of trapped electrons, an inner belt extending to 2.8 earth radii (R_e) and an outer belt extending from 2.8 to 12 R_e. Electrons in the outer zone have about 10 times the intensity of those in the inner zone and they are capable of having much higher energies. LDEF orbited well within the inner zone. Electrons in the inner zone are of low radiobiological significance when compared to protons in the same region. TLDs are sensitive to the trapped electron component, but the electron dose has a steep gradient with shielding depth. Detectors inside the spacecraft usually get a small fraction of their dose from electrons (from Bremsstrahlung).

(*ii*) Trapped Protons: Trapped protons, like trapped electrons, are contained in belts following the contours of the geomagnetic field. For the most part these trapped proton belts are above the altitude of the low earth orbit (LEO) of LDEF. Energies of trapped

protons range from tens to > 1000 MeV. There is a region between Africa and Brazil where the earth's magnetic field dips unusually close to the surface of the earth. This region is called the South Atlantic Anomaly (SAA) and orbits passing through this region receive a substantial dose from trapped protons. LDEF had a 28.5° inclination and for most of the mission an altitude of ~450 km, an orbit that passes through the SAA. TLDs are sensitive to the trapped proton spectra. CR-39 PNTDs are directly sensitive to the lower energy component of the trapped proton spectra and are sensitive to the higher energies through secondary particle production (to be covered later).

(*iii*) Trapped Anomalous Particles: Trapped anomalous particles are heavy ($Z > 1$) nuclei, single charged, with energies sufficiently low to allow capture by the Earth's magnetic field. The fluxes vary with time, sometimes disappearing. The fraction of total particle fluxes represented by anomalous trapped particles is very low and ranges in shielding are short (typically a few μm). Their contribution inside the LDEF experimental canisters is negligible.

For the LDEF orbit (28.5°, ~450 km), most ionizing radiation come from trapped protons in the SAA. While the geomagnetic field is approximately dipolar, it is not centered on the Earth. It is weakest over Brazil and the South Atlantic Ocean allowing the trapped radiation belts to dip closer to the Earth's surface. Trapped protons follow a helical path long the geomagnetic field lines (see Figure 5). The center of this helical trajectory is called the guiding center. As the strength of the field increases towards the poles, the gyroradius of the helical path and the angle between the field line and the velocity vector of the trapped proton (pitch angle) decrease. When the pitch angle reaches zero, the proton reverses direction and travels back up the field line. The point at which the pitch angle is zero is called the mirror point and nearly all protons in the SAA are near their mirror points. This causes the protons to intercept a spacecraft traversing the SAA at angles perpendicular to the local direction of the magnetic field lines. Thus the trapped proton environment in the SAA is anisotropic with the preferred directions for proton travel being from the East and West. Any protons not near their mirror points in the SAA have gyroradii which take them deep into the atmosphere where they are likely to undergo interactions with the air and be absorbed.

Protons travelling toward the East have guiding centers above the spacecraft and are

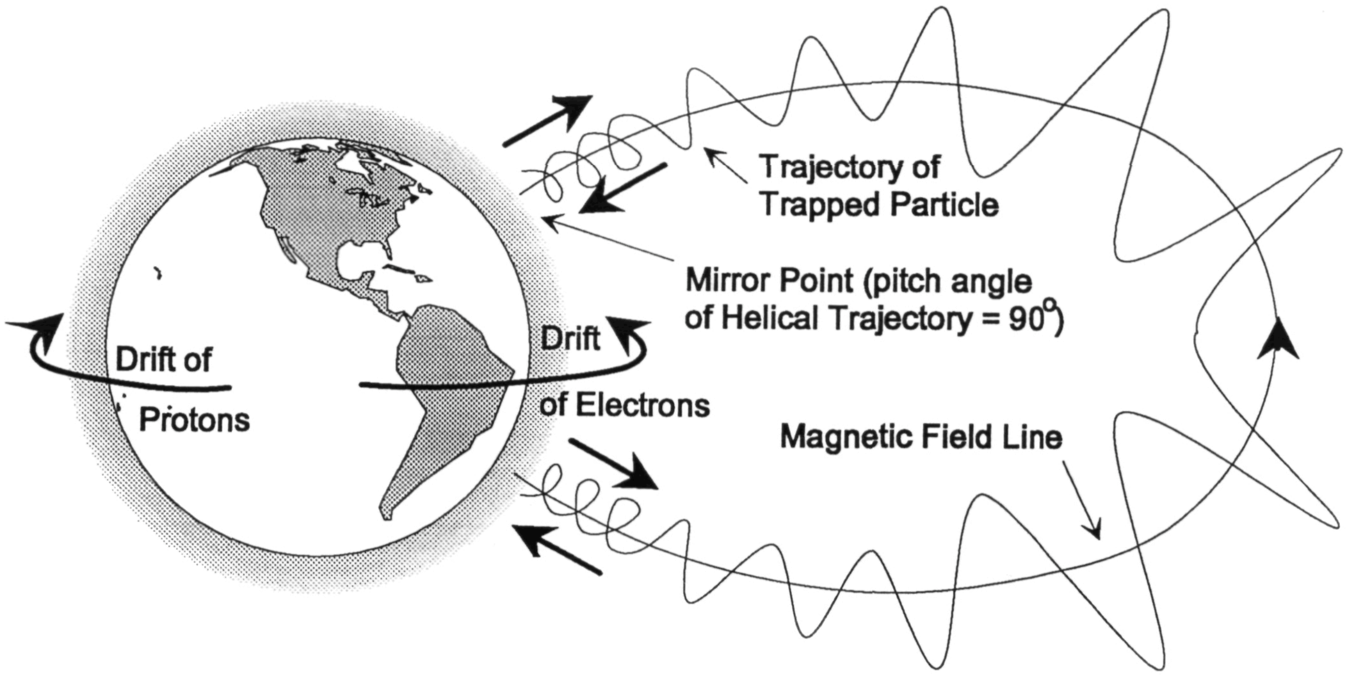

Figure 5: Trajectory of a charged particle trapped in the geomagnetic field.

moving down from space. Protons travelling toward the West have guiding centers below the spacecraft and are moving up from the Earth (see Figure 6). Because the gyroradius is of the same order of magnitude as the scale height of the atmosphere, those protons with guiding centers below the spacecraft are more likely to undergo interactions with the atmosphere and be absorbed. Thus an anisotropy exists between East and West moving protons with protons moving toward the East predicted to be of greater number than those moving toward the West. This is called the East/West trapped proton anisotropy (or East/West effect). Differences in absorbed dose and LET spectra measured on the East and West sides of LDEF confirmed the presence of the East/West effect.

(b) **Galactic Cosmic Radiation:** Galactic Cosmic Rays (GCR) are particles from beyond the solar system. 98% of the GCR component is made up of protons and heavier ions while the remaining 2% are electrons and positrons. Of the 98% baryon component, 87% are protons, 12% are helium ions, and 1% are heavy ions. Energy spectra of the GCR component are mainly in the ranges from 100 MeV to 10 GeV per nucleon. The heavy ion component of GCR is often referred to as HZE (high Z and Energy). While this is the smallest component in terms of fluence, the Linear Energy Transfer (LET) of heavy

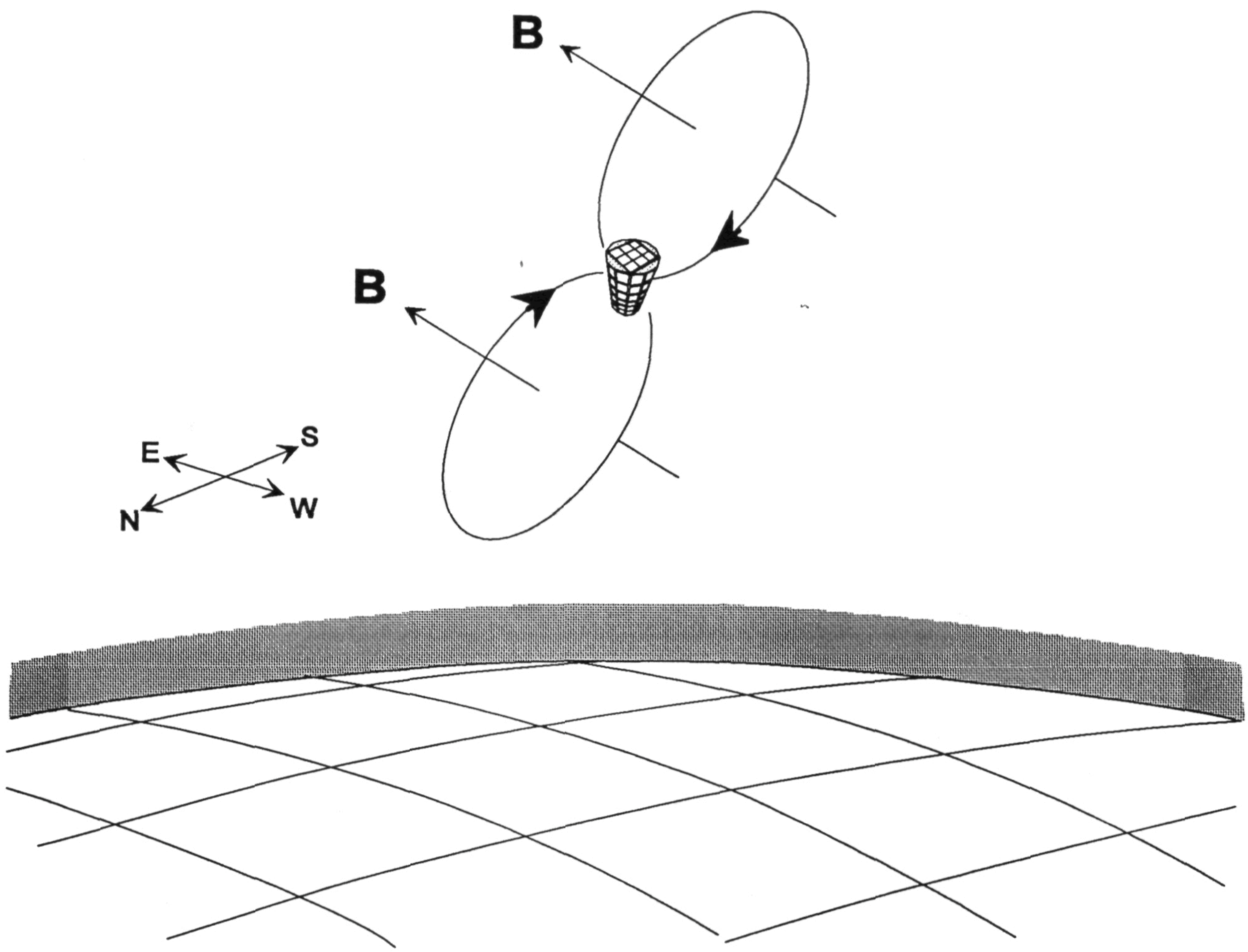

Figure 6: East/West trapped proton anisotropy.

ions increases as a function of the square of the atomic number Z, leading to a much greater Radiobiological Effect (RBE). The effect of HZE particles on electronics is also of importance due to higher LETs. Figure 7 is a histogram showing the abundances of GCR and a measure of the "ionizing power" of each element[21]. As an example, iron ions are only 10% as abundant as oxygen ions in the GCR spectrum. However, iron ions contribute nearly the same percentage to GCR dose as oxygen due to the larger Z of iron. In the LDEF orbit (28°, ~450 km), the geomagnetic cut-off prevents HZE particles with LETs greater than that of relativistic Fe from passing through the spacecraft. The lower LET portion (<5 keV/μm)

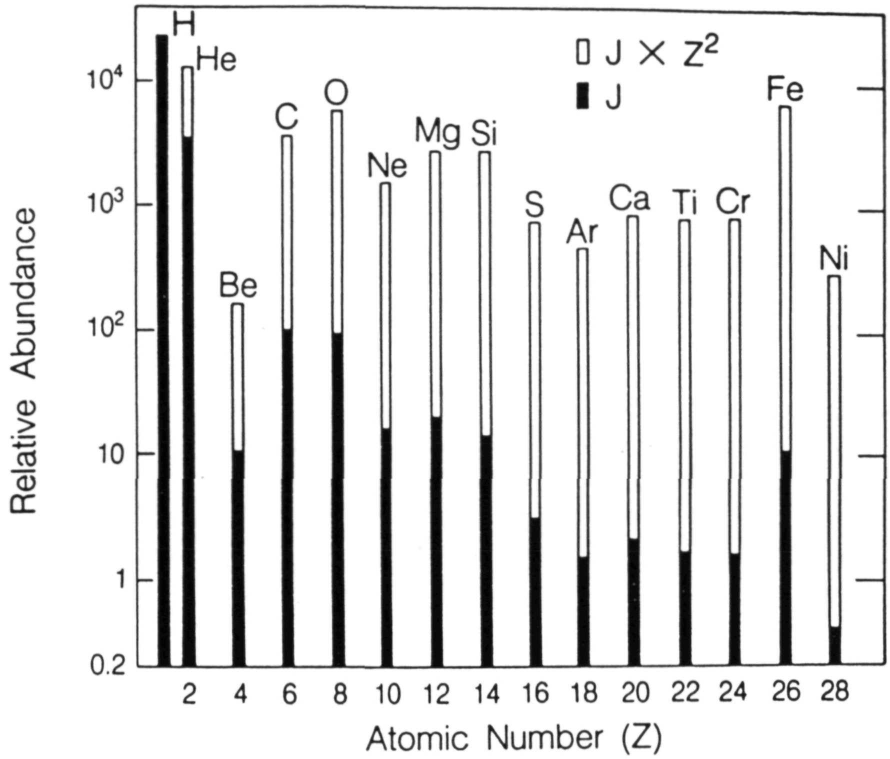

Figure 7: Histogram showing the relative abundances of the even numbered galactic cosmic ray (GCR) nuclei (solid bars) compared to their abundances weighted by the square of the particle's charge to give a measure of "ionizing power" of each element (open bars) (NCRP 1989).

of GCRs is detected efficiently by TLDs, but the higher LET portion has reduced efficiency. The higher LET portion of GCRs are detected primarily by the CR-39 PNTDs.

(c) **Solar Particle Events:** Solar particle events (SPE) refer to the charged particles emitted by the sun during a solar flare. The particles include protons, alpha particles, and heavy ions. SPEs tend to be of low energy. At low inclinations the geomagnetic field serves to protect spacecraft from SPE.

2.3 Proton-induced Secondary Radiation

High-LET (>100 keV/μm), short-range secondary radiation produced by high energy trapped protons make a significant contribution to the LET spectra of spacecraft in LDEF type orbits (28°, ~450 km). These particles produce a 'High-LET tail' that extends to LETs >1000 keV/μm, above the ~137 keV/μm geomagnetic cut-off imposed on GCR. Trapped

protons in the SAA, passing through the body of the spacecraft, undergo nuclear interactions with the nuclei of the stopping medium. These interactions can either be elastic (billiard ball collisions) or inelastic. In inelastic nuclear interactions, the incident proton is absorbed by the target nucleus. The target nucleus may become unstable and undergo decay, resulting in the generation of various secondary ions. The type of inelastic secondary produced is dependent on the charge of the target nucleus. Inelastic collisions may be either endothermic or exothermic.

Collisions of incident protons with hydrogen nuclei (proton-proton scattering) is nearly completely elastic for incident proton energies up to ~400 MeV. For the range of trapped proton energies found in the SAA, the cross section for elastic scattering of protons is on the order of 25 mbarn. These energies correspond to LETs below the threshold for registration in CR-39 PNTDs and these particles are not recorded. Nor does proton-proton elastic scattering contribute to the high-LET tail.

The type, energy and LET of secondary ions produced in inelastic scattering is dependent on the elemental composition of the stopping material. The elemental composition of CR-39 PNTD is $O_7C_{12}H_{18}$, while the elemental composition of polycarbonate PNTD is $O_3C_{16}H_{14}$. CR-39 is therefore nearly tissue equivalent. The high LET tail is through to be mainly due to heavy inelastic secondaries produced in collisions between trapped protons and the C and O nuclei of the PNTDs. The theoretical maximum LET for a recoils O is ~1500 kev. Cross sections for the production of various secondary ions can be found in references [18] and [6].

One of the significant findings of the ionizing radiation experiments included on LDEF was the major contribution proton-induced secondaries make to the LET spectra. Empirical studies at ground-based accelerators have shown that a fluence of 10^8 protons (~10 cGy) of an energy typically found in the trapped proton belts produces a fluence of $\sim 10^3$ tracks/cm^2 in CR-39 PNTDs. Due to the low inclination and high altitude of the LDEF orbit, GCR did not make a significant contribution to the LET spectra above ~137 keV/μm (due to the GCR geomagnetic cut-off and high fluxes of trapped protons). The LET spectra above this cut-off are thought to be caused almost wholly by interactions between trapped protons and the nuclei of the spacecraft and its experiments.

3 Measurements with CR-39 PNTDs

3.1 Response of CR-39 PNTDs

CR-39 PNTDs were included in the LDEF A0015 Experiment to measure ionizing radiation of $LET_\infty \cdot H_2O \geq 5$ keV/μm. This radiation component includes low energy trapped protons in the SAA, short-range high-LET secondaries produced by trapped protons, and GCR of atomic number $1 \leq Z \leq 92$. Integral and differential LET flux spectra were calculated using data measured from the CR-39 PNTDs.

The passage of a charged particle through a layer of CR-39 disrupts the chemical bonds of the polymer along the particle's trajectory. This path of broken bonds is highly reactive and is called the latent damage trail. Upon retrieval of the experiment, the CR-39 layers are chemically processed in a solution of 6.25 N NaOH (sodium hydroxide). The NaOH preferentially attacks the latent damage trail, leaving conical pits called nuclear tracks. The sizes of the elliptical openings of these tracks are a function of to the LET of the particles which produced the tracks. Measurements of the major and minor axes of the elliptical tracks are converted to LET values and are used to produce an LET flux spectrum.

For the A0015 Experiment, nuclear tracks on the processed CR-39 layers were measured using one of two methods: 1) Two-layer Coincident Spectroscopy and 2) Total Event Spectroscopy. In the two-layer coincident spectroscopy method two adjacent layers of CR-39 are reassembled into their original experimental configuration relative to one another, following chemical processing. Figure 8 shows a cross sectional diagram of a reassembled CR-39 pair. The second surface (lower surface of top layer) is scanned for particle tracks. When a track is found on the second surface, the third surface (upper surface of bottom layer) is examined for a companion track. The first (upper surface of top layer) and fourth (lower surface of bottom layer) surfaces are then examined for companion tracks. Tracks appearing on only one surface are disregarded. In this way, no background subtraction needs to be carried out since only events recorded during the experiment are accepted. The disadvantage of this method is that it neglects the shortest-range component.

Data from LET spectra measurements made using the coincident spectroscopy method are divided into three components: 1) short range—events having a range greater than

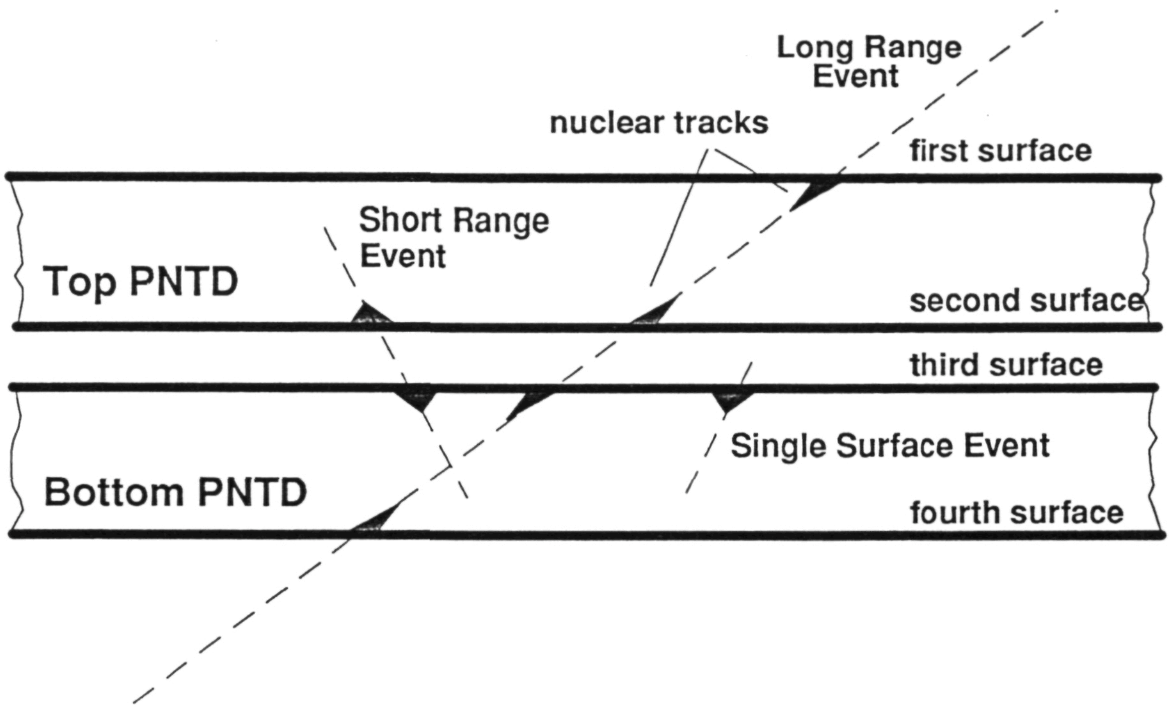

Figure 8: Cross sectional view of reassembled CR-39 PNTD pair shows examples of a long range (GCR) event and a short range (trapped proton) event.

16 μm and less than 2000 μm, 2) long range—events having a range greater than 2000 μm, and 3) total—short range plus long range events. The parameters of these components are dictated by the thickness of the detector layers ($\sim$1 mm) and the amount of material removed during etching ($\sim$8 μm for the 36 hr, 50°C 6.25 N NaOH etch of A0015 CR-39 detectors). Short range events consist of a pair of tracks on two adjacent surfaces of CR-39. The vertical distance between these two tracks is roughly two times the thickness removed during chemical processing (bulk etch B). For the LDEF CR-39 PNTDs this is $\sim$16 μm and represents the minimum range of a particle event measurable using the coincident spectroscopy technique. These short range events are principally the result of stopping primary protons and high-LET proton induced secondaries. The long range component consists of particle events that formed tracks on all four surface of the CR-39 doublet. Since the thickness of a layer of LDEF CR-39 is $\sim$1 mm, the vertical distance between tracks of a given event on the outermost surfaces of the doublet is $\sim$2 mm or $\sim$2000 μm. These events are caused by GCR and, in the case of LDEF, often by relativistic Fe. The total component consists of a sum of short and long range events and represents the LDEF spectra for charged particles with range

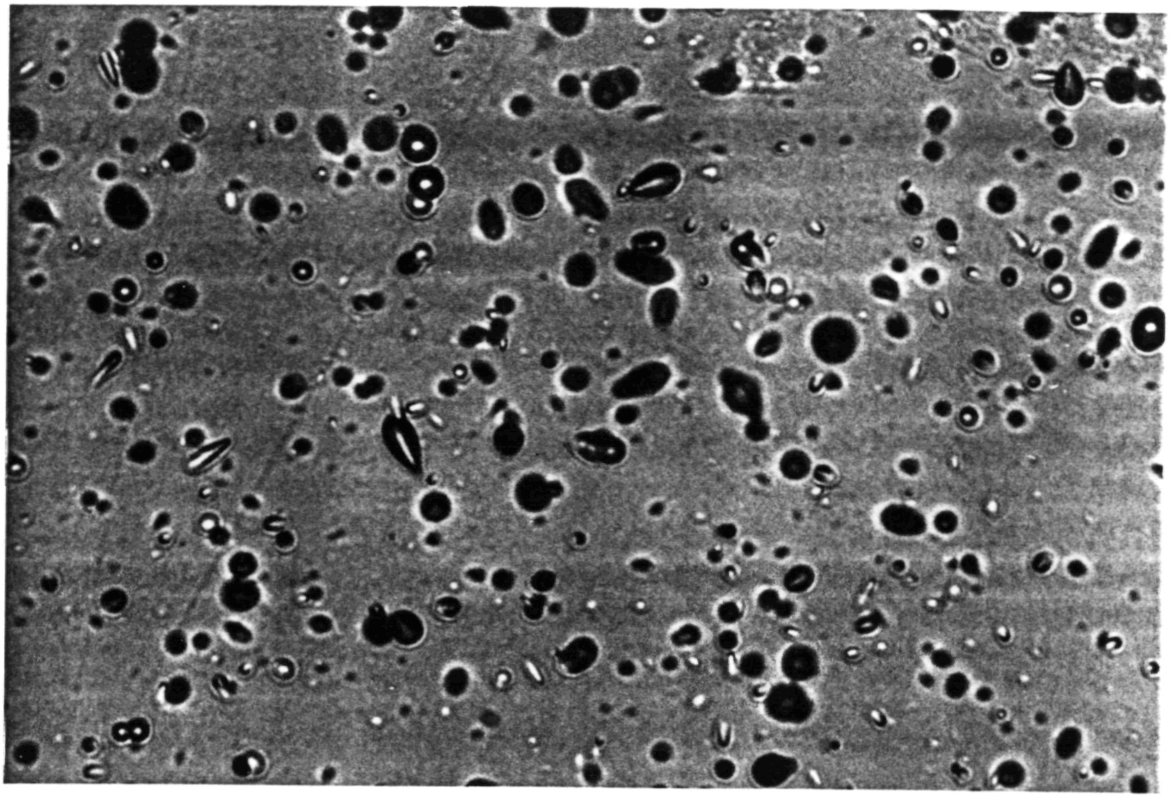

Figure 9: Photomicrograph of a typical field of view in a reassembled CR-39 pair. The image is focused on the upper surface. The scale is ~25μm/cm.

>16 μm.

Figures 9 and 10 are photomicrographs of two adjacent surface of CR-39 in the A0015 West-side stack following chemical processing and reassembly. Figure 9 shows a field of view focused on surface 2, the bottom surface of the upper layer of the reassembled CR-39 pair (see Figure 8). Figure 10 shows the same field of view focused on surface 3, the upper surface of the bottom layer of the CR-39 pair. Nearly all the object visible in the photomicrographs are tracks, many of them over-etched. Coincidence spectroscopy requires finding two tracks, one of each of the adjacent surfaces, produced by the same particle. The CR-39 layers may be realigned based on these tracks in order to make additional particle events easier to locate.

The total event spectroscopy method involves measuring all tracks on a single etched surface of CR-39 located in a given area. A similar measurement is made on a processed background layer of CR-39 and this background is subtracted from the experiment data set. For the etching regime used for the A0015 CR-39 detectors, the minimum range of a particle event measurable on a single layer of CR-39 is ~2 μm. No classification of events into short

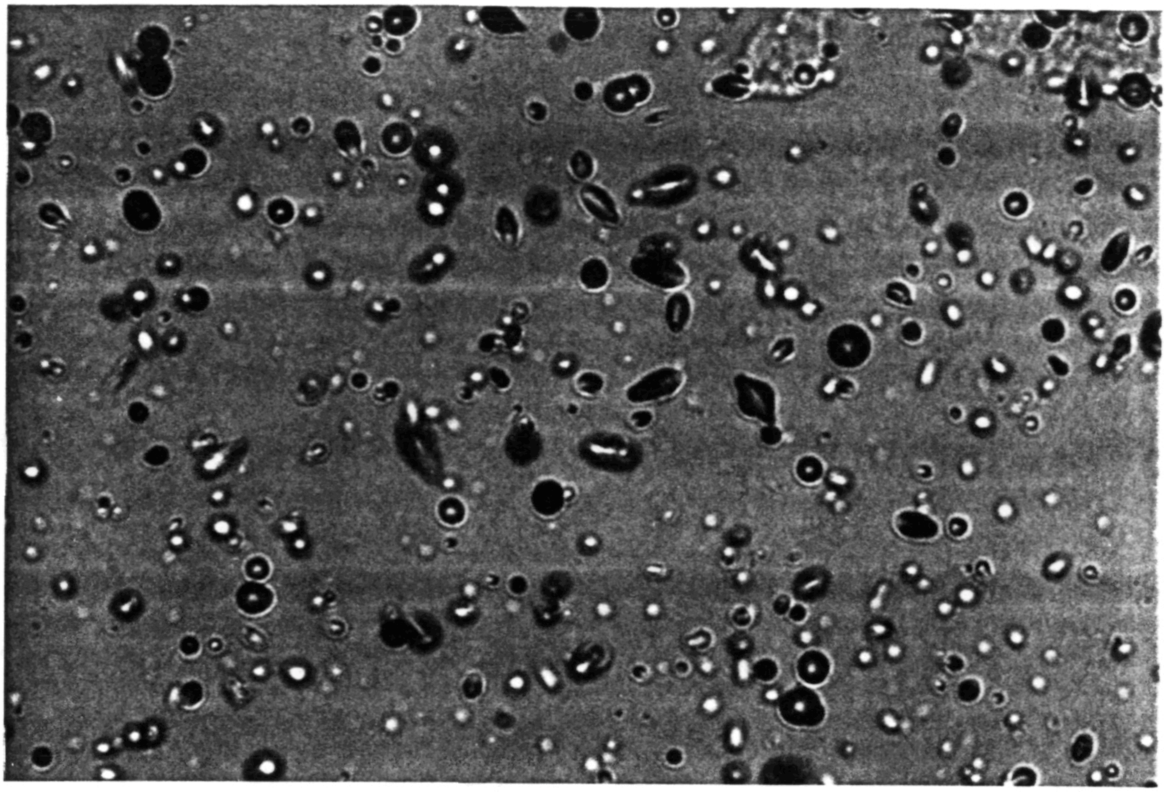

Figure 10: Photomicrograph of the same field of view now focused on the bottom surface.

range and long range components is carried out. The major advantage of this method is that it includes the very short range component. This is of special importance on LDEF where much of the high-LET tail takes the form of these very short range particles. The disadvantage of this method is that a fraction of the very short range component is produced by particles that did not intersect the pre-etch surface of the detector. LET values assigned to these events tend to be too low. The other disadvantage of this method is the subtraction of background, which can often be difficult.

3.2 Experiment

Three types of plastic nuclear track detectors (PNTDs) were included in the A0015 experiment—CR-39, Sheffield Polycarbonate, and Tuffak Polycarbonate. CR-39 is sensitive to ionizing radiation with a minimum $LET_\infty \cdot H_2O$ of $\sim$5 keV/μm. The two types of polycarbonate included, Tuffak and Sheffield, are sensitive to a minimum $LET_\infty \cdot H_2O$ of $\sim$250 keV/μm.

A number of studies of environmental effects on latent tracks in the three PNTD materials

were undertaken and the results may be found in reference[17]

Determination of chemical processing regimes was carried out using the results of analysis from the P0006 experiment. CR-39 detectors flown on a typical STS mission are usually processed for 168 hours at 50°C in a solution of 6.25 N NaOH. Due to the unprecedented length of the LDEF mission, the track fluence in the CR-39 detectors aboard LDEF was anticipated to be very high. A fluence of approximately 10^5 tracks/cm^2 is sufficient to saturate the CR-39 PNTDs and the etched tracks will overlap, making track measurements difficult to impossible. Samples of CR-39 were etched for various periods of time in a 50°C 6.25 N NaOH solution in order to determine optimal etch conditions. Processing times varied from 24 to 168 hr. Following chemical processing, the detectors were measured under an optical microscope and the fluences of single surface and two surface tracks were measured. The surface of the CR-39 detector processed for 168 hours was over-etched and the elliptical dimensions of the tracks could no longer be accurately measured. The fluences on the CR-39 test etch detectors were comparable to one another and determination of etch time was based on track size and ability to measure the track parameters. A visual judgment was made to determine which processing duration produced detectors which could be most easily and most accurately measured. For LDEF CR-39 PNTDs, a period of 36 hours was found to be optimal. The 36 hr, 50°C, 6.25 N NaOH processing regime was adopted for the CR-39 PNTDs in the A0015 experiment.

3.2.1 Calibration of PNTDs

Due to the reduction in chemical processing time and to environmental changes in the sensitivity of the PNTDs, A0015 control detectors, portions of the flight material, and PNTD material of the same manufactured batches as that included in A0015 were exposed to a variety of heavy ion beams at the Lawrence Berkeley Laboratory Bevalac accelerator for purposes of calibration. The PNTDs were irradiated to ions of known energy and known LET. Table 3 is a summary of the accelerator based irradiations. Calibration detectors are scanned in order to obtain the reduced track etch rate V_R for the particular ion/energy combination. A plot of V_R versus LET is then generated for all the calibration ions and a detector response equation is found for the material.

Table 3: Summary of A0015 Calibration Irradiations at the LBL Bevalac Accelerator

Ion	Energy MeV/amu	Range (cm H_2O)	$LET_\infty \cdot H_2O$ (keV/μm)	$LET_{200} \cdot$CR-39 (keV/μm)
Kr	1367	32.3	266	179
Au	1150	12.6	1320	888
Fe	1691	54.5	136.2	91.6
U	928	8.36	1882	1266
Ag	1452	26.7	451	303

For the specific batches of CR-39 and Polycarbonate PNTDs flown on LDEF, calibration response equations had already been determined. However, these response functions neglected the environmental changes in sensitivity of the material. In addition, these response equations were for a standard chemical processing duration of 168 hours. After the irradiation of a selection of the A0015 PNTDs at the LBL Bevalac accelerator, the new calibration points (V_R, LET) were added and the response equations were adjusted to reflect this change in sensitivity. Figure 11 is the adjusted calibration plot generated for Sheffield and Tuffak polycarbonate. Figure 12 is the adjusted calibration plot generated for CR-39. The points labeled "A" are the calibration points from the 168 hour etch adjusted for change in etch duration and environmental effects. The detector response equations derived from these graphs were used to generate the LET spectra for the A0015 detectors.

3.3 LET Measurements

3.3.1 LET Measurements as a Function of Location

Due to the fixed orientation of LDEF relative to the Earth, track density and LET spectra measured at different locations on LDEF are dependent on detector orientation. One A0015 stack was located on the Earth-facing end of LDEF while the other A0015 stacks were located on the West-facing trailing edge of LDEF. LET spectra was measured under 10.2 g/cm^2 in the A0015 Earth-side stack and under three shielding depths (2.6, 4.4, and 9.2 g/cm^2) in the A0015 West-side stack. In addition, LET spectra was measured under 6.1 g/cm^2 in the P0004 experiment, also on the West side of LDEF. All measurements were carried out using

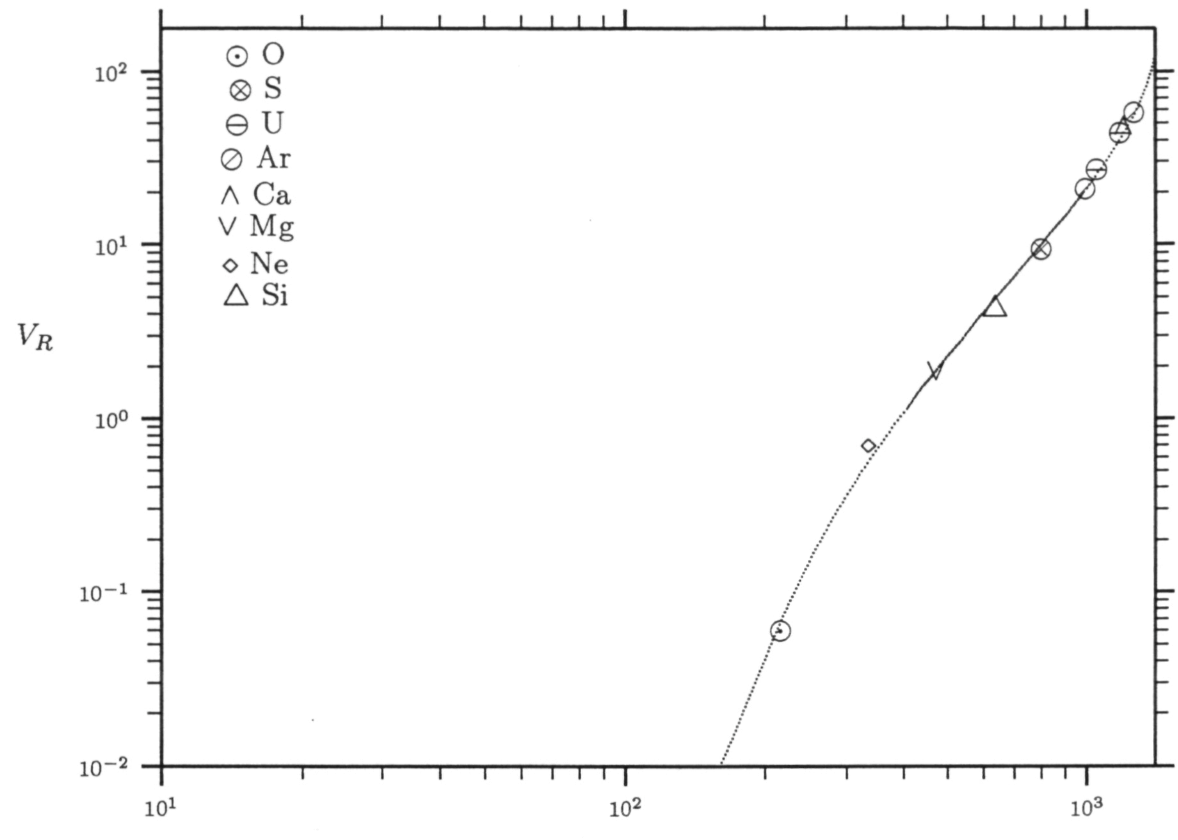

Figure 11: Polycarbonate PNTD response plot of measured V_R versus LET$_{200}$·CR-39 for LDEF A0015 experiment.

the standard coincident spectroscopy technique. Results are broken down into short range, long range and total components. Shielding for the given LET spectra represents only the vertical self-shielding of the experiment and not the total shielding from LDEF and other experiments.

Figure 13 shows the integral LET flux spectra measured under 10.2 g/cm^2 shielding in the A0015 Earth-side stack. The spectra are dominated by short range particles in the regions above ~150 keV/μm and below ~50 keV/μm. The region above 150 keV/μm consists largely of high-LET secondaries produced by interactions between high energy trapped protons and the O and C nuclei of the CR-39. The region below 50 keV/μm is most likely made up of

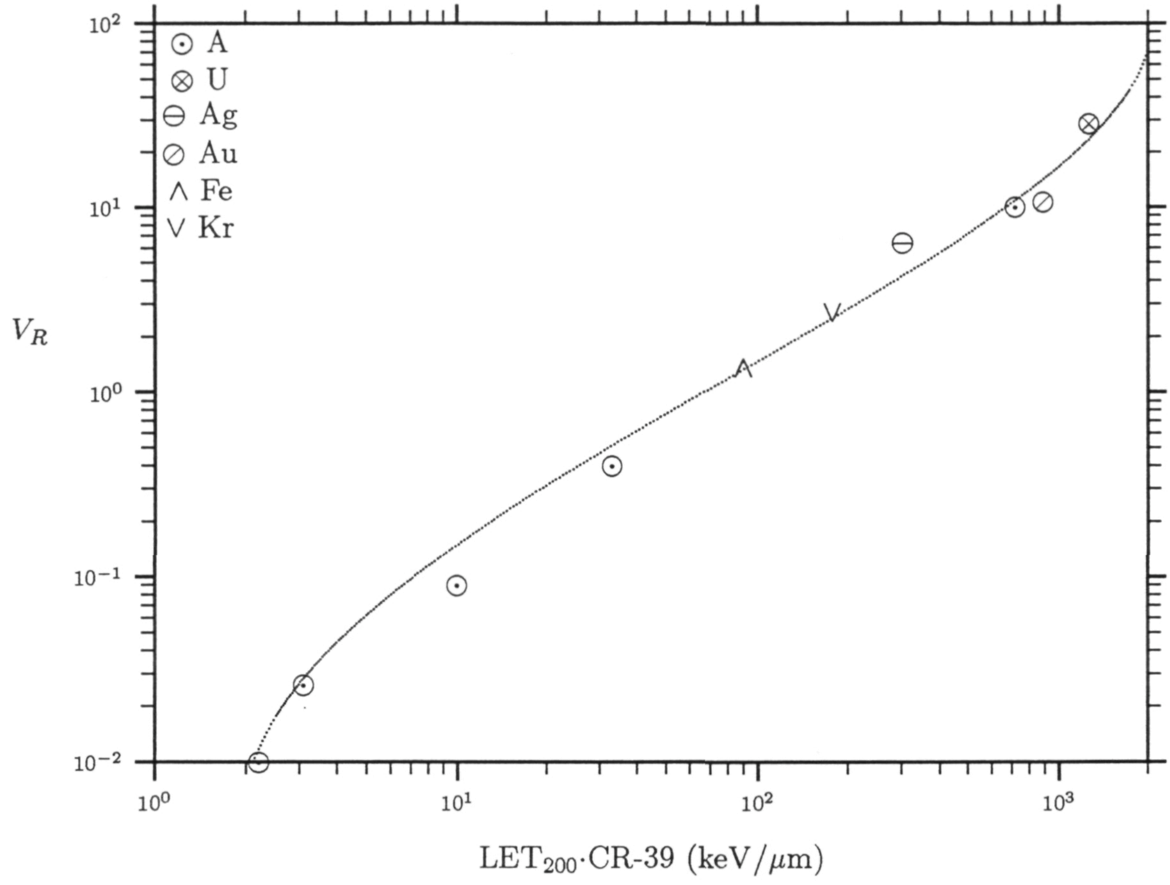

Figure 12: CR-39 PNTD response plot of measured V_R versus LET$_{200}$·CR-39 for LDEF A0015 experiment. Points labeled "A" are from 168 hour etch for this material adjusted to etch conditions of the A0015 CR-39 detectors.

stopping primary protons (both trapped and galactic) and inelastic proton secondaries from trapped proton interactions with C and O nuclei. The contribution of GCR to the LET spectra can be seen between ~50 and ~150 keV/μm. Reading the curve from right to left, there is a sharp rise in the long range spectrum around ~137 keV/μm, the geomagnetic cutoff for relativistic Fe, and then a leveling of toward lower LETs. Even in the region between 50 and 150 keV/μm, the contribution from short range particles is greater than long range particles, illustrating the relatively modest GCR component in the LET spectra for an orbit of this inclination and altitude.

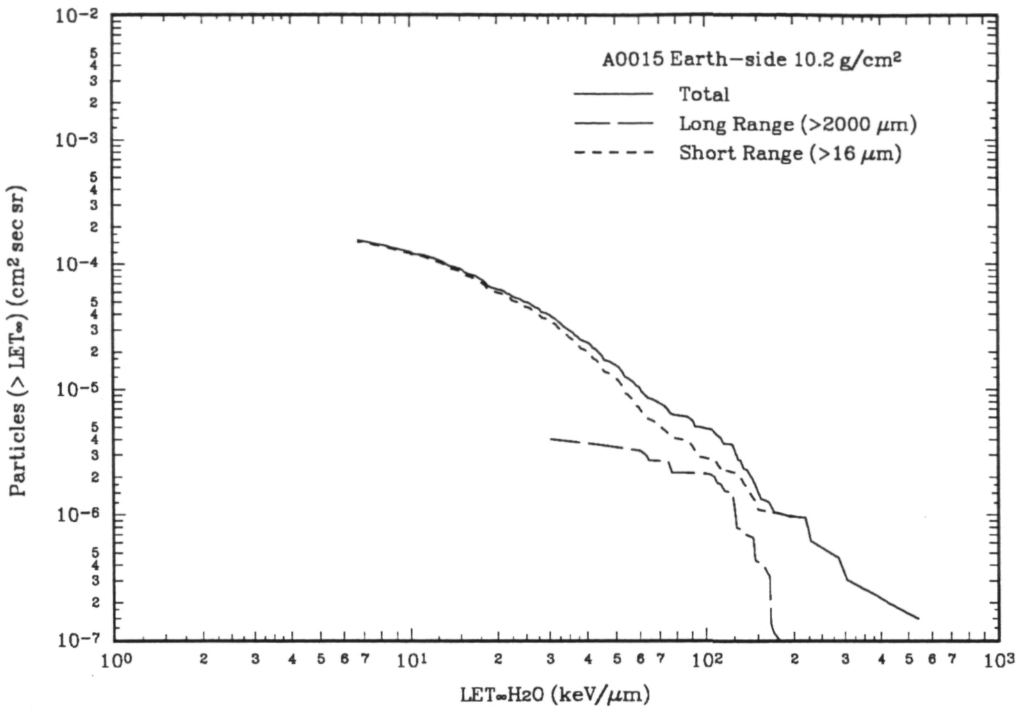

Figure 13: Integral LET Flux Spectra measured under 10.2 g/cm^2 shielding in the LDEF A0015 Earth-side stack.

Figures 14, 15, and 16 are integral LET flux spectra measured in the A0015 West-side stack under 2.6, 4.4, and 9.2 g/cm^2, respectively. As with the Earth-side LET spectra measurement, all three West-side spectra were measured using the two layer coincident method. Shielding values represent only the vertical self-shielding of the experiment and not the shielding from surrounding experiments or from the spacecraft itself. Analysis of the West-side spectra is similar to that of the Earth-side, with GCR make a relatively small contribution when compared with short range particles. The short range component is most likely C and O recoils and fragments at high LETs and inelastic proton secondaries and stopping primary protons at lower LETs. LET spectra measured under 4.4 g/cm^2 (Figure 15) showed a greater contribution from long range events in the middle of the spectra (50–150 keV/μm) when compared with the LET spectra measured at the other two shielding depths. The reason for this difference is not presently known and may reflect some complicated effect of the

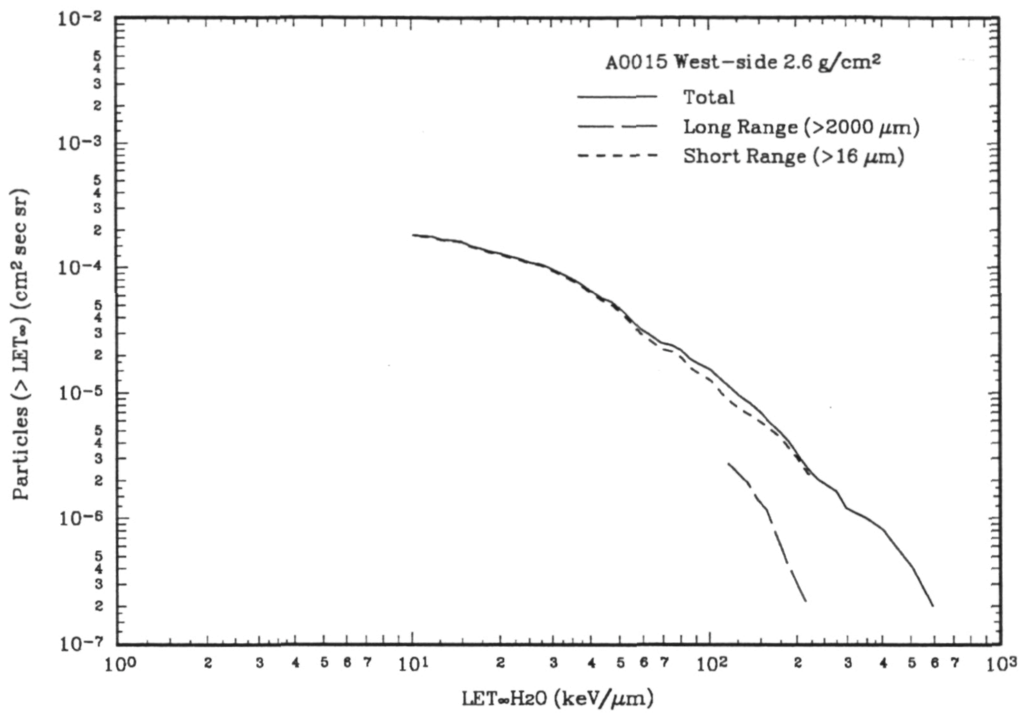

Figure 14: Integral LET flux spectra measured under 2.6 g/cm^2 shielding in the LDEF A0015 West-side stack using the coincident spectroscopy technique.

overall shielding geometry of the experiment. This set of spectra (4.4 g/cm^2) was measured before the other two sets of spectra and may simply reflect measurement inefficiency.

The A0015 West-side stack faced toward the West, the direction of highest trapped proton flux. This most likely explains the higher overall spectra measured on the West-side compared to the Earth-side. Figure 17 show the total LET spectra measured in the A0015 West-side stack under 2.6 g/cm^2 and similar LET spectra measurements made under 2.74 g/cm^2 in the M0004 experiment. The M0004 experiment was located on the East (leading edge) side of LDEF. The East-side spectrum is significantly lower than that measured on the West side, especially at higher LETs, showing the effect of the East/West trapped proton anisotropy. The larger flux of trapped protons entering the spacecraft on the West side than the East side led to a higher fluence of secondary particles produced in the West-side experiments compared to experiments on the East-side and elsewhere on LDEF.

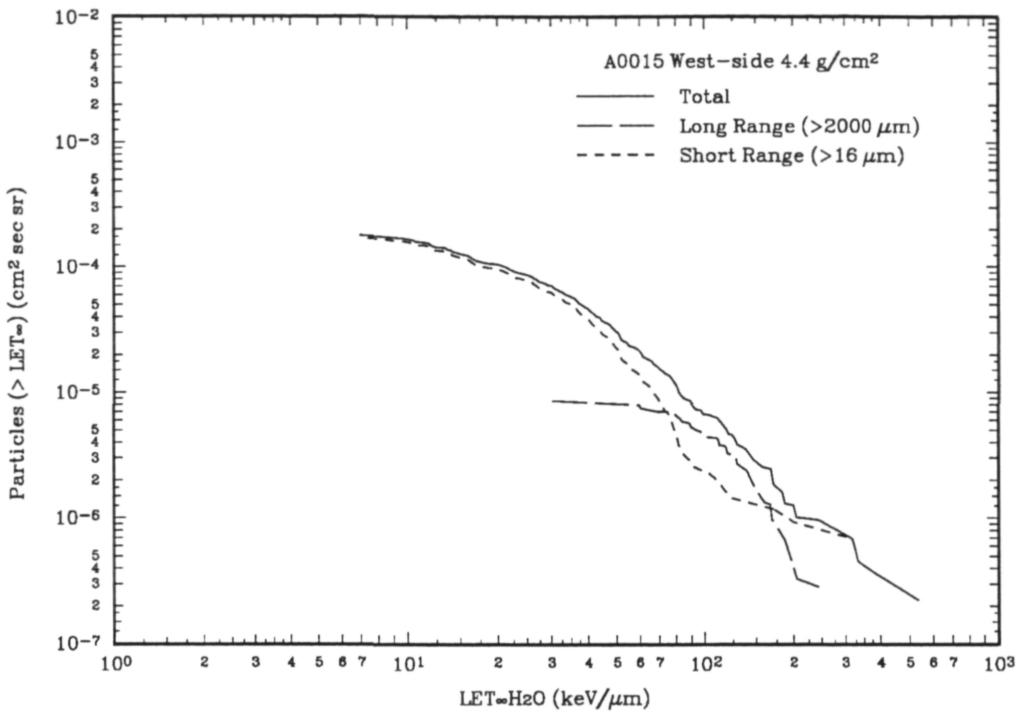

Figure 15: Integral LET flux spectra measured under 4.4 g/cm^2 shielding in the LDEF A0015 West-side stack using the coincident spectroscopy technique.

Figure 18 is the integral LET flux spectra measured under 6.1 g/cm^2 in the P0004 SEEDS experiment on the West side of LDEF. It is comparable to LET spectra measured in the A0015 West-side stack, showing the same dominance of short range events over long range GCR events.

Figures 19 and 20 are photomicrographs of typical fields of view on the LDEF A0015 CR-39 under 100x and 400x, respectively. Nearly all the objects visible in the photomicrographs are nuclear tracks, though many of them are over-etched and difficult to measure. An over-etched track is one which no longer possesses a pointed tip, but instead a rounded end. Particles that form over-etched tracks stopped in the volume occupied by the track. The track etched along the latent damage trail until it ended. The bulk etch continued in all directions, enlarging the pointed tip of the track into a spherical bowl shape. Short-range secondary particles often leave over-etched tracks. If a particle's path ended just beneath the

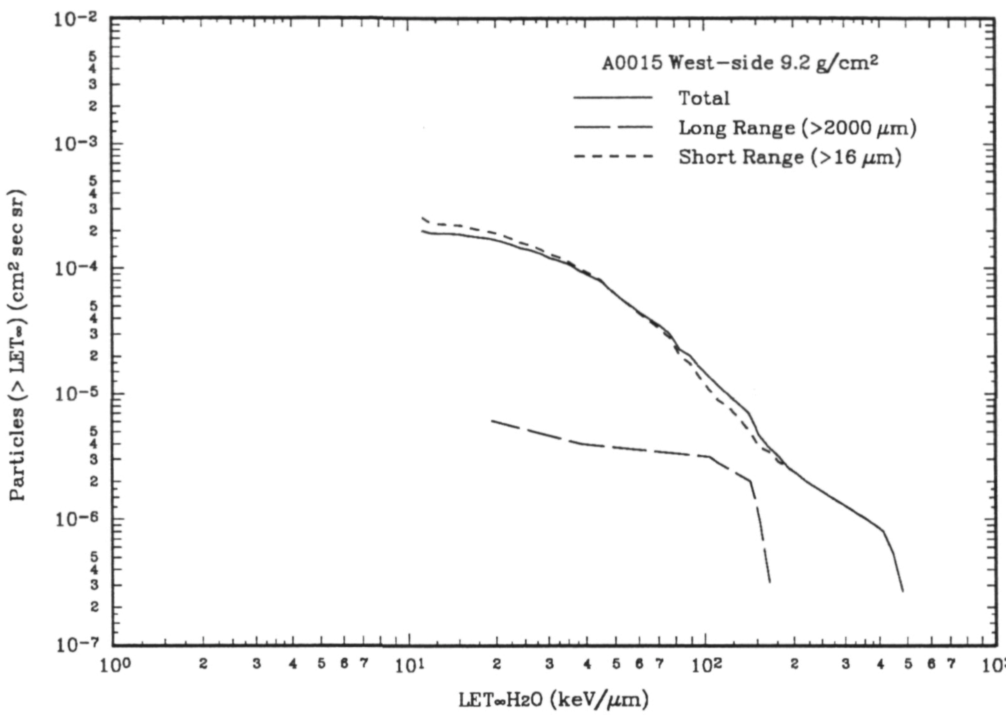

Figure 16: Integral LET flux spectra measured under 9.2 g/cm^2 shielding in the LDEF A0015 West-side stack using the coincident spectroscopy technique.

pre-etch surface of the detector, the particle may completely etch out into a hemispherical pit. Several of these tracks are visible in Figure 20, appearing as dark circles. The darkness of the track is often related to its dip angle, the angle between the particle's trajectory and the surface of the detector. Tracks with shallow dip angles tend to be lighter and of lower contrast with the surrounding background. These tracks also have more eccentric elliptical openings. Tracks from particles which passed through the detector surface at near right angles tend to be much darker and their openings are more circular in shape.

3.4 LET Measurements as a Function of Shielding

3.4.1 Track Density Measurements as a Function of Shielding

As a preliminary study to the measurement of LET spectra at different shielding depths in the A0015 stack, total track density (total number of particle tracks per unit area) was

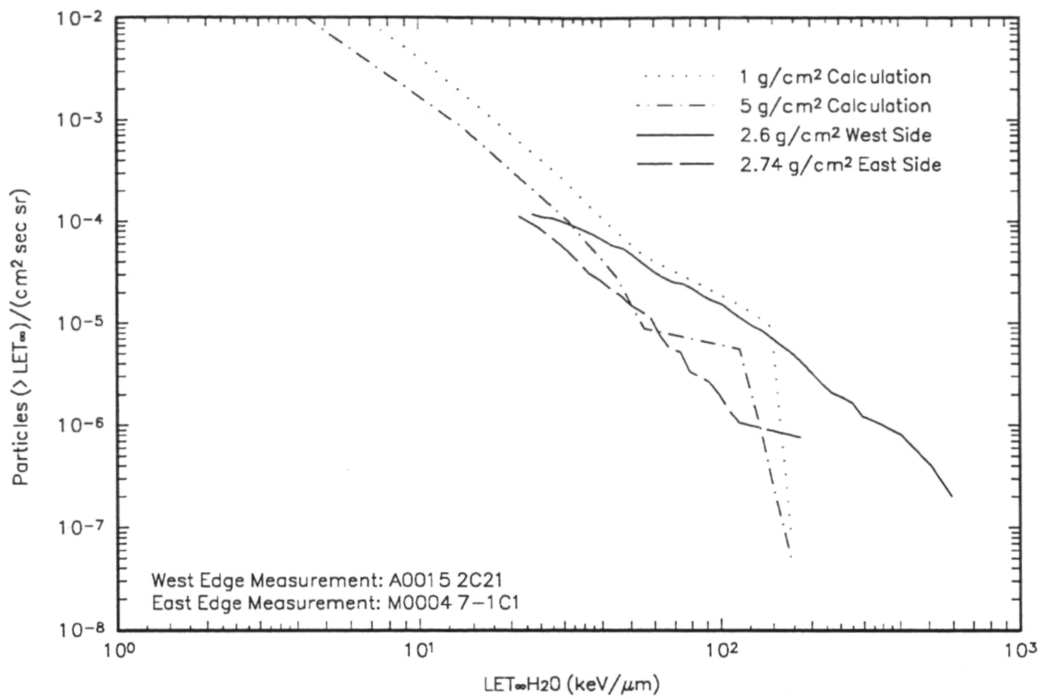

Figure 17: Integral LET flux spectra measured under 2.6 g/cm^2 in the A0015 West-side stack and under 2.74 g/cm^2 in the M0004 East-side stack, showing the effect of the East/West trapped proton anisotropy. Also included are model calculations of LDEF LET spectra under 1 and 5 g/cm^2 from the LDEF Pre-recovery Estimates.

counted at five shielding depths. Track density was counted in single layers of CR-39 PNTD. Track selection criteria for counting included both conical and round (stopping) tracks. Spherical etch pits, which could have been produced by either particles or defects in the PNTD material, were not counted. All tracks from particles of range down to $\sim$1 μm were counted. The CR-39 detector layers were 7$\times$7 cm^2 in area. Track density was counted in a 13$\times$13 array. Each field of view was separated by 5 mm. The area of each field of view was 0.0018 cm^2.

The track density measurements for the A0015 experiment were plotted as a function of x-y coordinates to produce track density profiles. Figures 21, 22, 23, 24, and 25 are track density contour plots for the West-side A0015 CR-39 layers under 2.6, 5.7, 8.2, 9.2, and 11.9 g/cm^2, respectively. For CR-39 layers under 2.6 and 5.7 g/cm^2, there appears to be

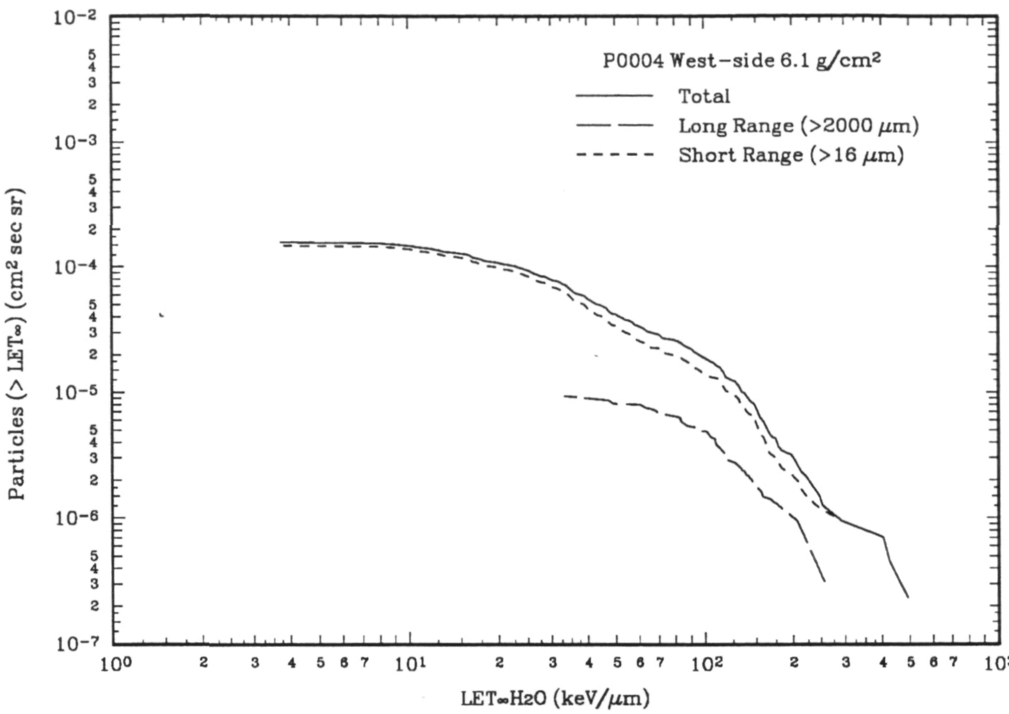

Figure 18: Integral LET flux spectra measured in the LDEF P0004 SEEDS experiment on the West side of LDEF under 6.1 g/cm^2.

a dearth of particle tracks in the upper-left corner of the detectors. CR-39 layers under 8.2 and 9.2 g/cm^2 appear more uniform. A large concentration of tracks appears in the upper-left corner of the 11.9 g/cm^2 layer. These changes in track density probably reflect the complicated shielding geometry surrounding the A0015 West-side stack.

Figure 26 shows the profiles for all five of the layers counted along with shielding depth of each counted layer at the left of the corresponding profile. While there appears to be little discernible structure in the total track density as a function of x-y position on the detector surface, total mean track density is seen to increase as a function of shielding. The mean track density on the front-side of the CR-39 detector under 2.6 g/cm^2 shielding was 1.08×10^5 tracks/cm^2. This increased to 1.62×10^5 tracks/cm^2 under 11.9 g/cm^2. Total mean track density measurements were also made on the backside surface of each detector. The backside of the 2.6 g/cm^2 detector had a mean track density of 1.09×10^5 tracks/cm^2.

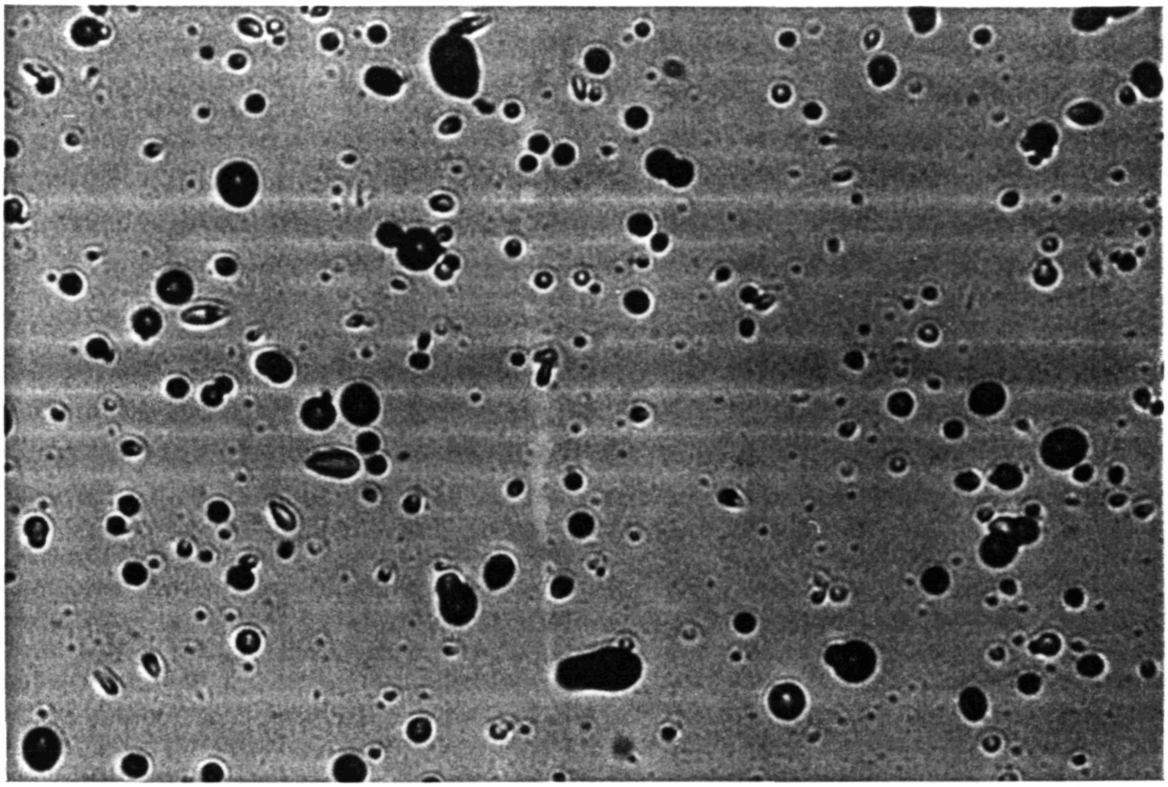

Figure 19: Photomicrograph of a typical field of view on a CR-39 layer from the LDEF A0015 experiment at 100× magnification. Nearly all the objects visible in the photograph are tracks. Scale is ~25μm/cm.

Under 11.9 g/cm^2, the total mean track density was 1.38 $\times$ 10^5 tracks/cm^2 on the backside. Figure 28 shows track density as a function of shielding for the A0015 West-side stack CR-39 PNTDs.

Figure 27 is a comparison of the total track density measurements and measured doses from TLDs as functions of shielding depth in the A0015 West-side stack. The TLD dose is seen to decrease with depth, reflecting the attenuation of lower LET particles as a function of shielding. These lower LET particles do not register as tracks in CR-39 PNTDs. Track density is seen to increase as a function of shielding in the experiment stack.

To understand the effect of shielding on LET spectra in the A0015 experiment, a ground-based study was carried out to simulate the exposure of CR-39 PNTDs on LDEF. The experiment consisted of a thick stack of CR-39 PNTDs interspersed with layers of Al absorber and was exposed to 154 MeV protons at the Harvard Cyclotron. Protons of this energy are close to the peak energy of the trapped proton energy spectrum[2]. The stack was exposed

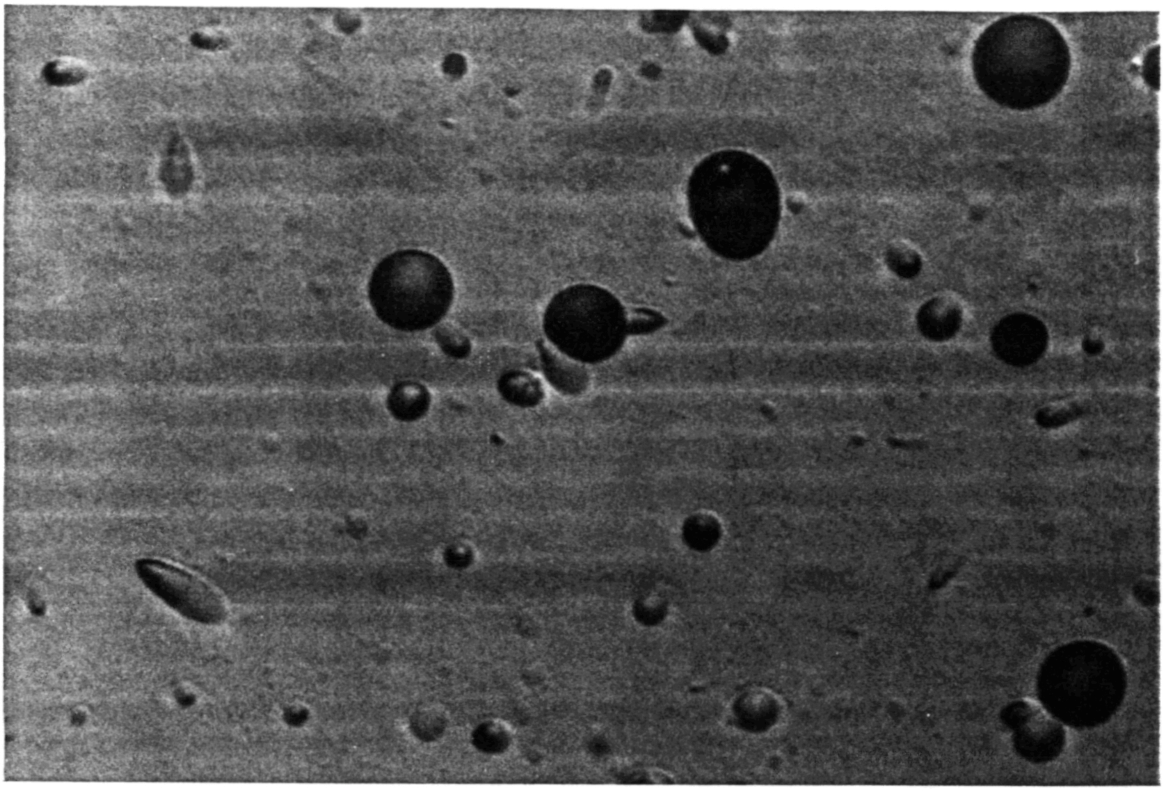

Figure 20: Photomicrograph of a typical field of view on a CR-39 layer from the LDEF A0015 experiment at 400× magnification. Scale is ~6μm/cm.

to ~10 rads or ~10^8 protons/cm^2. The stack was oriented normal to the incident proton beam. The range of 154 MeV protons in Al is ~21 g/cm^2. Under the lesser shielding depths in which the track densities were counted in the A0015 stack, 154 MeV protons cannot form visible tracks since their LET is below the threshold for track registration. Hence all tracks seen under this shielding are the result of secondary particles. These tracks are from elastic and inelastic collisions between the primary protons and hydrogen, carbon and oxygen nuclei of the stopping material. The CR-39 PNTDs from the 154 MeV proton experiment were processed and readout in the same manner as those from the LDEF experiment. Figure 28 shows track density as a function of shielding as measured in the CR-39/Al stack exposed to 154 MeV protons. Track density was normalized to the A0015 2.6 g/cm^2 track density. Track density is also seen to increase as a function of shielding until the stopping point for 154 MeV protons at ~21 g/cm^2. Between ~18 and ~22 g/cm^2 shielding, the CR-39 detectors were saturated with tracks making it impossible to accurately count the total track density in this region. However, in the region below 11.9 g/cm^2, the total shielding thickness of the

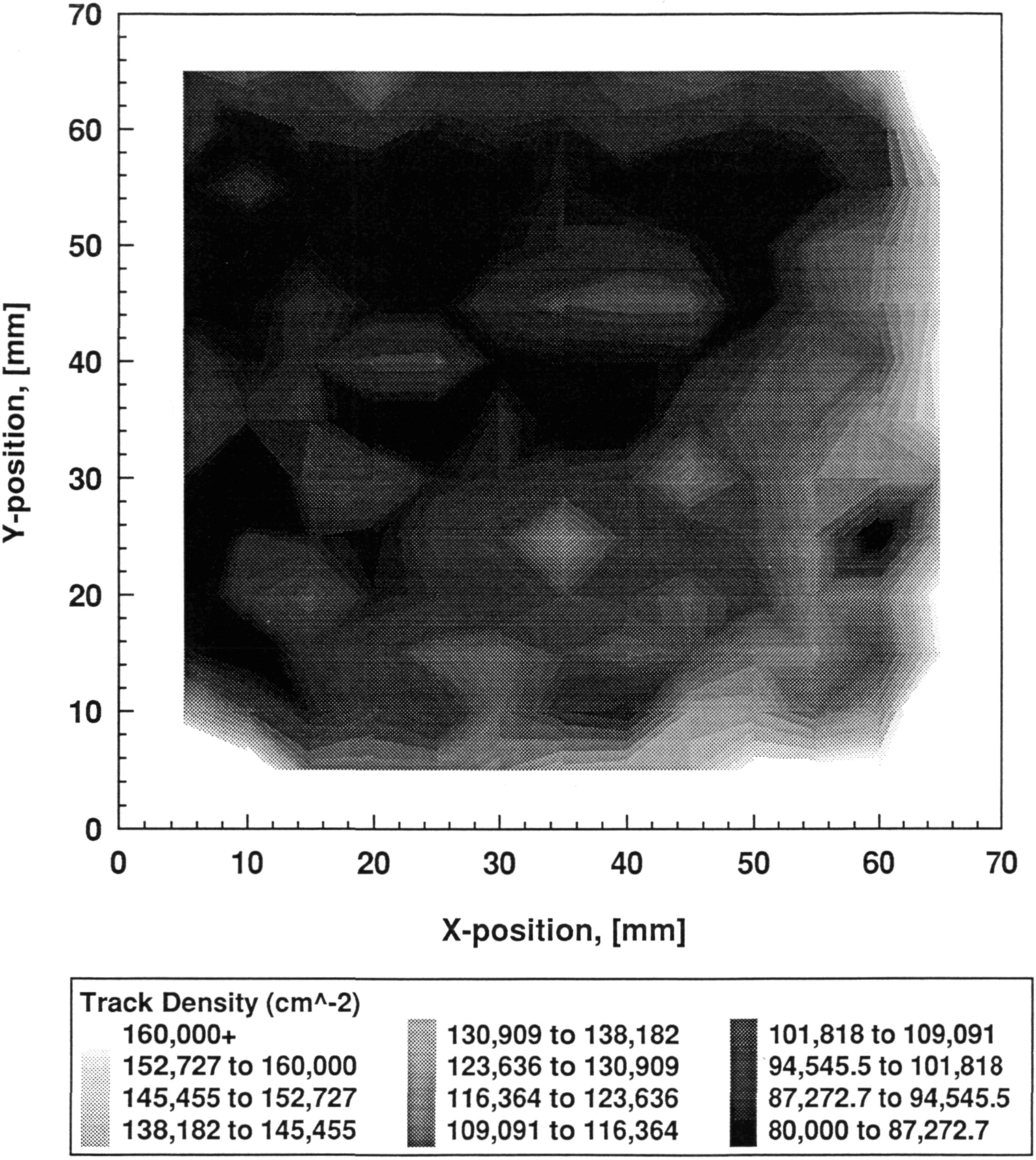

Figure 21: Track density profile of A0015 West-side CR-39 layer 2C21 under 2.6 g/cm^2.

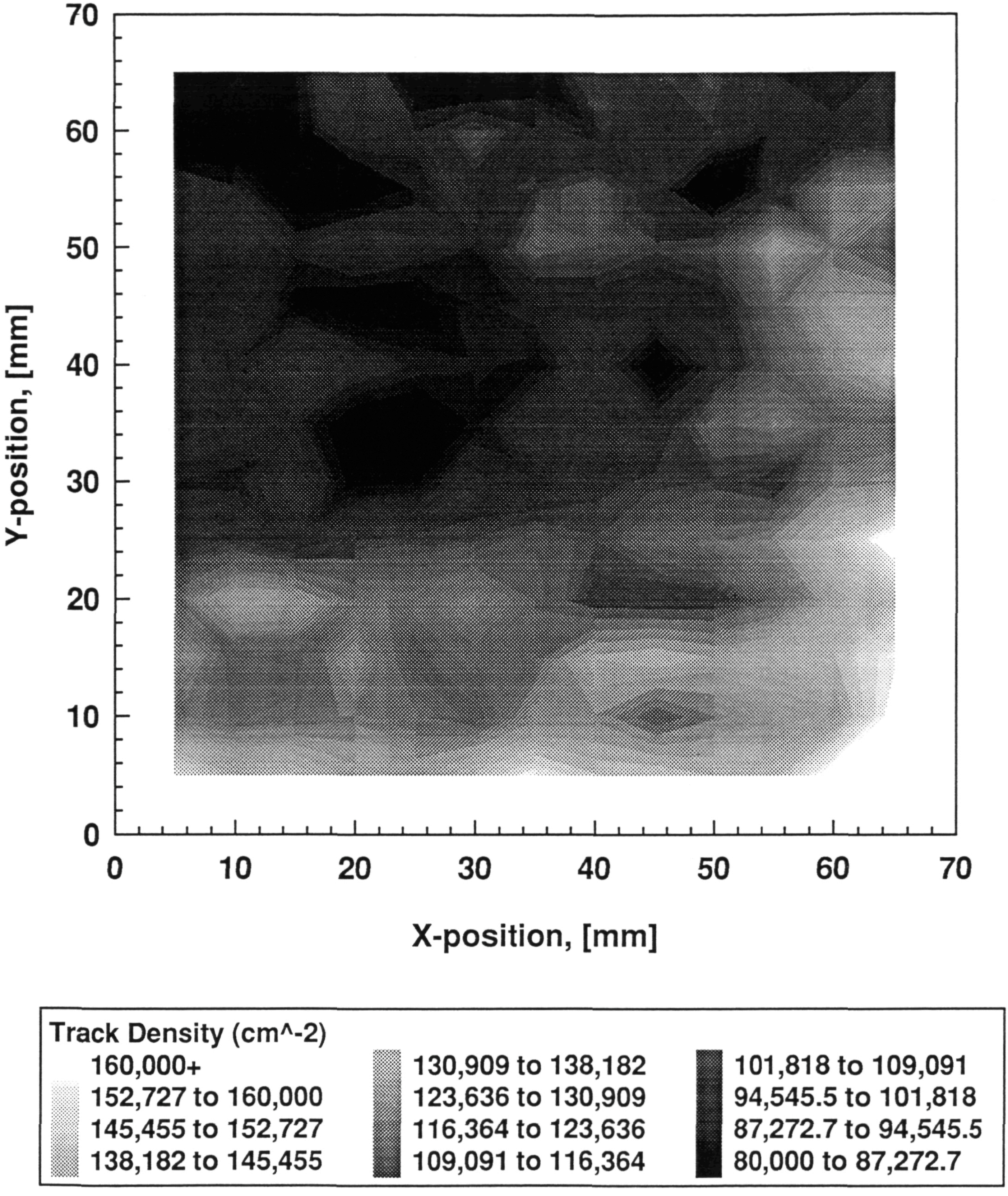

Figure 22: Track density profile of A0015 West-side CR-39 layer 2C65 under 5.7 g/cm^2.

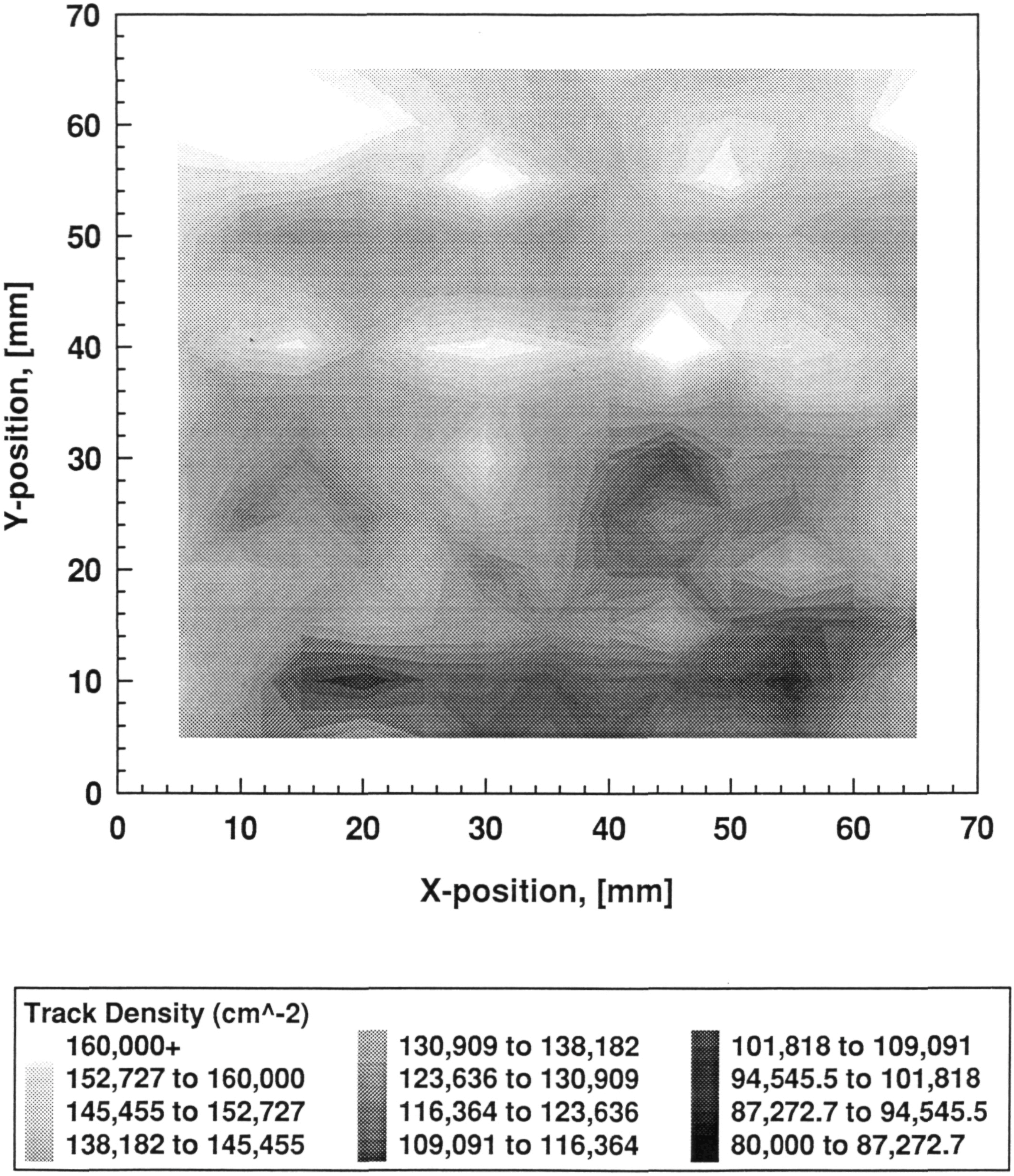

Figure 23: Track density profile of A0015 West-side CR-39 layer 2C101 under 8.2 g/cm^2.

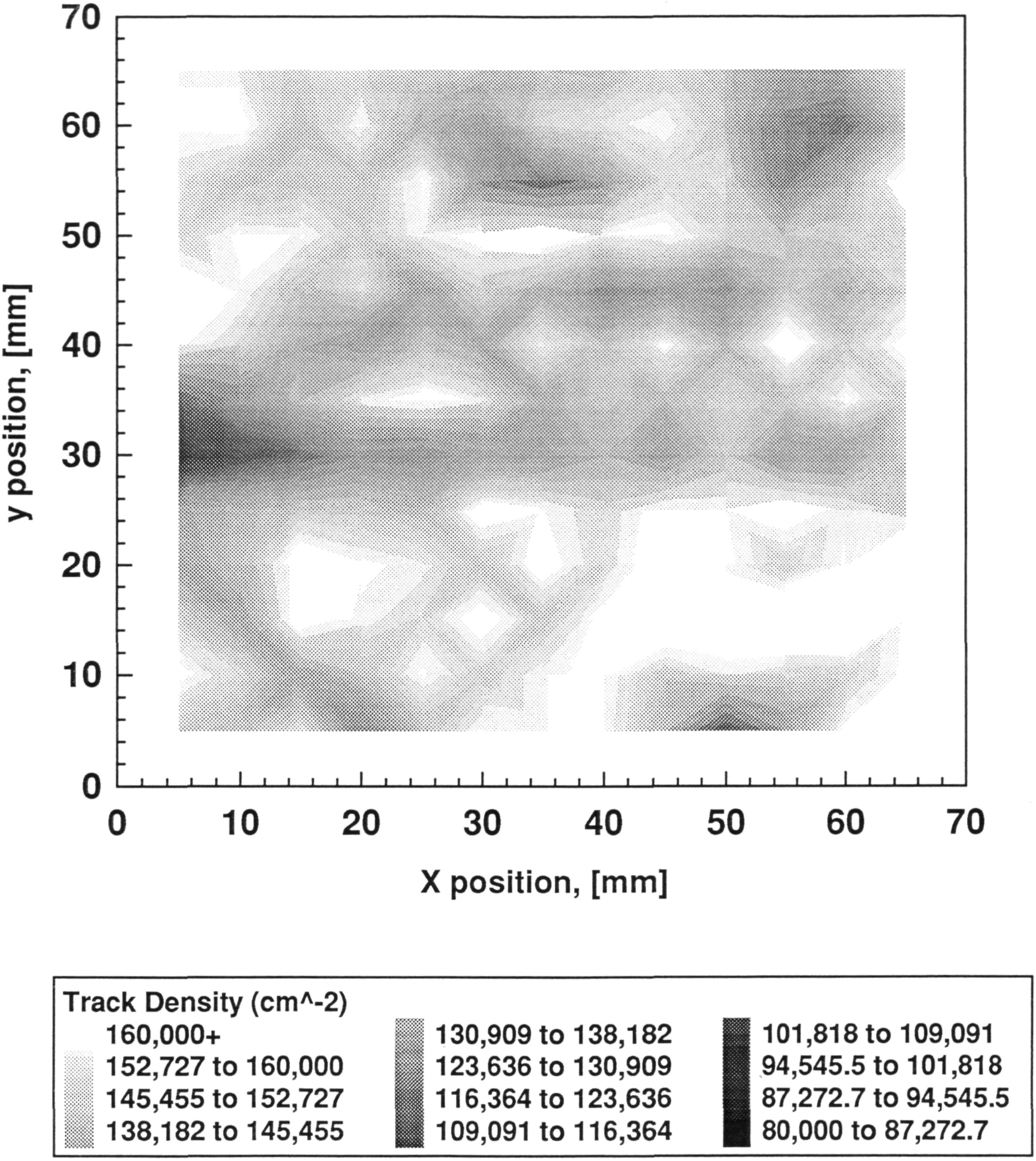

Figure 24: Track density profile of A0015 West-side CR-39 layer 2C121 under 9.2 g/cm^2.

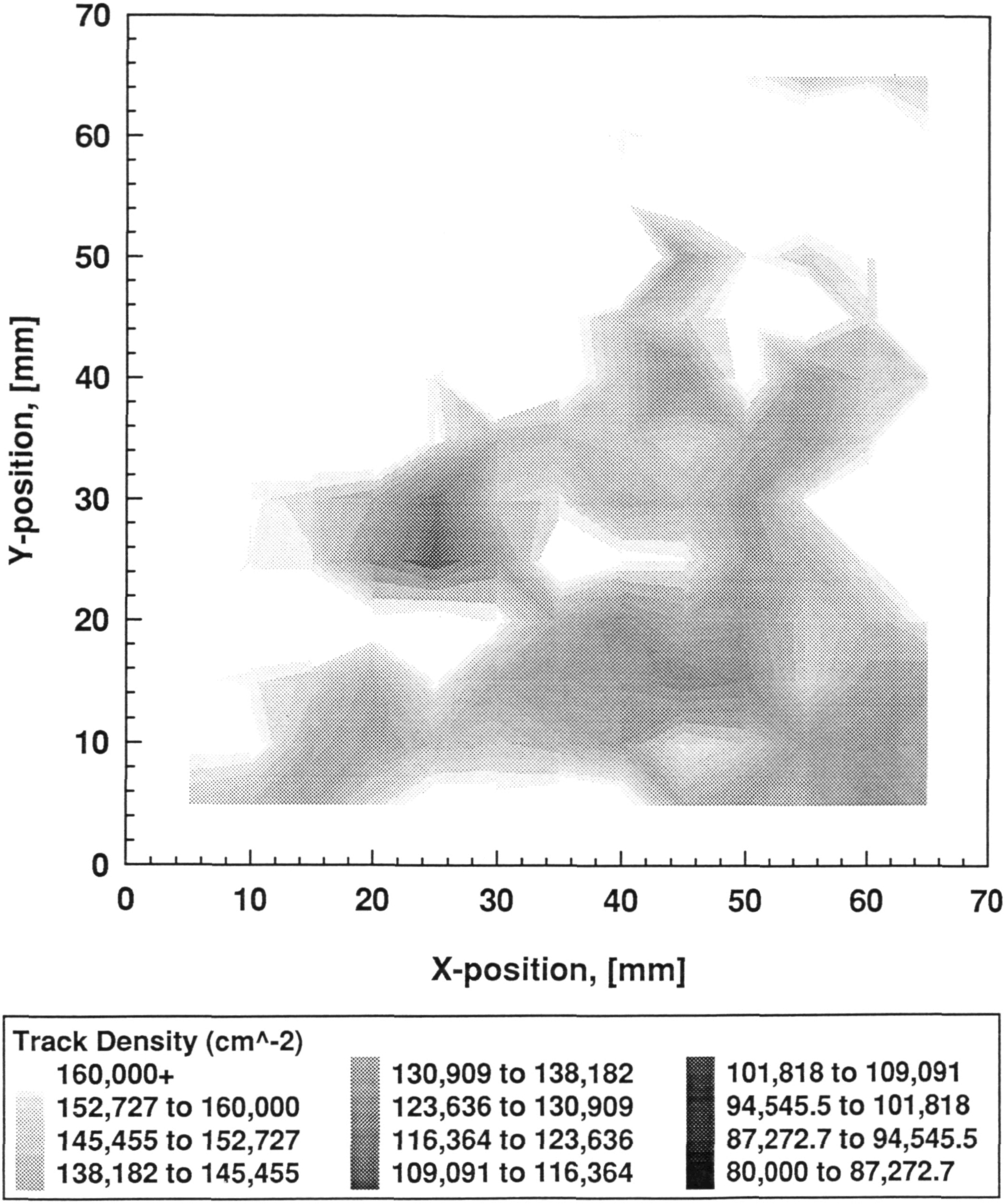

Figure 25: Track density profile of A0015 West-side CR-39 layer 2C161 under 11.9 g/cm^2.

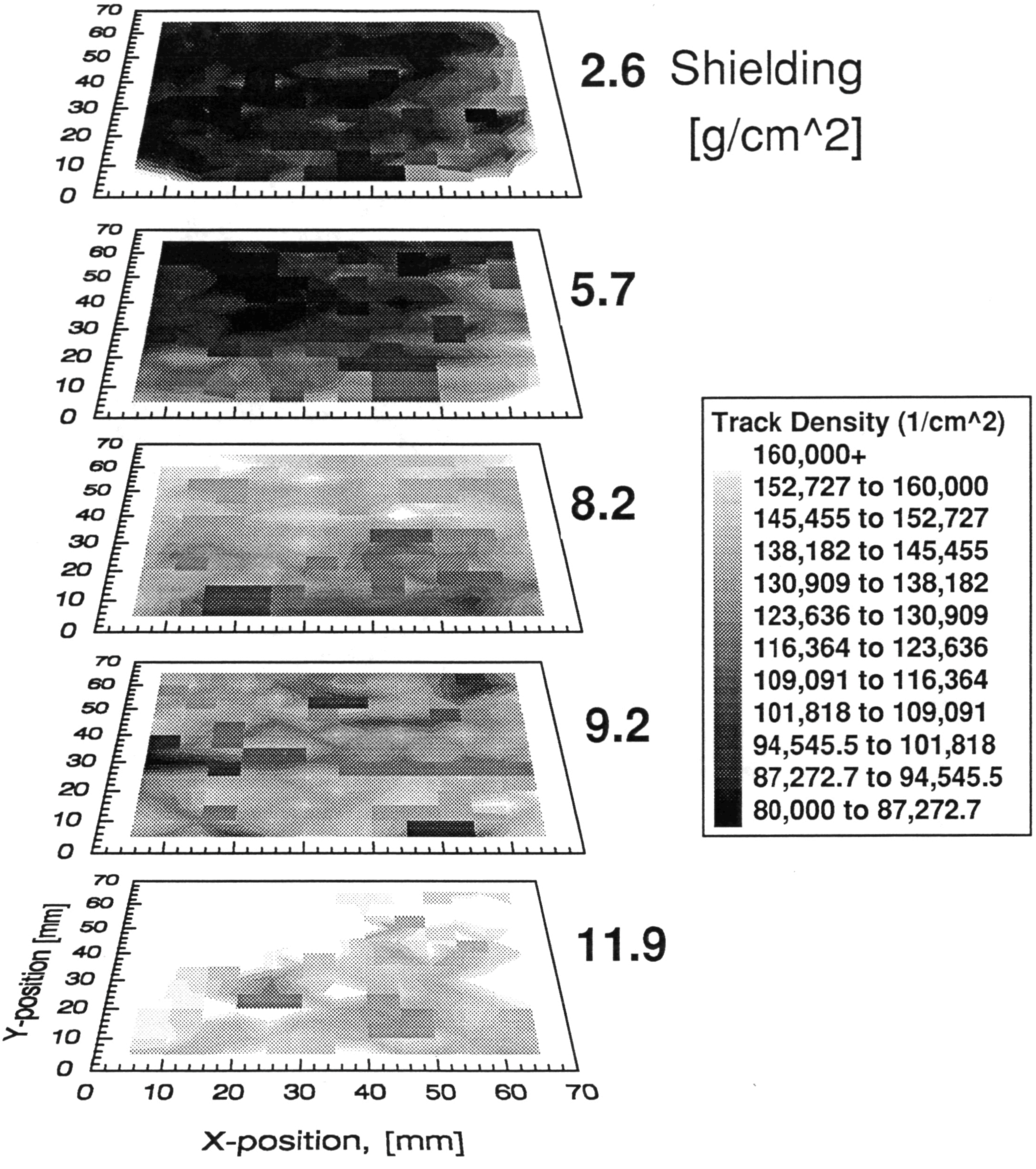

Figure 26: Total track density plots under five shielding depths for the A0015 West-side stack. Track density is seen to increase with greater shielding.

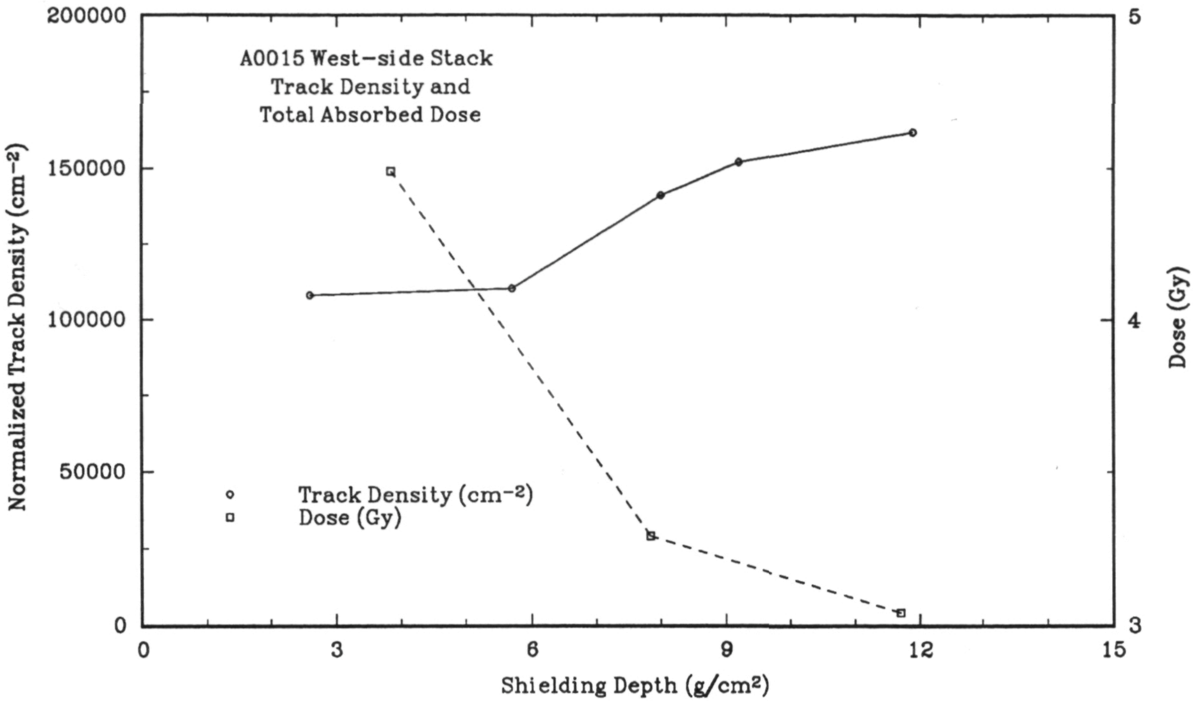

Figure 27: Comparison of total track density measurements with total absorbed dose measurements as a function of shielding for the A0015 West-side stack.

A0015 West-side stack, the LET of the protons is below that for the registration of latent tracks. All tracks seen in this region are the result of secondaries produced by interactions with the 154 MeV primary protons. Total track density increases from an absolute value of 6.69×10^5 and a normalized value of 1.07×10^5 tracks/cm^2 under 2.9 g/cm^2 to an absolute track density of 8.26×10^5 and a normalized track density of 1.32×10^5 tracks/cm^2 under 11.41 g/cm^2. The curve showing the increase in total track density for the 154 MeV proton exposure is similar to those from the A0015 experiment, especially on the back surfaces of the A0015 detectors, for shielding below 11.9 g/cm^2. Since it is known that the tracks in the 154 MeV proton detectors are from secondaries, the similarity between the 154 MeV proton and LDEF curves confirms that a significant fraction of the tracks being counted in the LDEF detectors are the result of secondaries.

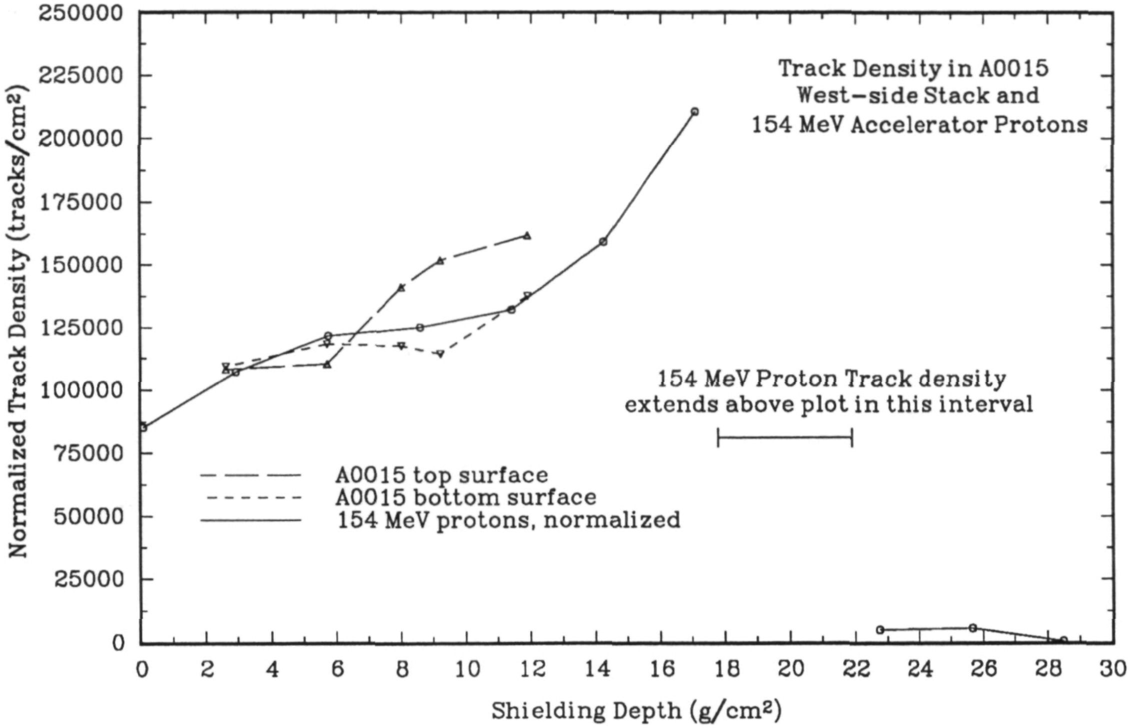

Figure 28: Total track density as a function of shielding depth for the front and back surfaces of the A0015 West-side stack detectors and the front surfaces of the 154 MeV proton detectors. The track density counted in the 154 MeV proton detectors is normalized to the A0015 results under 2.6 g/cm^2.

3.4.2 LET Measurements

LET spectra were measured under three shielding depths of the A0015 West-side stack, 2.6, 4.4 and 9.2 g/cm^2, and under three shielding depths in the 154 MeV proton stack, 2.9, 8.5 and 14.4 g/cm^2. Tracks were selected for measurement using the two-layer coincident method. Since the amount of material removed from each surface (bulk etch) was $\sim$8 μm, all measured events, both primary and secondary, are from particles of range $>$16 μm.

The standard method used by this laboratory to reduce particle track data into LET spectra involves the assumptions that the flux of particles is isotropic. For both the A0015 and the 154 MeV proton experiments, this was not the case. The beam of protons was incident normal to the surface of the CR-39 PNTDs for the ground-based exposure while

there was a preferred direction of arrival from the West, nearly normal to the detector surface, for the A0015 West-side stack. While it might be argued that isotropy is still valid in the case of inelastic collisions, there is a directional dependence, based on the directionality of the primary protons, for elastic collisions. Instead of generating integral LET spectra based on the assumption of isotropy, the track data was reduced in such a way as to yield the average differential LET spectra for a given solid angle. A solid angle of 20° normal to the detector surface was chosen. This angle was a compromise between a small angle which is better from the point of view of detector efficiency, and an angle large enough to measure enough tracks for good statistics. Measured tracks that did not fall within this acceptance angle were rejected.

LET spectrum data was collected by measuring the major and minor axes of 300 track pairs in each detector. These track parameters, along with the bulk etch, were then transformed into LET values by a calibration function. For the detectors on the A0015 West-side stack, an additional 50 long range events were measured. Long range events are from particles which left tracks on each of the four surfaces of the reassembled detector pair. These events are considered to be from relativistic Fe and were used as part of an internal calibration. They were not included in the LET spectra.

Differential LET fluence spectra was measured under two shielding depths, 2.6 and 9.2 g/cm^2, of the A0015 West-side stack, and under three shielding depths, 2.9, 8.5, and 14.4 g/cm^2, in the 154 MeV proton stack. Figure 29 is the differential LET fluence spectra measured in the A0015 West-side stack under 2.6 g/cm^2 and is plotted with error bars. Similar errors were calculated for the other spectra. Note that the y-axis is a logarithmic scale so while the error appears to decrease with increasing fluence, it is actually increasing. Figure 30 shows the differential LET spectra measured in the A0015 West-side stack under 2.6 and 9.2 g/cm^2. There is close agreement between the two A0015 LDEF curves within the limits of error. At lower LETs (below 100 keV/μm) much of the spectra is made up of secondaries from elastic proton-proton collisions. Tracks from elastic and inelastic collisions between primary trapped protons and carbon and oxygen nuclei of the stopping material have higher LETs and contribute only to the right-most portion of the spectrum.

Figure 31 shows the differential LET spectra measured under 2.9, 8.5 and 14.4 g/cm^2 in

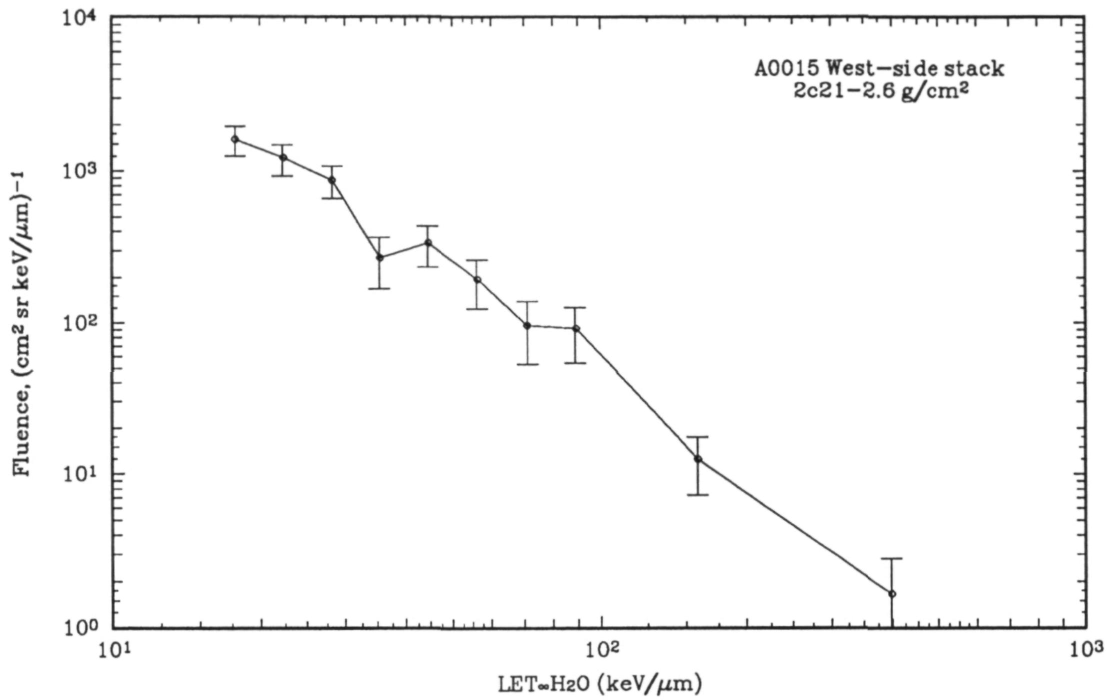

Figure 29: Differential LET fluence spectrum, including error bars, measured in CR-39 under 2.6 g/cm^2 in the A0015 West-side stack.

the 154 MeV proton stack. The slopes of the 154 MeV proton curves are similar to those measured in the LDEF detectors showing that a significant number of the tracks counted in the LDEF detectors are the result of secondaries. Although the three curves lie close together, the fluence increases with shielding depth, presumably because of the increase in cross-section with decreasing primary proton energy. Figure 29 is the differential LET fluence spectra measured in the 154 MeV proton stack under 2.9 g/cm^2 plotted with error bars. Errors were similar for the other two spectra measured in the accelerator proton experiment. The two sets of curves, A0015 West-side detectors and 154 MeV proton detectors, at similar shielding depths lie close together. The slopes are similar, especially for $LET_\infty{\cdot}H_2O<100$ keV/μm, the region dominated by elastic recoils. At higher LET, there appears to be a larger number of inelastic secondaries in the LDEF detectors. This result might be due to the fact that LDEF was exposed to the full spectrum of trapped proton energies and not to just one

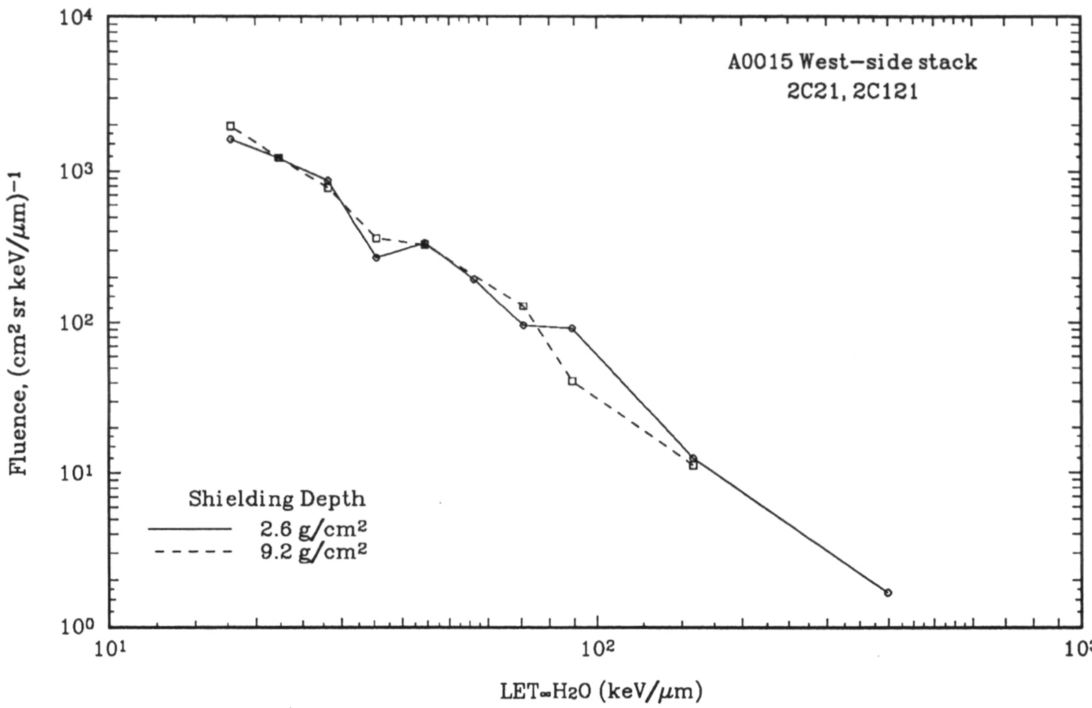

Figure 30: Differential LET fluence spectrum measured in CR-39 under 2.6 and 9.2 g/cm^2 in the A0015 West-side stack.

mono-energetic proton beam.

3.4.3 Conclusions from Measurements as a Function of Shielding

As has been suggested in earlier work proton-induced, short range secondaries were found to make a significant contribution to the LET spectra[7]. The similarity in slopes between the differential LET spectra measured in the LDEF A0015 West-side detectors and the CR-39 PNTD stack exposed to 154 MeV accelerator protons normally incident to the detector surface supports the conclusion that a substantial fraction of the tracks seen in the LDEF detectors are the result of secondaries. An increase in track density as a function of shielding depth was measured and can be explained by an increase in the cross section for the production of secondaries as the primary proton energy is attenuated. A pronounced increase in fluence as a function of shielding depth was not seen in the differential LET spectra. This is

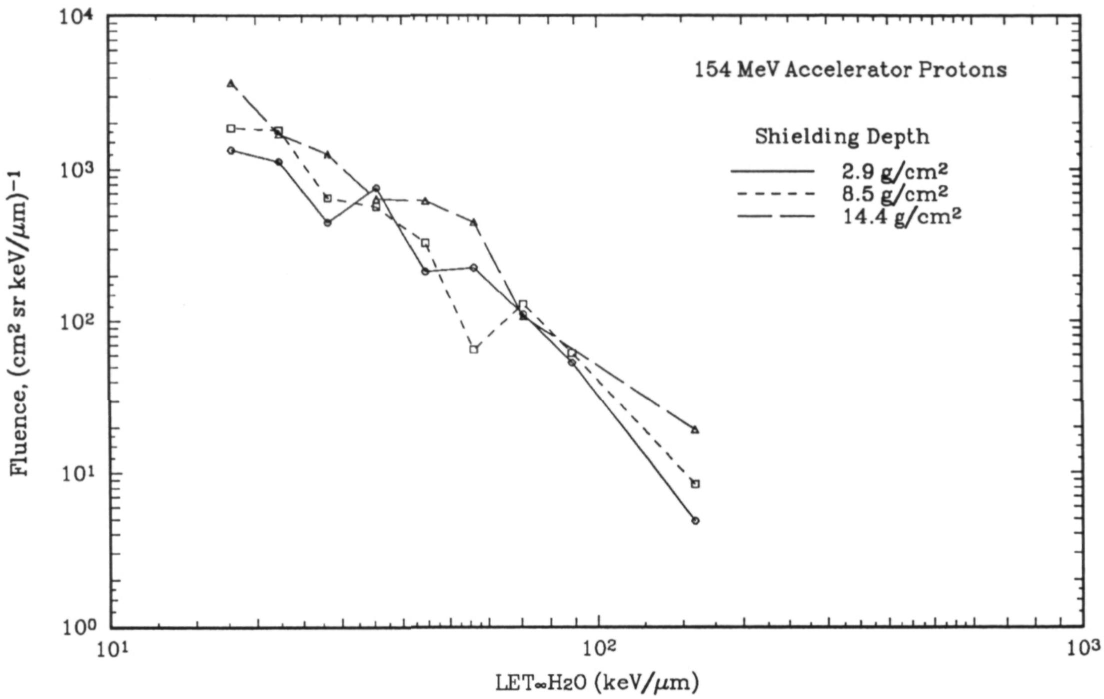

Figure 31: Differential LET fluence spectrum in CR-39 PNTDs under 2.9, 8.5, and 14.4 g/cm^2 for a 154 MeV proton exposure.

due to the difference in track selection criteria between the two types of measurements. The total track density measurements included all tracks from particles with a range greater than $\sim$1 μm while the differential LET spectra measurements consisted of all tracks from particles with range >16 μm. This indicates that the number of short range secondaries increased more rapidly than the number of longer range secondaries as a function of shielding.

3.5 High LET Tail

Measurement of LET spectra using the two-surface coincidence spectroscopy method had the disadvantage of excluding all tracks from particles with range less than a certain value (16 μm for A0015 CR-39), as explained above. A large fraction of the proton-induced high-LET secondary particles have a range less than 16 μm. The total event spectroscopy method was used to measure LET spectra from particles of range >2 μm in two layer of the A0015

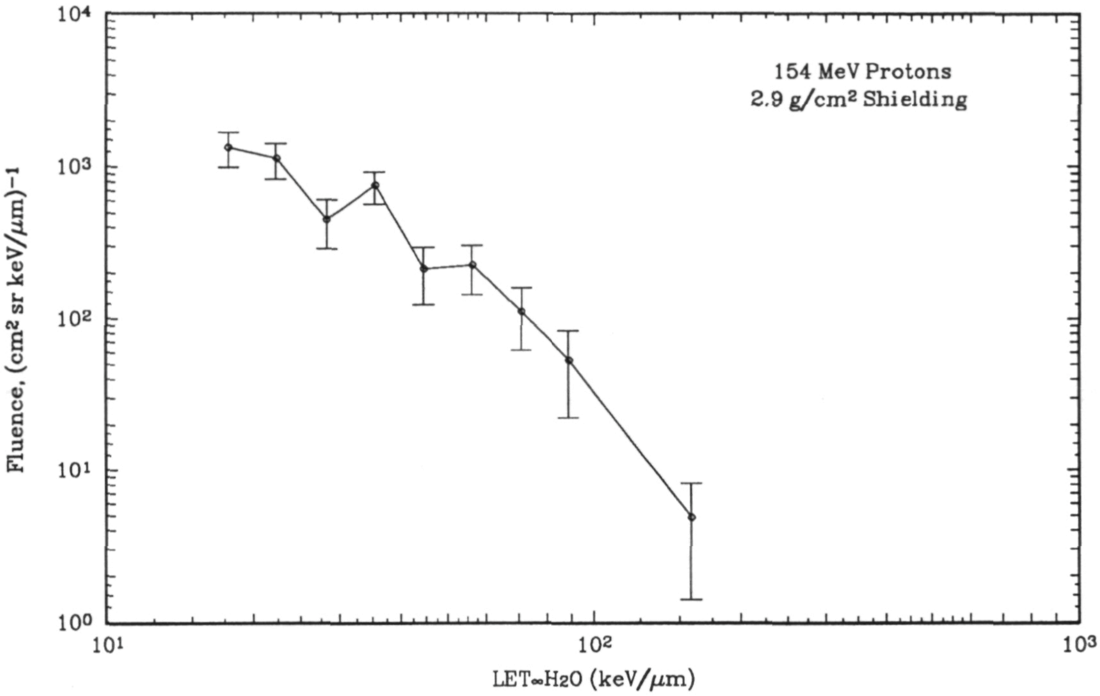

Figure 32: Differential LET fluence spectrum, including error bars, measured in CR-39 under 2.9 g/cm^2 in the 154 MeV proton stack.

West-side stack (2C21 under 2.6 g/cm^2 and 2C121 under 9.2 g/cm^2). Tracks from particles with range less than 2 μm are not readily measurable in CR-39 processed for 36 hr in 50°C 6.25 *N* NaOH. While shorter range (<2 μm) secondary particles were undoubtedly formed by trapped protons in the A0015 CR-39 layers, their contribution to the LET spectra was not measurable. In addition, some secondary particles were formed in the region of detector material removed by the etching process. These particles leave measurable tracks, but did not pass through the pre-etch surface of the detector, making the LET values determined for such tracks are too low. While the total event spectroscopy method is an improvement over the coincidence method in that it includes secondary particles of shorter range, it cannot be considered a 'complete' LET spectrum.

Figure 33 shows integral LET flux spectra measured under 2.6 g/cm^2 in the A0015 West-side stack using the total event and coincidence spectroscopy techniques. For the most part,

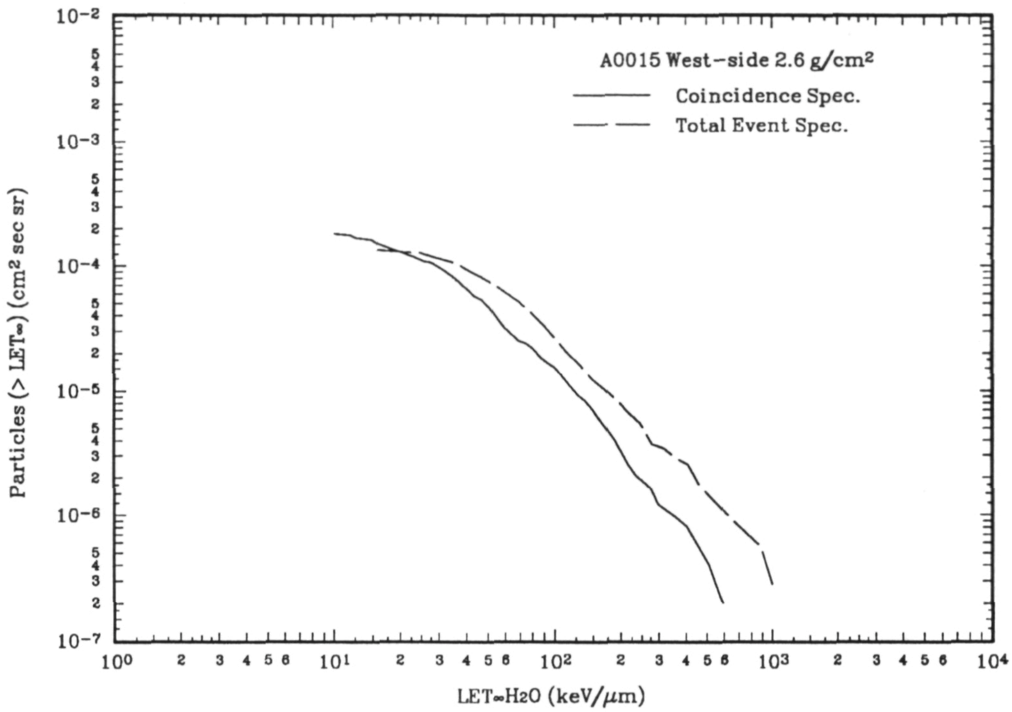

Figure 33: Integral LET flux spectra measured under shielding of 2.6 g/cm^2 in the A0015 West-side stack using both the two-layer coincidence spectroscopy method and the total event spectroscopy method.

the total event curve lies above the coincidence curve, especially at high LETs. This shows the contribution of the relatively large fraction secondary particles with ranges between 2 and 16 μm. As LET increases, the range of secondaries appears to decrease. At lower LETs ($\sim$20 keV/μm) the two curve converge. Particle tracks with low LET are quite small and of low visual contrast compared to the background surface of the detector making them difficult to measure. In addition, tracks with low LETs are approaching the LET threshold for registration in CR-39 ($\sim$5 keV/μm) and are recorded with less than perfect efficiency.

Figure 34 shows integral LET flux spectra measured using total event and coincidence methods under 9.2 g/cm^2 shielding in the A0015 West-side stack. As with the spectra measured under 2.6 g/cm^2, the total event curve lies above the coincidence curve, illustrating the relative contribution to the LET spectra from particles with range between 2 and 16 μm.

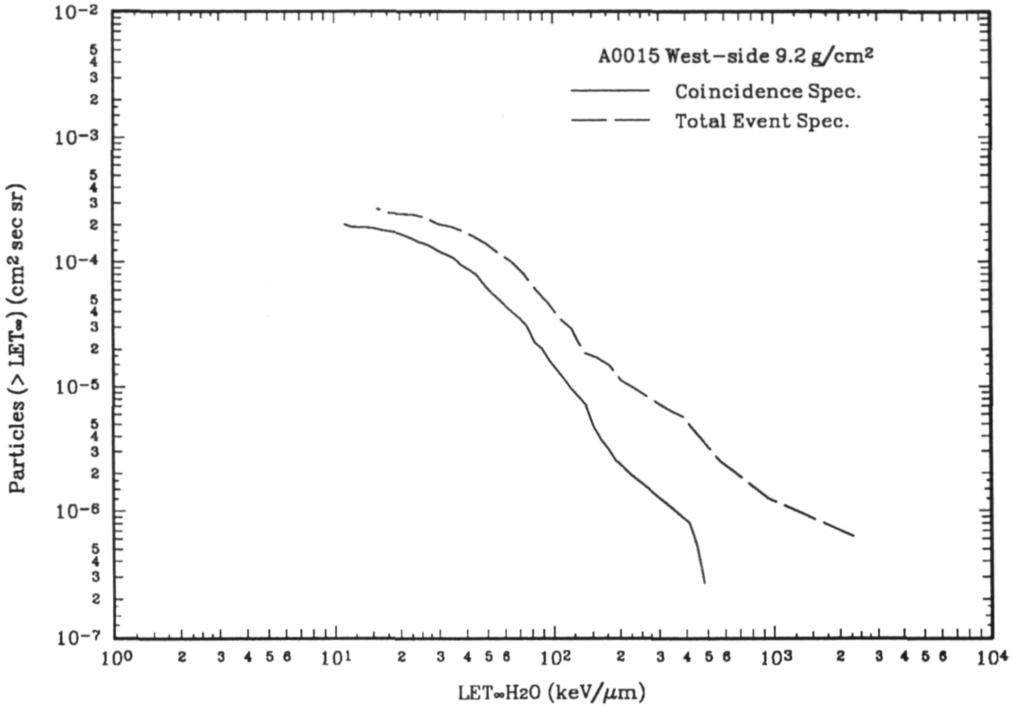

Figure 34: Integral LET flux spectra measured under shielding of 9.2 g/cm^2 in the A0015 West-side stack using both the two-layer coincidence spectroscopy method and the total event spectroscopy method.

The total event curve also extends to much higher LET (~2000 keV/μm) than does the coincidence curve, showing the decrease in range of secondary particles as LET increases.

Data for both sets of curves (two-layer coincidence and total event methods) were reduced using the assumption that the flux of particles was isotropic. For LDEF, this is not the case since trapped protons have a preferred direction of travel from West to East in the SAA and the spacecraft travelled through the SAA in a fixed orientation. Elastic secondaries and high energy inelastic secondaries will also show this directional preference since forward scattering angles are favored in these types of collisions. However for lower energy inelastic secondary particles, there is less of a preferred angle of scatter and the flux of these particles may be considered isotropic within the detector. The short range, high LET secondaries that make up the high-LET tail are of relatively low energy, making the assumption of isotropy valid

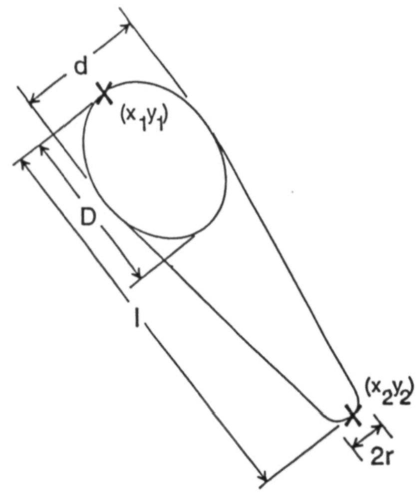

Track Selection Criteria

$d > 8\ \mu m$
$l > D + 5\ \mu m$
$r > 1\ \mu m$

Figure 35: Track selection criteria used in measurements of "energetic recoils".

for this component. At lower LETs, this assumption is probably not valid.

3.6 Charge, Range, and Directionality Measurements of Energetic Secondaries

Charge, range, and directionality distributions of energetic secondaries were measured on the top and bottom surfaces of detector layer 1C20. 1C20 was under 10.2 g/cm^2 shielding in the Earth-side stack. For this set of measurements, an "energetic secondary" is defined as a track having the following parameters: minor axis $>8\ \mu$m, track length > major axis + 5μm and tip radius $>1\ \mu$m. Figure 35 illustrates the track selection criteria. It was not possible to accurately determine a charge distribution for tracks that did not meet these selection criteria. Of the 400 tracks measured, 200 tracks were selected as "energetic", meaning that the particle had a range greater than 20 μm.

Figures 36 and 37 are photomicrographs of a stopping track focused on the post-etch

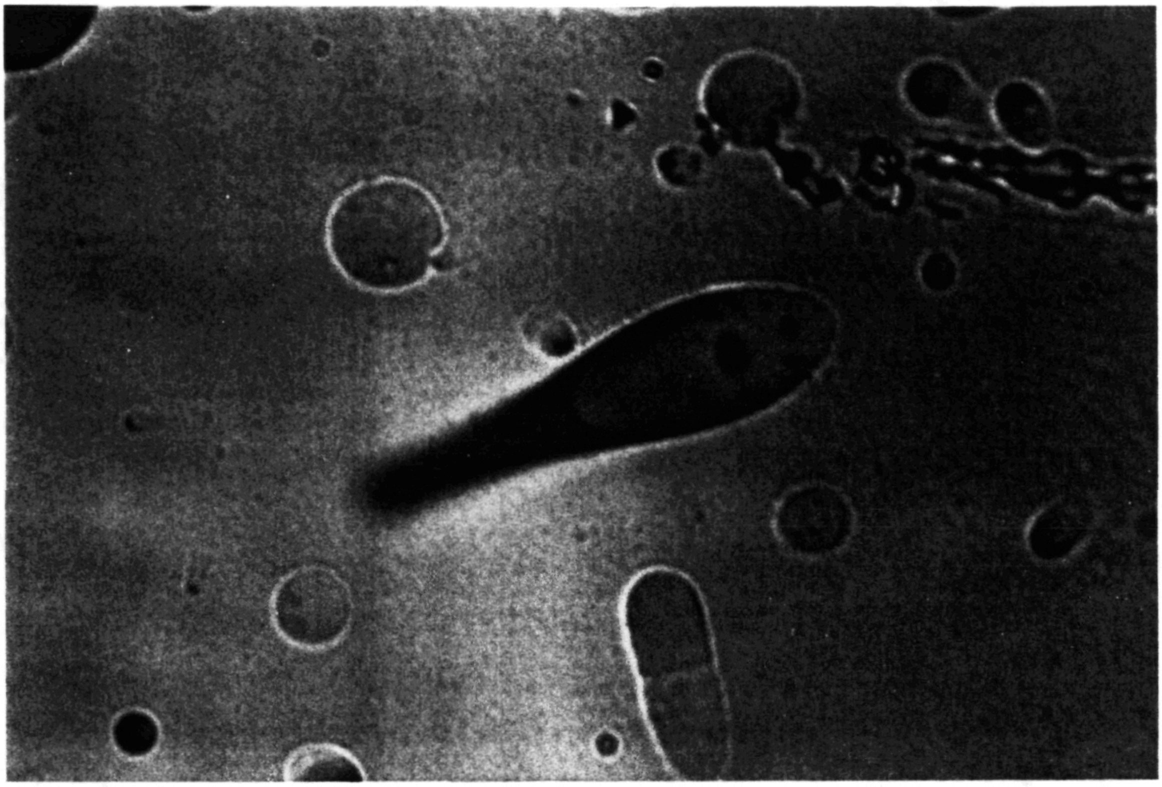

Figure 36: Photomicrograph of a stopping track focused on the post-etch detector surface. Scale is $\sim 4\mu m/cm$.

surface and the rounded tip of the track, respectively. These photomicrographs illustrated the track selection criteria used in measuring charge, energy and azimuthal angle of energetic secondaries. The major and minor axes, D and d, are measurable in Figure 36. The track length, l, is measured from the back of the track in Figure 36 to the tip of the track in Figure 37. The tip radius is half the width of the tip as seen in Figure 37. The track has a rounded tip, indicated that the particle stopped within the volume of the etch pit, at a point one tip radius behind the front of the track. The bulk etch continued after the track etch ceased, causing the tip to enlarge into a spherical end.

3.6.1 Directionality Measurements

Figures 38 and 39 are the directionality distributions of the energetic secondary tracks in the top and bottom surfaces of layer 1C20. The azimuthal angle is the angle of the projection of the particle trajectory onto the detector surface measured from an arbitrary x–axis on the detector sheet. The top surface plot shows a peak near an azimuthal angle of 180°. The

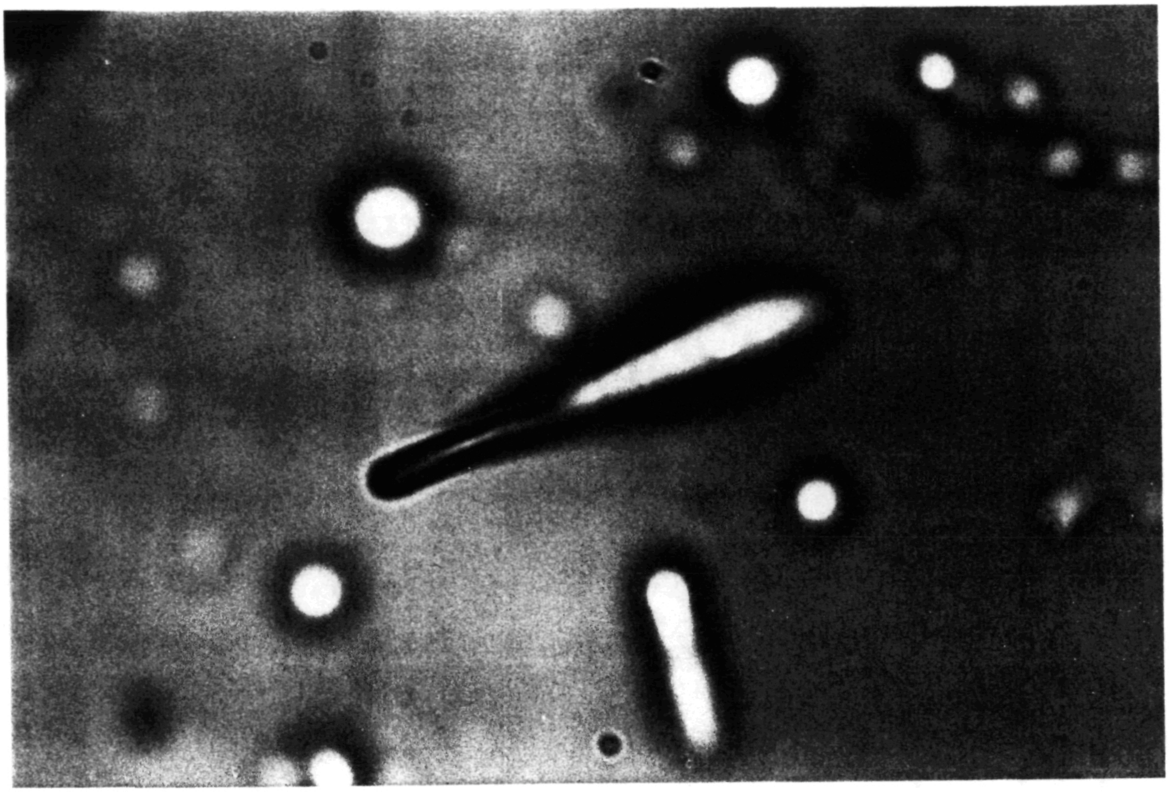

Figure 37: Photomicrograph of a stopping track focused on the tip of the track, beneath the detector surface. Scale is $\sim 4\mu m/cm$.

bottom surface plot shows a peak near 110°.

A similar study of the azimuthal angle of secondaries was carried out for CR-39 stacks exposed to a beam of 200 MeV protons at the Brookhaven Proton Linac. Figure 40 shows similar directionality distributions for detector stacks exposed at three different angles of incidence. For protons penetrating the detector at an incident angle of 90° relative to the surface, no discernible peak can be seen in the directionality distribution of secondaries. At an incident angle of 45°, a peak can be seen starting to develop near an angle of 180°. For protons at a incident angle of 0° relative to the surface of the detector, a peak in the directionality distribution is clearly seen at an azimuthal angle of 180°. This corresponds to the forward scattering direction in the detector. The comparison of these distributions with that obtained from the LDEF sample confirm the anisotropic nature of the primary proton fluence by which these energetic heavy recoils were produced in the case of the LDEF. If it is assumed that the peaks in the LDEF azimuthal angle distribution correspond to trapped particles entering the side of the Earth-side canister from the West, the arbitrary x-axis

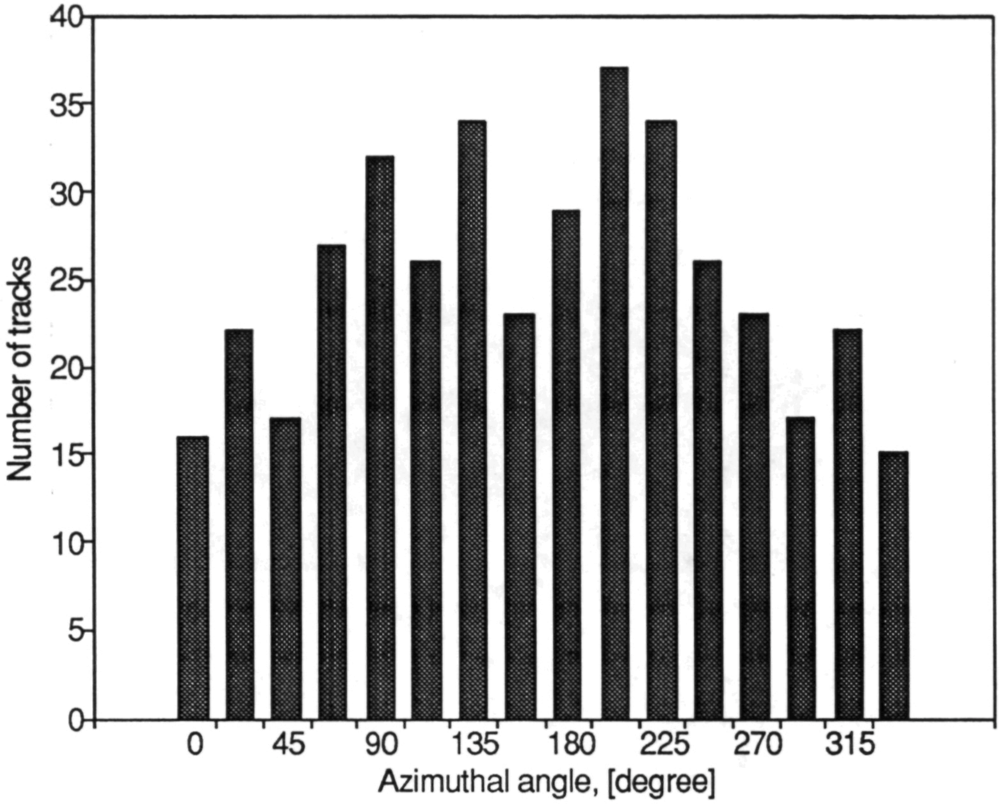

Figure 38: Angular distribution of energetic secondaries measured in the top surface of detector 1C20 on the Earth-side.

of the detector surface of the A0015 Earth-side detectors can be normalized to the West direction.

3.6.2 Charge and Range Distribution Measurements

In measuring the charge distribution of energetic recoils, an internal calibration needed to be made in order to assign a charge to a given set of measurements. For tracks measured on the bottom surface of 1C20, a detector response function was used to fit the reduced etch rate ratio $(V_r - 1)$ as a function of LET. This fit takes the form of a power function in LET:

$$V_r - 1 = a\mathrm{LET}^b, \tag{1}$$

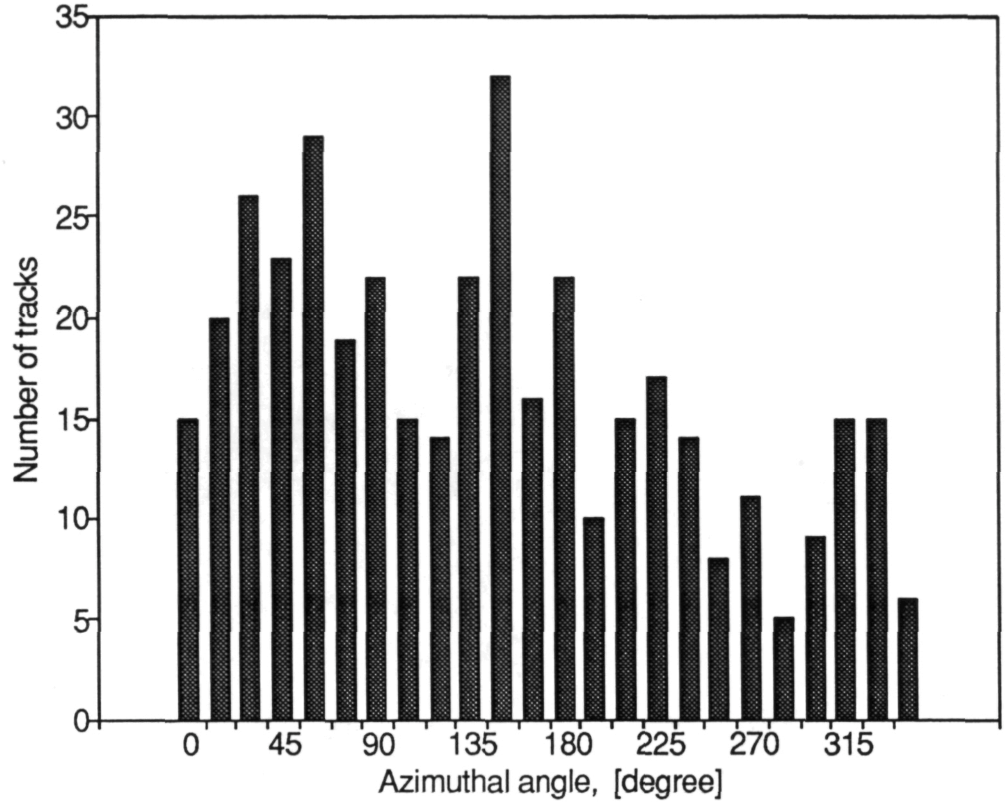

Figure 39: Angular distribution of energetic secondaries measured in the bottom surface of detector 1C20 on the west-side.

and LET is assumed to be a function of charge and residual range:

$$\mathrm{LET} = AZ^m R^n. \tag{2}$$

A, m, and n are fitted parameters from range/energy relations and are independent of the detector. a and b are the detector dependent fitted parameters. The calibration curve for 1C20 bottom surface can be seen in Figure 41 and the charge distribution can be seen in Figure 42. In doing the fit, the highest charge was assumed to be 8 corresponding to O in the CR-39.

The same form of the LET dependent response function was used for 1C20 top surface. However, the charge distribution had poor resolution and it was decided that a different form of calibration was needed. A Particle Response function was found that fit the reduced

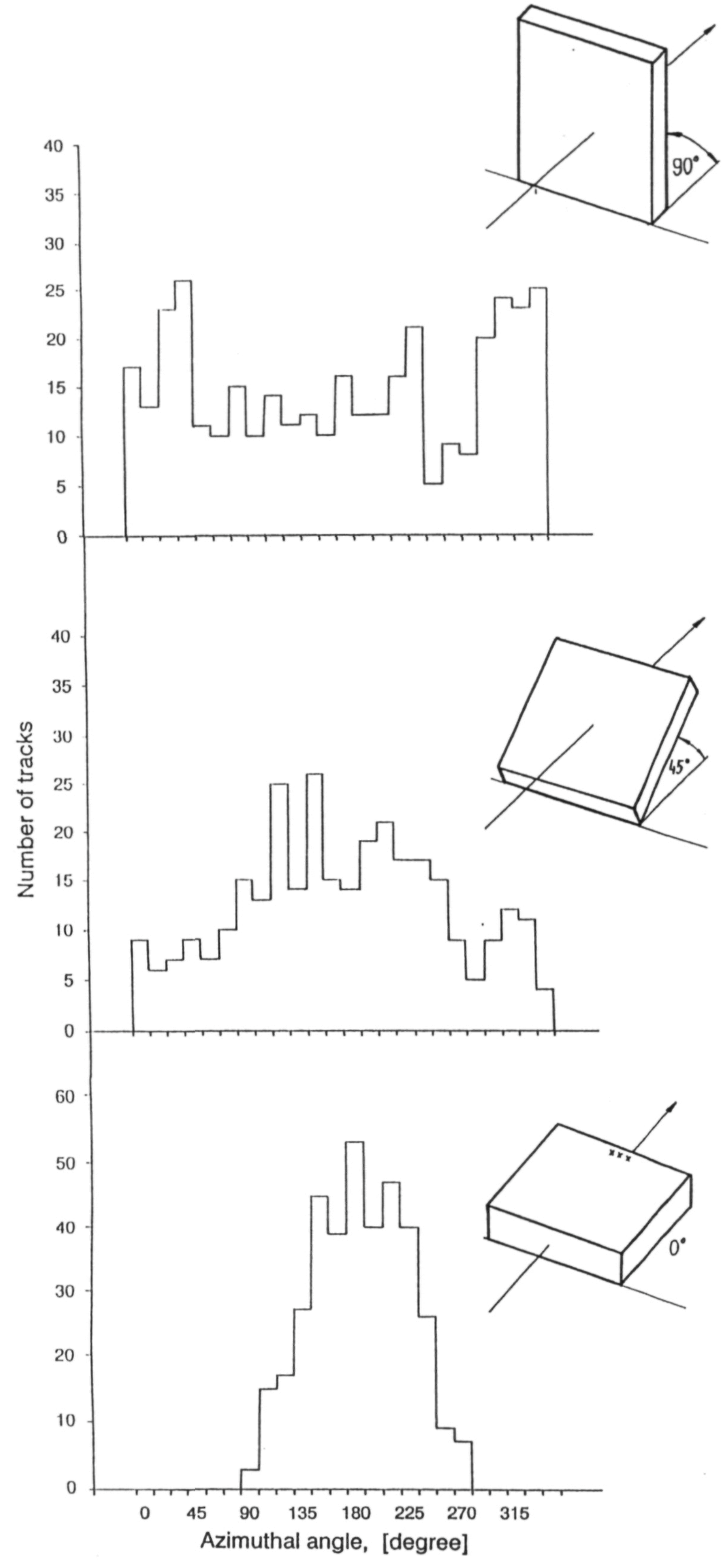

Figure 40: Angular distribution of energetic secondaries from 200 MeV protons in CR-39 at incident angles of 90°, 45°, and 0° relative to the sensitive surface of the detector.

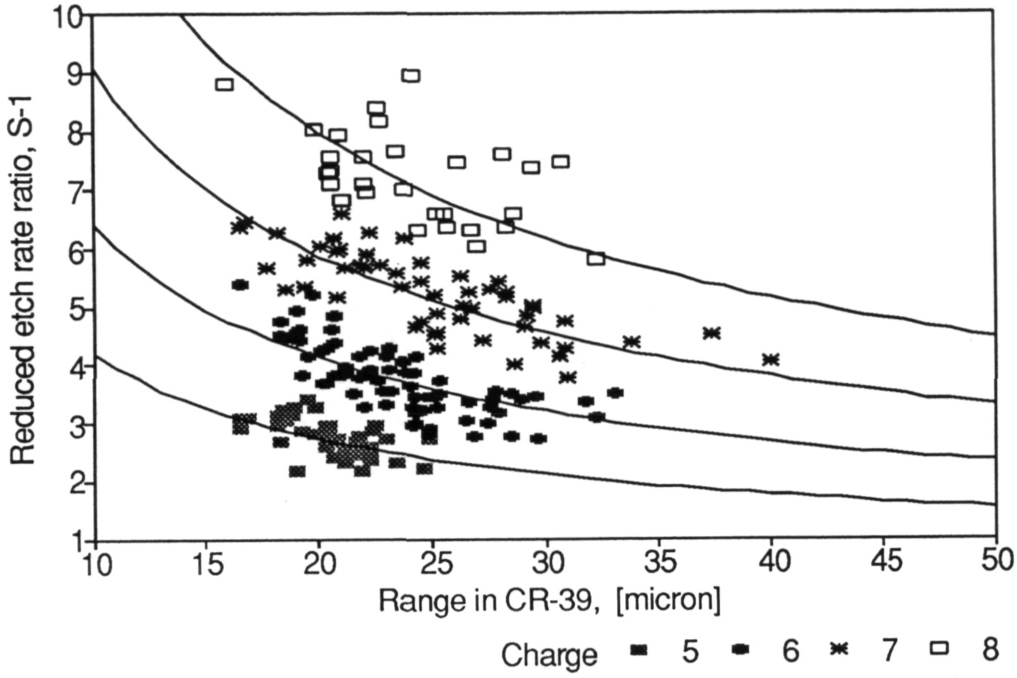

Figure 41: Internal calibration of measurements made on bottom surface of layer 1C20. Lines represent the fitted detector response function.

etch rate ratio ($V_r - 1$) as a power function in residual range and an exponential function in charge:

$$V_r - 1 = \alpha e^{\beta Z} R^{\gamma} \tag{3}$$

where α, β, and γ are fitted parameters. For this calibration fit, the lowest and highest charges were assumed to be 3 (Li) and 8 (O). Figure 43 is the calibration plot for 1C20 top surface while Figure 44 is the charge distribution for this surface. The charge resolution on the top surface is superior to that on the bottom, with peaks clearly visible for charges 3, 5, 6, and 8.

Figure 45 is a plot of dip angle versus residual range for tracks measured in 1C20 top surface. Charges are differentiated by different grey-values. It can be seen that while there is a lower limit in residual range for a particular charge, the data for each charge does not fit into a simply shaped region in the parameter space. The parameter space region for a

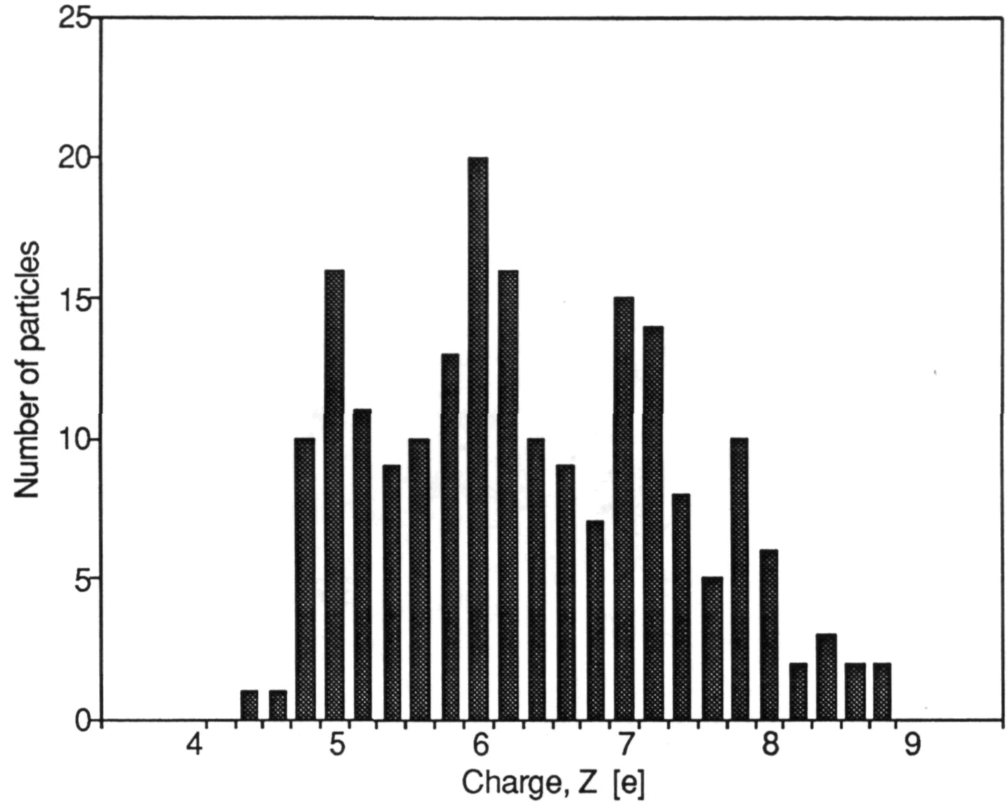

Figure 42: Charge spectrum for bottom surface of layer 1C20.

given charge overlaps that of other charges.

It was found that charge and energy spectra of selected energetic recoil particles can be measured in CR–39 samples with acceptable charged resolution in the case of the LDEF samples. Together with detailed detection efficiency calculations these spectra can be compared with theoretical results to validate model calculations.

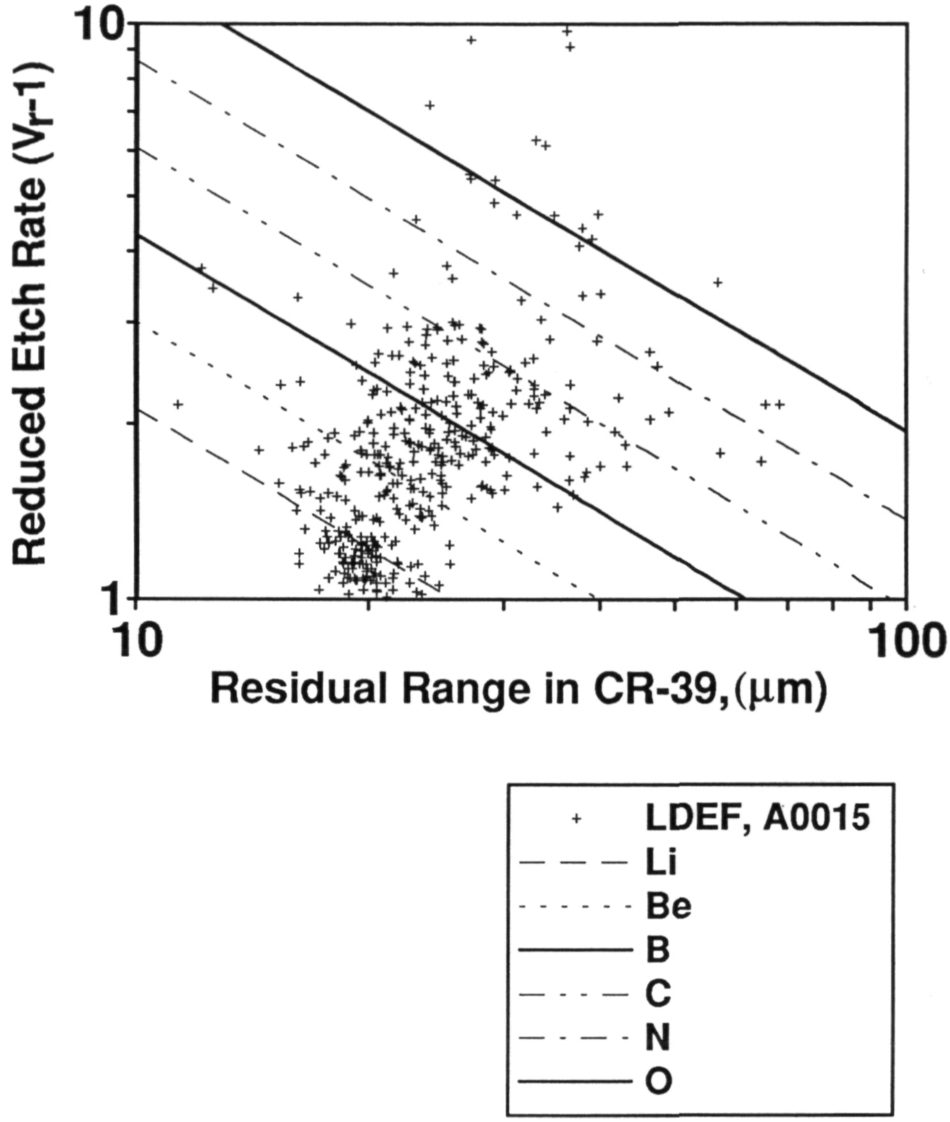

Figure 43: Internal calibration for measurements made on the top surface of detector layer 1C20. Lines are the fitted particle response function.

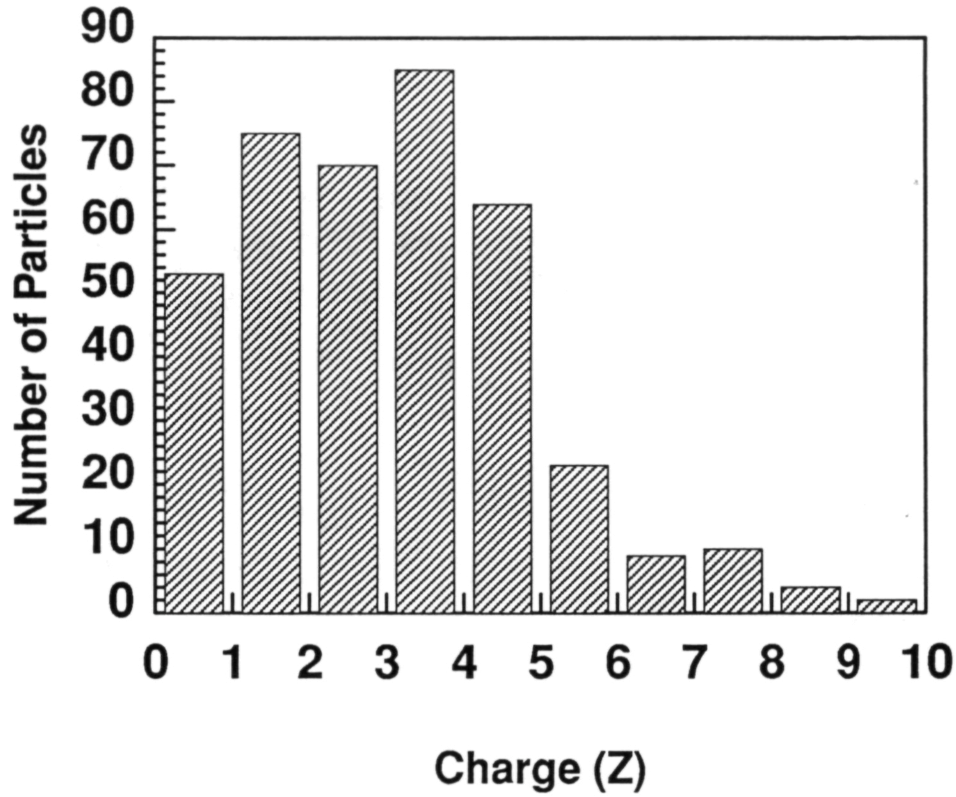

Figure 44: Charge spectrum measured on the top surface of detector 1C20.

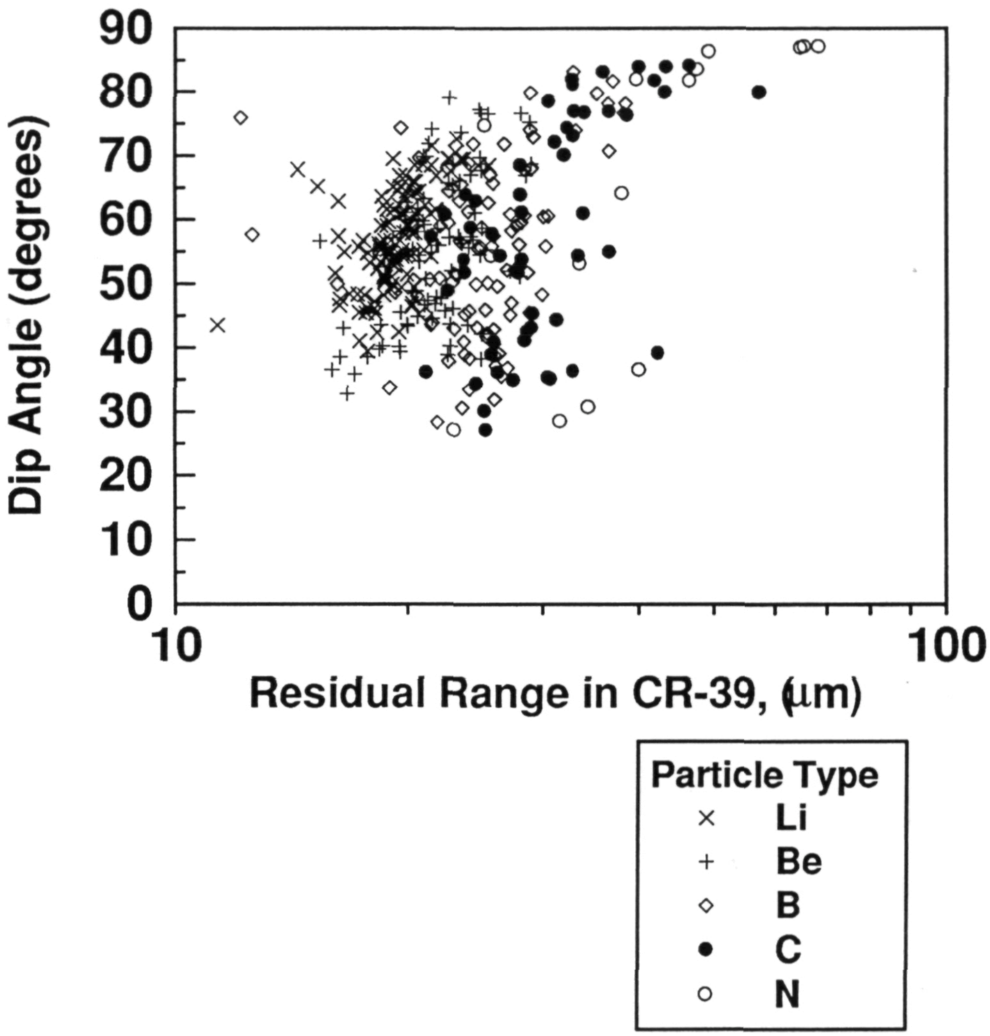

Figure 45: Dip angle as a function of residual range for tracks measured in top surface of layer 1C20. Note that the points for a given charge do not fall neatly into a particular region.

4 Absorbed Dose Measurements with TLDs

Total absorbed dose was measured in the A0015 using thermoluminescent detectors (TLDs). These measurements can be used to define the radiation environment, to measure shielding and locational effects and to map the radiation environment for LDEF type orbits (28.5° inclination, ~450 km altitude). A0015 total absorbed dose measurements are compared with calculations using modeling of the incident radiation and propagation through shielding. These calculations were made by Armstrong *et al.*[2] using the Marshall Space Flight Center Proton Transport Code, a 3-D mass model of LDEF and detailed knowledge of the experimental shielding materials. A separate set of calculations based on different models was carried out by Atwell *et al.*[4] and are included for comparison.

4.1 Response of TLDs

Thermoluminescent Detectors (TLDs) are sensitive to γ-radiation and to ionizing radiation of low LET. The efficiency of detection of TLDs decreases as LET increases. TLDs record the cumulative doses of trapped electrons and protons and the proton component in SPE and GCR with high efficiency.

TLDs used in the LDEF A0015 Experiment were type TLD-700, consisting of extruded ^{7}LiF crystal. The TLD stores the cumulative signal from all radiation sources. Upon retrieval, the TLD is placed in a reader and heated. The heated TLD emits light in proportion to the total accumulated radiation dose. The light is amplified by a photomultiplier tube and measured. Calibrations with standard sources allow the light measurements to be converted to total dose measurements.

4.2 Experiment

The A0015 experiment contained a number of TLD-700 (^{7}LiF) type TLDs manufactured by Harshaw in each of the three experiment canisters. The Earth-side and Trailing Edge sealed canisters each contained three acrylic holders, each mounted with eight TLDs. A single acrylic holder with eight TLDs was included in the Trailing Edge, non-sealed container (see Figures 2 and 3). The dimensions of the TLD chips were 0.25×0.25×0.035". The TLD

holders were 7.0×7.0 cm square and 0.062" in thickness. The TLD chips were inserted inside 0.375" diameter holes and held in place by layers of filter paper and teflon tape.

Since the LDEF mission lasted nearly six times longer than anticipated, accumulated doses were much greater than originally designed for in the experiment. Calibrations of ground control TLDs were carried out for the duration of the mission. These calibrations included accounting for the fading of stored signal in the TLDs over the length of the experiment.

4.2.1 Calibrations

Calibrations were carried out using TLDs of the same manufactured batches as those included in the flight experiment. Flight, control and calibration sets of TLDs were annealed together prior to the experiment. To duplicate the fading of stored signal taking place in the experimental TLDs in the calibration TLDs, they were exposed to a mean dose of 6.284 rad (tissue equivalent) from a standard ^{137}Cs γ-ray source at two-month intervals (33 individual exposures) during the LDEF mission. The total accumulated dose was 207.36 rad. Dose calibration factors were determined in units of rad/nC (the TLD reader results are in units of nanocoulombs).

4.2.2 TLD Fading Study

A fading study for TLD-700s was carried out to determine the magnitude of fading of accumulated signal with time. TLDs were exposed to a dose of 1053 mrad from a standard ^{137}Cs γ-ray source and then stored at a constant temperature of 38°C, the highest projected temperature that the LDEF experiments would reach and, thus a worst-case situation. Groups of six TLDs were removed at various intervals and read out. Newly irradiated TLDs of the same batch were read out simultaneously for comparison.

Figure 46 shows the ratio of stored dose to newly-exposed dose as a function of storage time. After an initial decline during the first 6 weeks, the ratio of faded to newly irradiated doses levels off. No pre-heating of the TLDs was carried out and the low temperature glow peak in LiF is included in the measurement. The initial decline comes from the decaying out of this low temperature glow peak. When pre-heating is employed (heating the TLDs

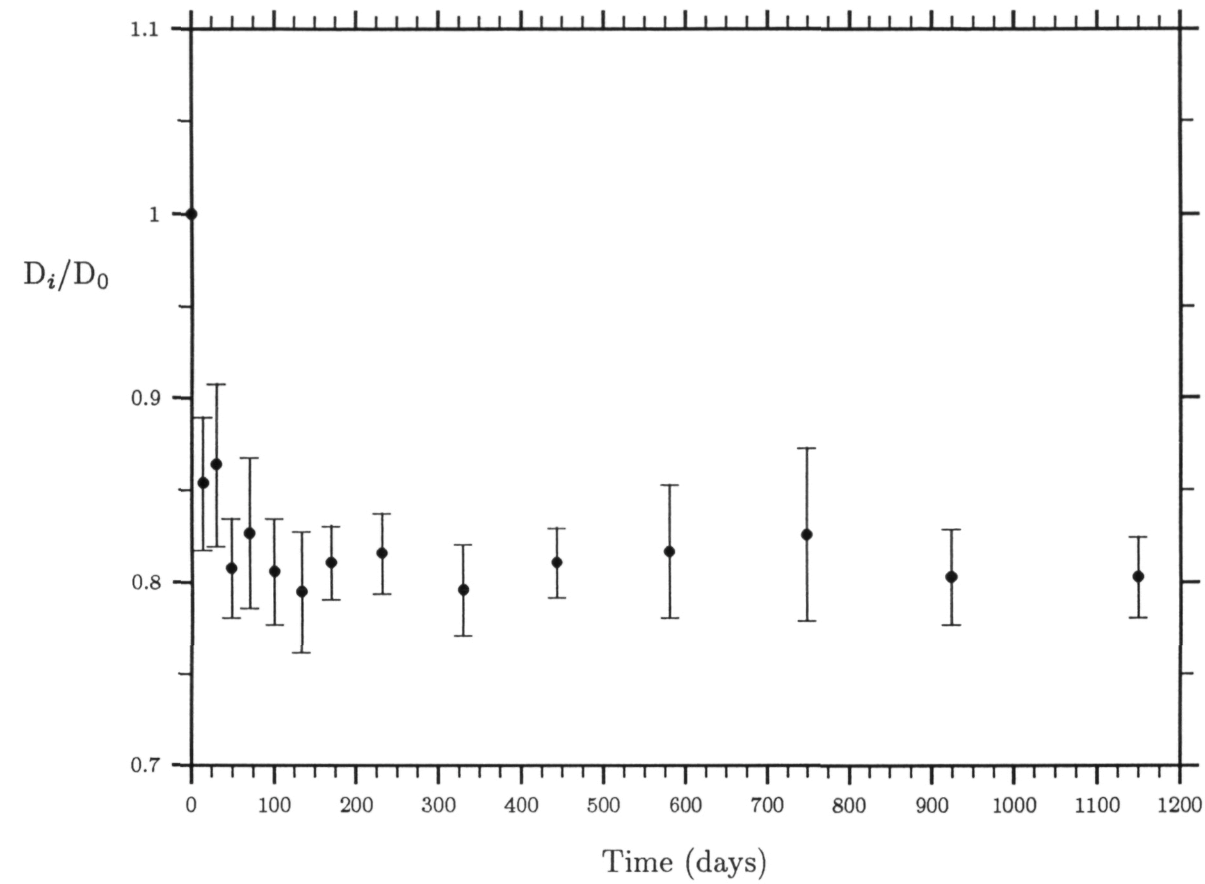

Figure 46: The fading of thermoluminescence in TLD-700 chips irradiated to 1.053 rad, then stored at 38°C, where D_i and D_0 were the doses measured on the stored TLDs and newly irradiated TLDs, respectively.

to 120°C for 10 sec, for example) the low temperature glow peak is eliminated from the measurement and the response is approximately flat from the first readout. These results indicate that compensating for fading is not a serious problem in TLD-700 at temperatures under 38°C.

4.2.3 High Dose Supralinearity

Due to the high doses accumulated in the LDEF TLDs, it was necessary to compensate for the supralinearity in the integrating picoammeter measurements. Supralinearity becomes a

significant problem at doses of 100 rad and greater[14]. Figure 47 shows a calibration to measure this effect.

4.2.4 TLD Readout

Flight, background and calibration TLDs were read out at the same time. Due to high doses accumulated during the LDEF mission, a 100/1 (nominal) neutral density filter was inserted beneath the photomultiplier tube to reduce the light transmission from the heated TLDs. The readout cycle employed was a pre-heating at 120°C for 10 sec. followed by a 7°C/sec. heating ramp to a maximum temperature of 325°C. The current output from the photomultiplier unit was integrated between 120°C and 260°C for dose determination, but glow peaks were measured up to 325°C to examine possible dose- or LET-dependent effects.

4.3 Experimental Results

4.3.1 A0015 Dose Measurements

Absorbed dose measurements in TLDs from the A0015 experiment are presented in Table 4. All the TLDs in a given holder were read out together and a mean value of dose for that holder is reported. Also shown are values of shielding of the TLD plates in each stack. In the Earth-side container, the measured dose varied from a minimum of 2.41 Gy under 1.66 g/cm^2 Al equivalent shielding to a maximum of 3.93 Gy under 1.66 g/cm^2 Al equivalent shielding. In the Trailing Edge seal canister (#2) the minimum measured dose was 3.04 Gy under 11.7 g/cm^2 and the maximum measured dose was 4.49 Gy under 3.85 g/cm^2. A dose of 3.47 Gy was measured in the Trailing edge, non-sealed canister. The shielding for this TLD set is not known. Values of uncertainty in measured doses ranged from 0.04 to 0.32 Gy. The doses measured in the Trailing Edge canister are higher due to the favorable position of this experiment with regard to the East/West trapped proton anisotropy.

4.3.2 Dose Measurements in other LDEF Experiments

Measured doses in the A0015 Biostack canisters can be compared with other dose measurements made in the Biostack experiment[23]. Table 5 shows an approximate agreement of

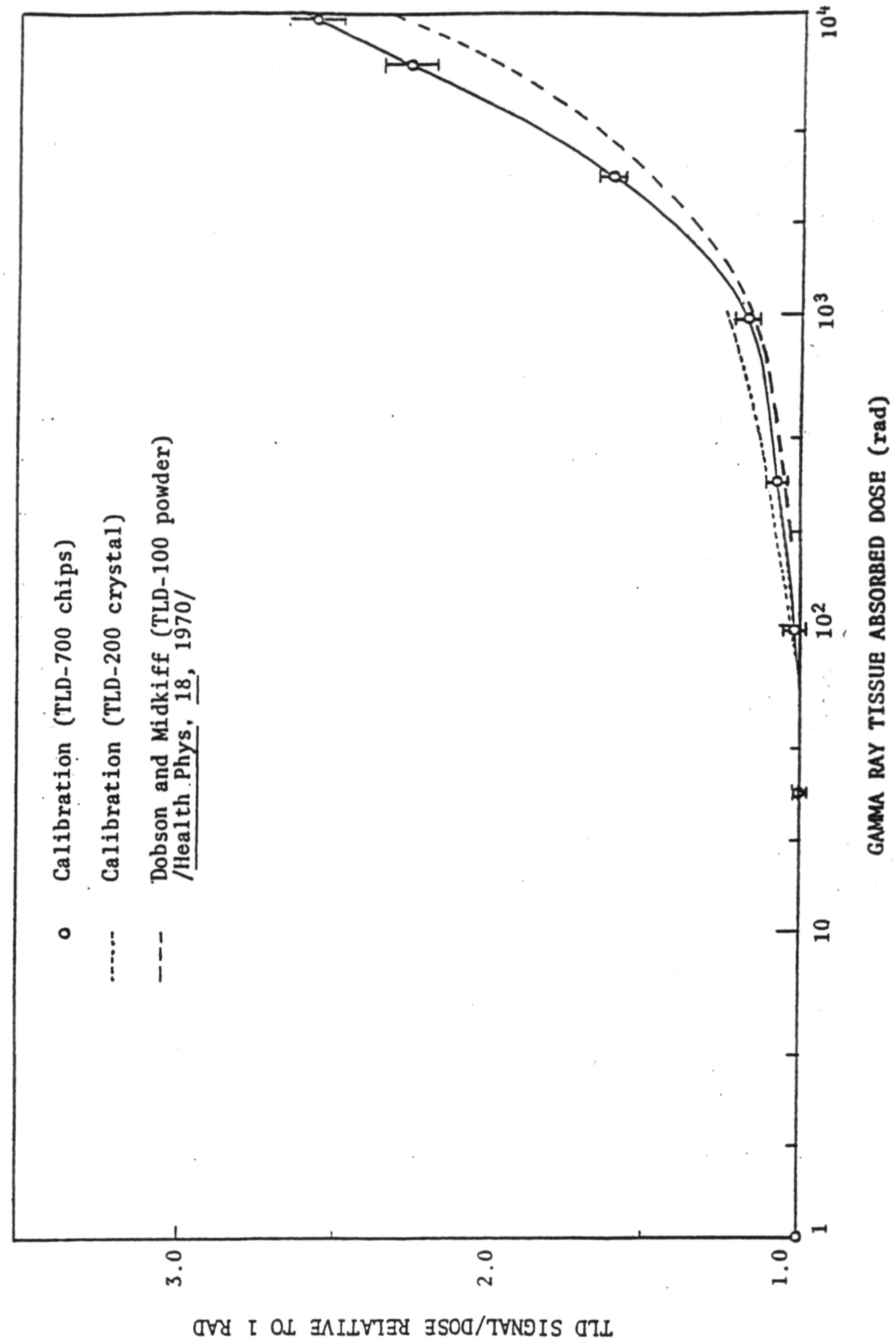

Figure 47: Calibrations of TLDs demonstrating the supralinearity at high doses.

Table 4: A0015: LDEF Absorbed Dose Measurements with TLD-700.

Canister No.*	TLD Plate No.	Tissue Absorbed Dose (Gy)	Dose Rate (mGy/d)	Al Equivalent Shielding (g/cm^2)
1	1	3.93 ± 0.08	1.86 ± 0.04	1.66
	2	2.74 ± 0.23	1.30 ± 0.11	6.23
	3	2.41 ± 0.18	1.14 ± 0.09	10.0
2	1	4.49 ± 0.11	2.12 ± 0.05	3.85
	2	3.29 ± 0.22	1.56 ± 0.10	7.83
	3	3.04 ± 0.32	1.44 ± 0.15	11.7
3	1	3.47 ± 0.22	1.64 ± 0.10	—

*Canister #1 was to Earth-side.
*Canister #2 was at the trailing edge.
*Canister #3 was vented to space and at the trailing edge.
Minimum shielding to the side (for only the detector assembly) of the individual TLDs was 2.52 to 5.31 g/cm^2 Al equivalent.
All shielding materials were converted to Al equivalent on the basis of the relative ranges of 100 MeV protons in the materials.

measured doses at the trailing edge and at the Earth end, as functions of vertical shielding thickness. Only rough agreement is expected since the measurements are from different canisters with different contents, internal geometries and horizontal distributions of TLDs.

TLDs were included in three other LDEF experiments: the P0006 LETSME, the P0004 SEEDS, and the M0004 Fiber Optics Experiment. Two types of TLD were included in the P0006 experiment, TLD-200 (CaF_2) and TLD-700 (^7LiF), both produced by Harshaw. The TLDs were arrayed inside five acrylic holders which, in turn, were distributed throughout the main stack of the P0006 experiment. The TLD holders were 4.5×4.5×0.062". As in the A0015 experiment, the TLD chips were inserted inside 0.375" diameter holes and held in place by layers of filter paper and teflon tape. TLD-200 and -700 were distributed alternately in the acrylic holder.

The TLD dose measurements are given in Table 6. Mission doses are seen to vary between 266 rad (maximum shielding) and 648 rad (minimum shielding). Also included in

Table 5: Comparison of LDEF A0015 Absorbed Doses from TLD-700.

Location	Laboratory	Tissue Absorbed Dose (Gy)	Vertical Shielding (g/cm^2)
Earth-side	ERI*	3.93 ± 0.08	1.66
	DLR**	3.79 ± 0.17	0.7
		3.89 ± 0.19	0.7
	ERI	2.41 ± 0.18	10.0
	DLR	2.22 ± 0.30	12.0
		1.99 ± 0.25	14.0
Trailing Edge	ERI	4.49 ± 0.11	3.85
	DLR	4.73 ± 0.26	0.7
		3.88 ± 0.64	2.0
	ERI	3.04 ± 0.32	12.0
	DLR	2.38 ± 0.22	12.0
		2.46 ± 0.26	12.0

*Eril Research, Inc.
**DLR Institut für Flugmedizin[23]

Table 6 are the measured shielding thicknesses of each TLD holder in the P0006 main stack. Within the statistical uncertainty (σ) of the measurements, the TLD-200 and -700 chips gave equal readings. The standard deviations of measurement (σ) of Plates 3, 4, and 5 were not calculated directly from the spread in the individual TLD readings since their differences also included real dose differences. At the larger depths in the stack, TLDs near the sides of the canister were less shielded than those in the middle. There was a non-uniform dose across these plates. The σs were scaled from Plates 1 and 2. The minimum doses of Plates 3, 4, and 5 were about 303, 242 and 227 rad, respectively.

In the P0004 experiment, small plastic holders containing four TLD-700 chips were placed in six Al canisters carrying seeds (five canisters of tomato seeds, one canister with a variety of seeds). The canister interiors were 31 cm in diameter with average depths of about 12.5 cm, and they had rounded lids. They were arrayed, 3×2, in Tray F2. The TLDs were centered

Table 6: Dose measurements from P0006 TLDs.

TLD Plate No.	TLD Type	Tissue Absorbed Dose (rad)	Dose Rate (mrad/d)	Al Equiv. Shielding (g/cm^2)
1	200	628 ± 21	297 ± 10	0.48
	700	648 ± 24	307 ± 11	
2	200	392 ± 21	185 ± 10	4.10
	700	392 ± 21	185 ± 10	
3	200	320 ± 15	151 ± 7	8.34
	700	316 ± 15	149 ± 7	
4	200	282 ± 13	133 ± 6	12.2
	700	276 ± 13	131 ± 6	
5	200	266 ± 12	129 ± 6	15.4
	700	266 ± 12	126 ± 6	

The doses were approximately uniform over Plates 1 and 2 and were non-uniform over Plates 3, 4 and 5 (due to lesser shielding through the sides than through the top for the deeper TLD plates). The minimum shielding to the side (canister only) for the individual TLDs was 0.64 g/cm^2 Al plus 1.06 to 4.84 g/cm^2 plastic.

in the canisters, either at the top or bottom or at a position roughly centered within the seeds.

The M0004 experiment included two small Al canisters (interior dimensions of 4.8 cm diameter and 1.3 cm depth) containing two TLD plates each, which were separated by plastic stacks. Each plate contained either 3 or 4 TLD-700 chips. The canisters were mounted, canted 90° to each other, next to other flight components of the experiment in Tray F8 near the leading edge.

The dose measurements from these two experiments are given in Tables 7, and 8. The highest doses are seen to be near the trailing edge under thin shielding. Doses are lower by more than a factor of two near the leading edge, taking shielding into account, and doses at the Earth end are intermediate between the leading and trailing edges. This distribution of doses is due to trapped proton anisotropy combined with the shielding from the LDEF vehicle, which together yield a dose maximum at the western side of the vehicle.

Table 7: P0004: LDEF Absorbed Dose Measurements with TLD-700.

Detector No.	Canister No.	Tissue Absorbed Dose (Gy)	Dose Rate (mGy/d)	Al Equivalent Shielding (g/cm^2)
1	6	6.64 ± 0.29	3.14 ± 0.14	0.48
2	6	2.91 ± 0.07	1.38 ± 0.03	11.1
3	6	3.88 ± 0.22	1.83 ± 0.10	$\sim$5
4	4	3.12 ± 0.08	1.48 ± 0.04	6.11
5	2	3.05 ± 0.08	1.44 ± 0.04	6.10
6	5	3.09 ± 0.08	1.46 ± 0.04	6.10
7	7	2.93 ± 0.10	1.39 ± 0.05	6.10
8	3	3.15 ± 0.08	1.49 ± 0.05	6.10
GC1		$3.2 \pm 0.2 \times 10^{-3}$	$1.3 \times 10^{-3*}$	
GC2		$3.2 \pm 0.2 \times 10^{-3}$	$1.3 \times 10^{-3*}$	

*For a total detector assembly time of 2418 days. The flight detectors are averaged over the LDEF orbital duration of 2115 days.
The minimum shielding to the side (for only the detector assembly) of the individual TLDs was $\sim$12.4 g/cm^2 Al equivalent. All shielding was converted to Al equivalent on the basis of the relative ranges of 100 MeV protons in the materials. The proton range in the seed was assumed to be equal (in units of g/cm^2) to that of polycarbonate plastic.

4.4 Comparison of Model Calculations with Measured Doses

Comparisons of calculations with measured doses for A0015, P0006, P0004, and M0004 experiments are summarized in Table 9. Calculations of absorbed dose on LDEF were performed by Armstrong and Colborn[2]. They are based on the calculations of Watts[26] for the trapped proton exposure, a detailed three dimensional geometry/mass model developed by Colborn and Armstrong[13] and the transport code of Burrell[12]. The proton exposure model is based on the AP8 omnidirectional proton flux model[24]. Atmospheric height, solar cycle information and a model of the trapped proton anisotropy were included in the calculations.

A second set of calculations were made by Atwell, Badhwar, Hardy and Weyland[4] at JSC. These are considered to be preliminary calculations. The proton flux is based

Table 8: M0004: LDEF Absorbed Dose Measurements with TLD-700.

Detector No.	TLD Plate No.	Tissue Absorbed Dose (Gy)	Dose Rate (mGy/d)	Al Equivalent Shielding (g/cm^2)
1	1	2.10 $\pm$ 0.13	0.99 $\pm$ 0.06	2.90
	2	2.37 $\pm$ 0.10	1.12 $\pm$ 0.05	1.37
2	1	2.19 $\pm$ 0.12	1.04 $\pm$ 0.06	2.90
	2	2.58 $\pm$ 0.09	1.22 $\pm$ 0.04	1.37
3(GC)	1	2.9 $\pm$ 0.2 $\times$ 10^{-3}	1.3 $\pm$ 0.1 $\times$ 10^{-3*}	
	2	3.2 $\pm$ 0.2 $\times$ 10^{-3}	1.4 $\pm$ 0.1 $\times$ 10^{-3*}	
4(GC)	1	2.9 $\pm$ 0.2 $\times$ 10^{-3}	1.3 $\pm$ 0.1 $\times$ 10^{-3*}	
	2	2.9 $\pm$ 0.2 $\times$ 10^{-3}	1.3 $\pm$ 0.1 $\times$ 10^{-3*}	

*For a total detector assembly time of 2271 days. The flight detectors are averaged over the LDEF orbital duration of 2115 days.
All shielding materials were converted to Al equivalent on the basis of the relative ranges of 100 MeV protons in the materials.

on the AP8 omnidirectional proton flux model[24] and a vector flux model of Kern[19]. Atmospheric scale height and solar cycle were modeled, but the trapped proton anisotropy was not included in the calculations. A simple mass model of the LDEF was used to model the distribution of shielding.

Figure 48 is a comparison of total absorbed dose measurements in TLDs from this laboratory (ERI) and DLR and with the calculations of Armstrong and Atwell. There is close agreement between the two sets of measurements. The Atwell calculations lie quite close to the DLR measurements, but fall below the ERI measurements while Armstrong's calculations fall below both sets of measurements.

Figure 49 is a comparison of TLD measurements and calculations of absorbed dose in the P0006 experiment. Both sets of model calculations lie below measured values. The largest discrepancy is for the least shielded point ($\sim$0.5 g/cm^2) where the calculations fall below measurements by nearly a factor of two. Also plotted in Figure 49 are the pre-recovery estimates of total absorbed dose using planar and spherical geometry models. The spherical

Table 9: LDEF Absorbed Dose Calculations of Armstrong *et al.*: Comparison with TLD Measurements.

	Detector	Location	Shielding Min. Al. Equiv. (g/cm^2)	Absorbed Dose in Tissue (cGy) Measured	Calculated	Ratio: Calculated/ Measured
Exp. P0004	#1	Can. #6	0.48	664 ± 29	338	0.51
	#3	Can. #6	~5	388 ± 22	170(a)	0.44
	#4	Can. #4	6.1	312 ± 8	172	0.55
Tray F2	#5	Can. #2	6.1	305 ± 8	170	0.56
Near Trailing	#6	Can. #5	6.1	309 ± 8	172	0.56
Edge	#7	Can. #7	6.1	293 ± 10	167	0.57
	#8	Can. #3	6.1	315 ± 8	172	0.55
	#2	Can. #6	11.1	291 ± 7	141	0.48
Exp. P0006	TLD Plate #1		0.48	630(b)	327	0.52
	TLD Plate #2		4.1	367	182	0.50
Tray F2	TLD Plate #3		8.3	275	138	0.50
Near Trailing	TLD Plate #4		12.2	218	118	0.54
Edge	TLD Plate #5		15.4	208	110	0.53
Exp. M0004	#1	Plate #2	1.37	237 ± 10	198	0.84
Tray F8	#1	Plate #1	2.90	210 ± 13	168	0.80
Near Leading	#2	Plate #2	1.37	258 ± 9	207	0.80
Edge	#2	Plate #1	2.90	219 ± 12	180	0.82
Exp. A0015	TLD Plate #1		1.66	393 ± 8	205(c)	0.52
Tray G2	TLD Plate #2		6.23	274 ± 23	127	0.46
Earth End	TLD Plate #3		10	241 ± 18	113	0.47

(a) Calculated at 6.1 g/cm^2 depth.
(b) Measured values at middle TLD plate (i.e. minimum TLD value in plate), corresponding to location used in calculations.
(c) Detailed geometry description of Tray G2 not included in calculations.

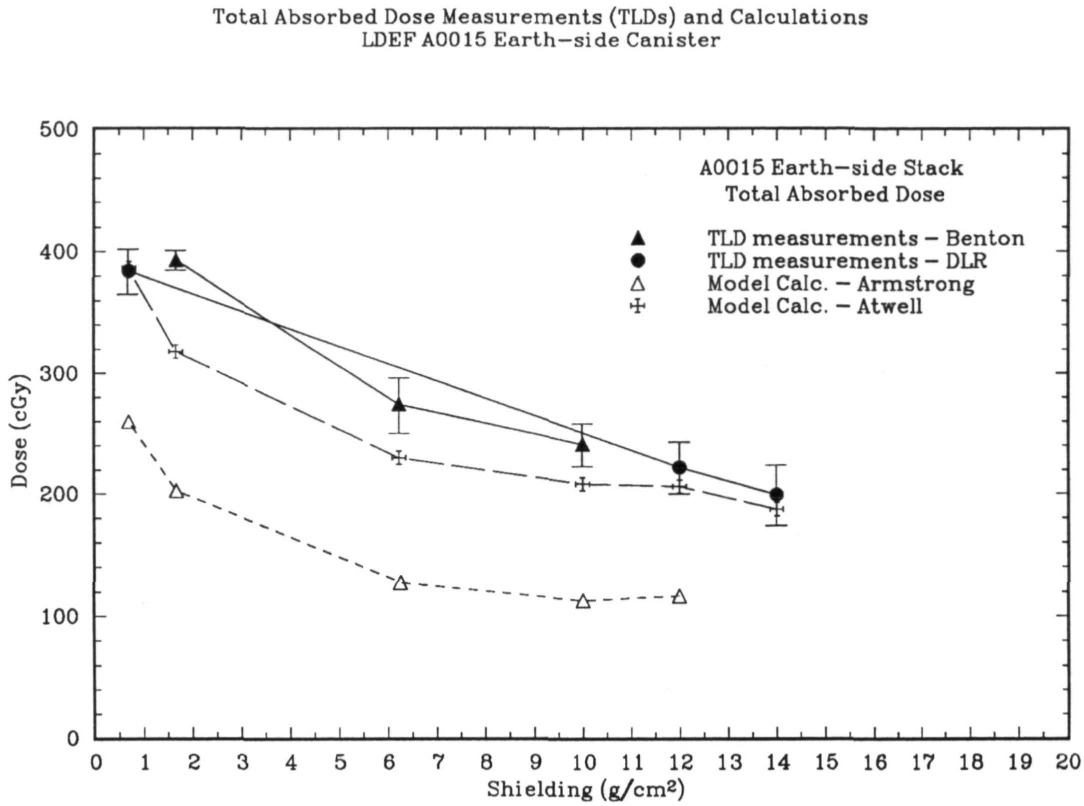

Figure 48: A0015 Total Absorbed Dose: comparison of measurements and calculations.

geometry model provides the closest agreement with measured values. Figure 50 compares measured absorbed doses from TLDs with calculations for the P0004 experiment as a function of shielding depth. Like Figure 49, both sets of calculations fall below the measured values and the biggest difference is for the least shielded point.

Figure 51 shows a comparison of dose measured in TLDs with calculations as a function of shielding for the M0004 experiment on the leading (East) edge of LDEF. The smaller measured and calculated doses of M0004 as compared with P0006 and P0004 show the effect of the East/West trapped proton anisotropy. The largest difference can be seen for the low shielding point (0.5–1.0 g/cm^2) where the dose on the West side exceeds that of the East side by about a factor of three. The calculations of Armstrong show a $\sim$1.5 times greater dose on the West side as compared to the East side under $\sim$1.5 g/cm^2. Atwell's calculations show little difference between doses (300 cGy Earth-side, 350 cGy West side) between East and West due to the fact that the East/West proton anisotropy was not accounted for in

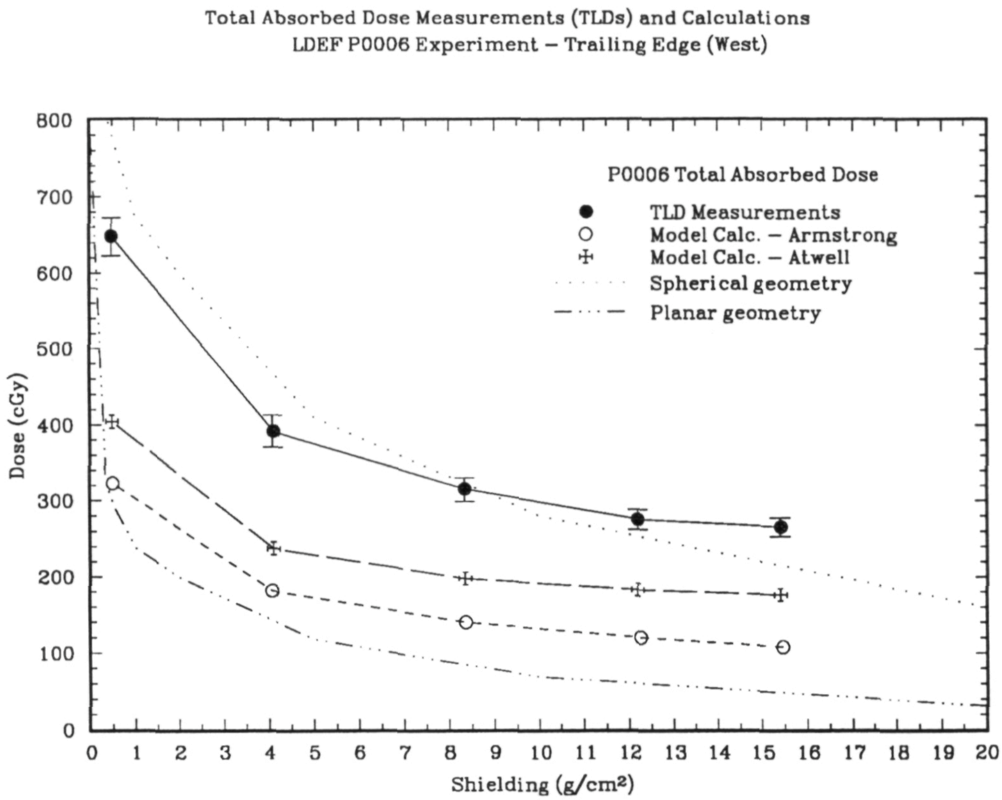

Figure 49: P0006 Total Absorbed Dose: comparison of measurements and calculations.

the calculations.

The calculations of Armstrong are consistently lower than measurement of dose by approximately a factor of two. This would seem to indicate that there is a systematic omission in the model. The calculations of Atwell fall on both sides of the measurements. There is close agreement with measured doses on the Earth side. Atwell's calculations exceed the measurements of the East side and fall below measurements made on the West side. One difference between the two sets of calculations is the vector flux model used. The Armstrong calculations are based on a vector flux model of Watts[26] and a comparatively high atmospheric scale height. The Atwell calculations are based on a newer vector flux model being developed by Kern[19] at JSC which uses a lower atmospheric scale height. Discrepancy between measurements and Armstrong's calculations might also be due to inadequacies in the trapped proton anisotropy model. While a ratio of 1.5 was calculated between doses on the West and East sides and agreed well with the measured ratio, the measured ratio only

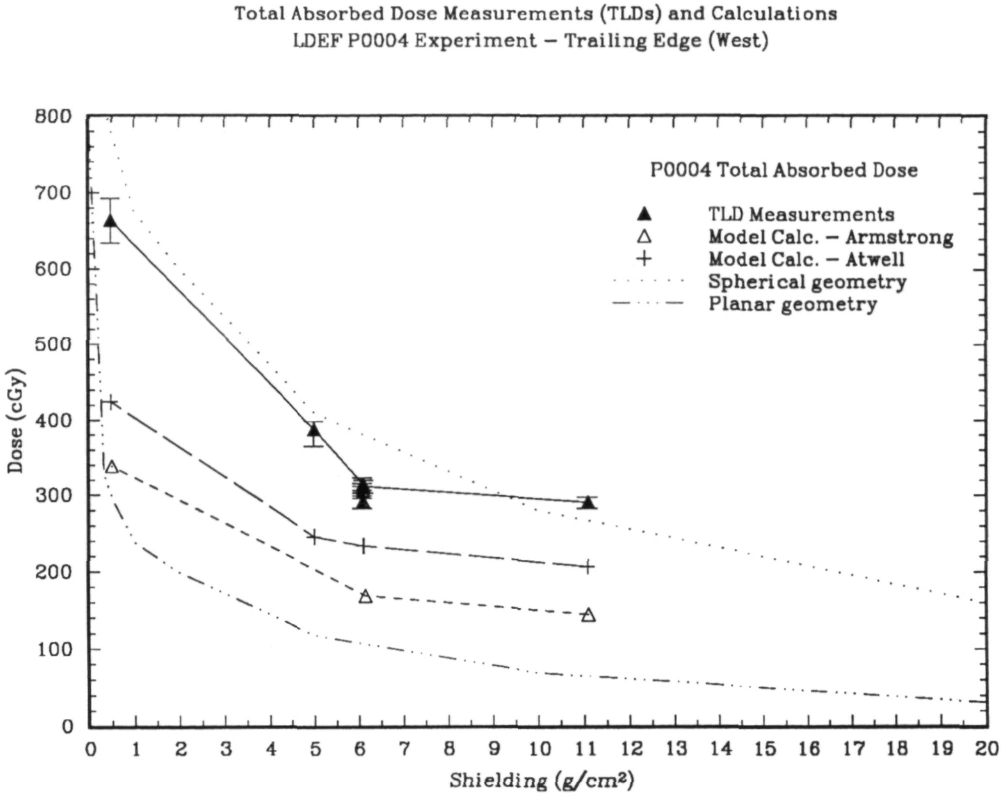

Figure 50: P0004 Total Absorbed Dose: comparison of measurements and calculations.

included the shielding of the experiment itself and not the shielding of the entire spacecraft, making the validity of this comparison questionable. The ratio of measurements of induced radioactivity on the West and East sides of the spacecraft is closer to a factor of three. Refinements are expected to be made to both models and new sets of calculations will soon be published.

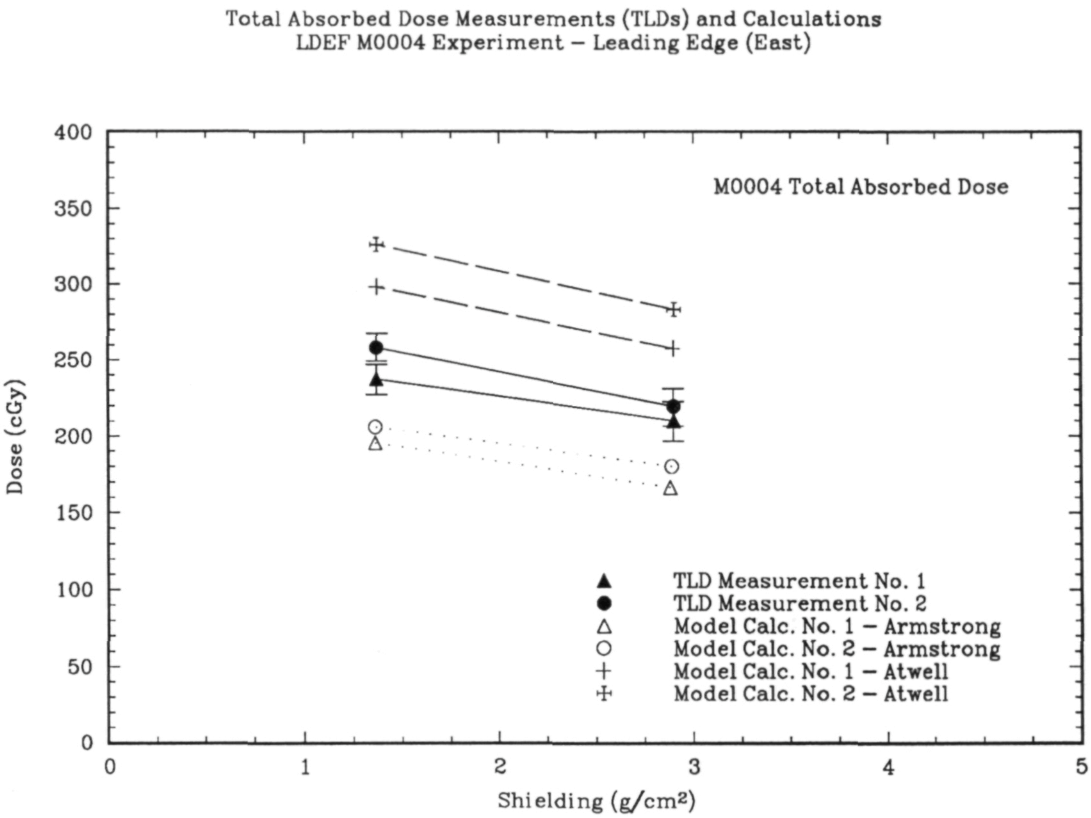

Figure 51: M0004 Total Absorbed Dose: comparison of measurements and calculations.

5 Thermal and Resonance Neutron Measurements with ^{6}LiF/CR-39 Detectors

5.1 Experiment

On A0015 there were two sets of ^{6}LiF/CR-39 low energy neutron detectors. The first set was in Canister #1 (Earth-side) under 12.3 g/cm^2 Al equivalent shielding. The second set was in Canister #2 (Trailing Edge) under 2.00 g/cm^2 Al equivalent shielding. Each set included two detectors each with and without Gd foil absorbers (0.00635 cm in thickness).

The ^{6}LiF foils were discs of 1.6 cm diameter with 4.5 mg/cm^2 of ^{6}LiF on a heavy paper backing. CR-39 PNTD discs were placed in direct contact with the ^{6}LiF. When the nuclear interaction ^{6}Li(n,α)T occurred the ^{6}LiF became a radiator foil and α-particles formed latent tracks in the CR-39. In the detectors with Gd foil covers the thermal neutrons were absorbed before reaching the ^{6}Li and the detector was sensitive to neutrons above an effective energy of 0.2 eV. The composite detector response can therefore be separated into thermal and resonance contributions.

5.2 Processing

After post-flight disassembly the CR-39 discs were processed in 6.25 *N* NaOH solution at 70°C for 1.25 hr to enlarge the latent α-particle tracks. Because of the high track densities accumulated in the CR-39 during the long LDEF exposure period, the processing time was only 25% of the standard processing time for space flights of a few days. A longer processing time would have resulted in overlapping tracks and difficulty in counting of track densities.

5.3 Readout

The α-particle track densities in the surfaces of the CR-39 discs were counted at 430× under an optical microscope. The power was increased from the standard 200× to compensate for the small track sizes. The short stopping α-particle tracks were discriminated from the greater part of the background tracks on the basis of size and geometry. For those background tracks similar to the stopping α tracks, the backsides of the CR-39 discs were

Table 10: Track Densities from the ^{6}LiF/CR-39 Detectors on A0015 (Background Subtracted).

Detector	Position	Gd Foil	Track Density (cm^{-2}
1	upper left	no	2.86 ± 0.11 × 10^4
	lower right	no	2.98 ± 0.11 × 10^4
	upper right	yes	1.25 ± 0.08 × 10^4
	lower left	yes	1.22 ± 0.08 × 10^4
2	upper left	no	3.05 ± 0.11 × 10^4
	lower right	no	2.97 ± 0.10 × 10^4
	upper right	yes	0.86 ± 0.06 × 10^4
	lower left	yes	0.86 ± 0.07 × 10^4

Detector	Neutron Energy Range	Average Track Density (cm^{-2})
1	<0.2 eV	1.69 ± 0.10 × 10^4
	0.2 eV – 1 MeV	1.24 ± 0.06 × 10^4
2	<0.2 eV	2.15 ± 0.09 × 10^4
	0.2 eV – 1 MeV	0.86 ± 0.05 × 10^4

counted. The background tracks consisted of GCRs, trapped particles and their secondaries plus ^{3}H nuclei from the ^{6}Li(n,α)T reaction. The track densities (background subtracted) are given in Table 10. The standard deviations given derive from counting statistics.

5.4 Results

The track densities were converted to neutron fluences and dose equivalents using calibrations determined by methods previously developed[10]. Neutrons are assumed to be well thermalized below 0.2 eV (the effective Gd foil absorption cutoff) and to follow a moderated neutron E_n^{-1} energy spectrum between 0.2 eV and 1 MeV. Dose equivalents were determined from the fluences using conversion factors from NCRP (1971) which incorporate QF values of 2 for thermal neutrons and 6.4 for resonance neutrons. The results are given in Table 11.

Table 11: Measured Low Energy Neutron Fluences and Dose Equivalents from A0015.

Detector	Position	Al Equivalent Shielding (g/cm^2)	Neutron Energy Range	Neutron Fluence (cm^{-2})
1	Earth-side	12.3	<0.2 eV	$3.45 \pm 0.20 \times 10^6$
			0.2 eV – 1 MeV	$4.84 \pm 0.23 \times 10^7$
2	Trailing Edge	2.00	<0.2 eV	$4.39 \pm 0.18 \times 10^6$
			0.2 eV – 1 MeV	$3.35 \pm 0.20 \times 10^7$

Detector	Neutron Energy Range	Dose Equivalent (mrem)	Dose Equivalent Rate (mrem/d)
1	<0.2 eV	3.50 ± 0.20	0.0017
	0.2 eV – 1 MeV	238 ± 11	0.113
2	<0.2 eV	4.46 ± 0.18	0.0021
	0.2 eV – 1 MeV	165 ± 10	0.078

Note: Standard deviations in the table are from counting statistics only. The necessary assumptions regarding neutron spectra in the thermal and resonance regions introduce errors which can only be estimated. The accuracy in thermal (<0.2 eV) region is estimated to be ±20%. The accuracy in the resonance (0.2 eV – 1 MeV) region is estimated to be ±50%.

6 Fission Foil Measurements of Neutron and Proton Fluences

6.1 Experiment

A0015 Canisters #1 and #2 on the Earth-side and Trailing Edge of LDEF, respectively, each contained a selection of fission foil detectors (FFDs). The FFDs consist of heavy metal foils in contact with muscovite mica films. The foil types included ^{181}Ta, ^{209}Bi, ^{232}Th and ^{238}U.

The shielding of the FFDs is given in Table 12. The aluminum equivalent values are given but most of the volume of the canisters was filled with plastics (polycarbonate, acrylic and CR-39). This has a significant effect on the scattering of neutrons in the vicinities of the FFDs. FFDs are at one end of the detector arrays and, from the shielding in Table 12, it is seen that the FFDs were oriented toward space in Canister #2 (trailing edge) but away from space in Canister #1 (Earth-side). There were 6-10 cm^2 of each of the four foil types in each canister.

After the return of LDEF, the FFDs were removed from the canisters and disassembled. The mica films were processed in 50% HF solution at 21°C for 1.25 hr in order to delineate the fission fragment tracks for counting. The mica was given a pre-flight processing for 3 hr to enlarge the fossil tracks. The films were then counted under an optical microscope at 200×.

6.2 Background

Heavy metal nuclei have significant cross sections for fission when irradiated with neutrons and protons. Each isotope is characterized by threshold energies for the fission reactions and particular energy-dependent cross sections. In the FFDs, fission fragments produced by the reactions are emitted from the foils and create latent particle tracks in the adjacent mica films. When the films are processed, surface tracks are formed which can be optically counted. The track densities are indications of the fluences and spectra of neutrons and/or protons.

Table 12: Shielding of LDEF A0015 Fission Foil Detectors.

Canister	Plate	Min.Vertical Shielding (g/cm^2) Al Equivalent	Min.-Max. Horizontal Shielding (g/cm^2) Al Equivalent
#1	^{209}Bi	12.7	2.75 - 10.0
	^{181}Ta	13.1	2.70 - 22.6
	^{232}Th	13.4	1.87 - 8.92
	^{238}U	13.6	1.87 - 13.4
#2	^{209}Bi	1.65	2.75 - 10.0
	^{181}Ta	1.42	2.70 - 22.6
	^{232}Th	1.20	1.87 - 8.92
	^{238}U	0.97	1.87 - 13.4

Canister #1 was located on the Earth-side end of LDEF and Canister #2 near the trailing edge (Tray C2).

FFDs have previously been used for spaceflight measurements[9, 5, 10, 16, 15]. In cases where the proton contribution to track densities can be subtracted out, the FFDs can be used as high energy (>1 MeV) neutron dosimeters. These detectors have been calibrated with neutrons of energies up to ~15 MeV and found to have efficiencies $\epsilon = 1.16 \times 10^{-5}$ tracks/neutron barn[22]. More recently, calibrations have been performed with high energy protons. At high energies, either proton or neutron calibrations are sufficient since the cross section data, plotted in Figure 52[20, 27, 25], show that the proton and neutron fission cross sections are approximately equal.

Detector efficiencies, plotted in Figure 53, have been found for the four FFD types by combining low energy neutron and high energy proton calibrations with the published fission cross sections to cover the energy region from 1 MeV to 100 GeV. Armstrong and Colborn[3] have shown that the energy range of interest in space applications extends to 100 GeV for proton/neutron spectra.

The FFD efficiencies $\epsilon(E)$, together with calculated proton or neutron energy spectra,

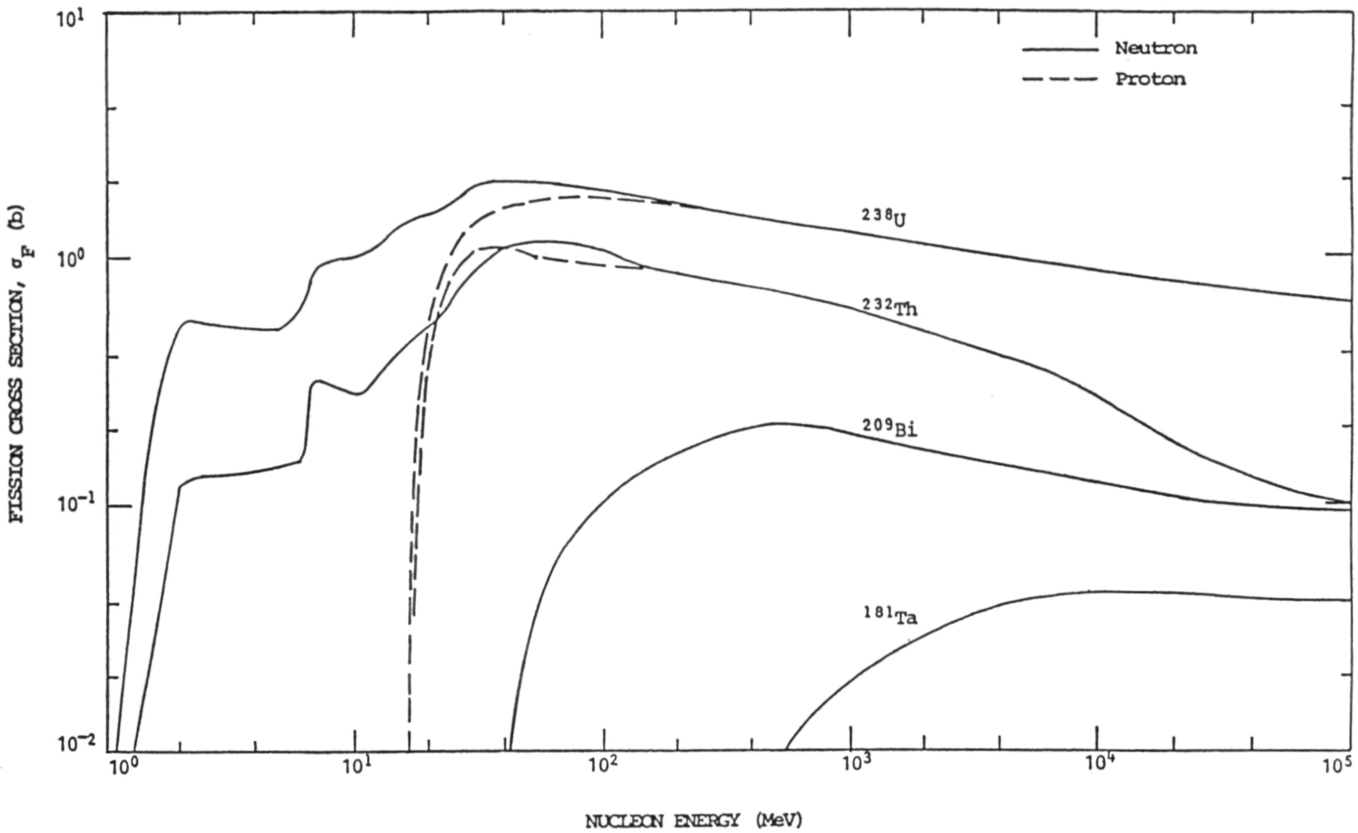

Figure 52: Fission cross sections for neutrons and protons incident on heavy metal foils.

$N(E)$, are used to generate predicted track densities. These values are then compared with measured track densities, for an evaluation of the calculated spectra and determination of LDEF fluences and doses.

6.3 Measurements

The average track densities from the mica films are given in Table 13. The standard deviations given are due to counting statistics. In addition, there were differences of up to 16% from the mean in track densities across the detector layers in Canister #1 and up to 37% in

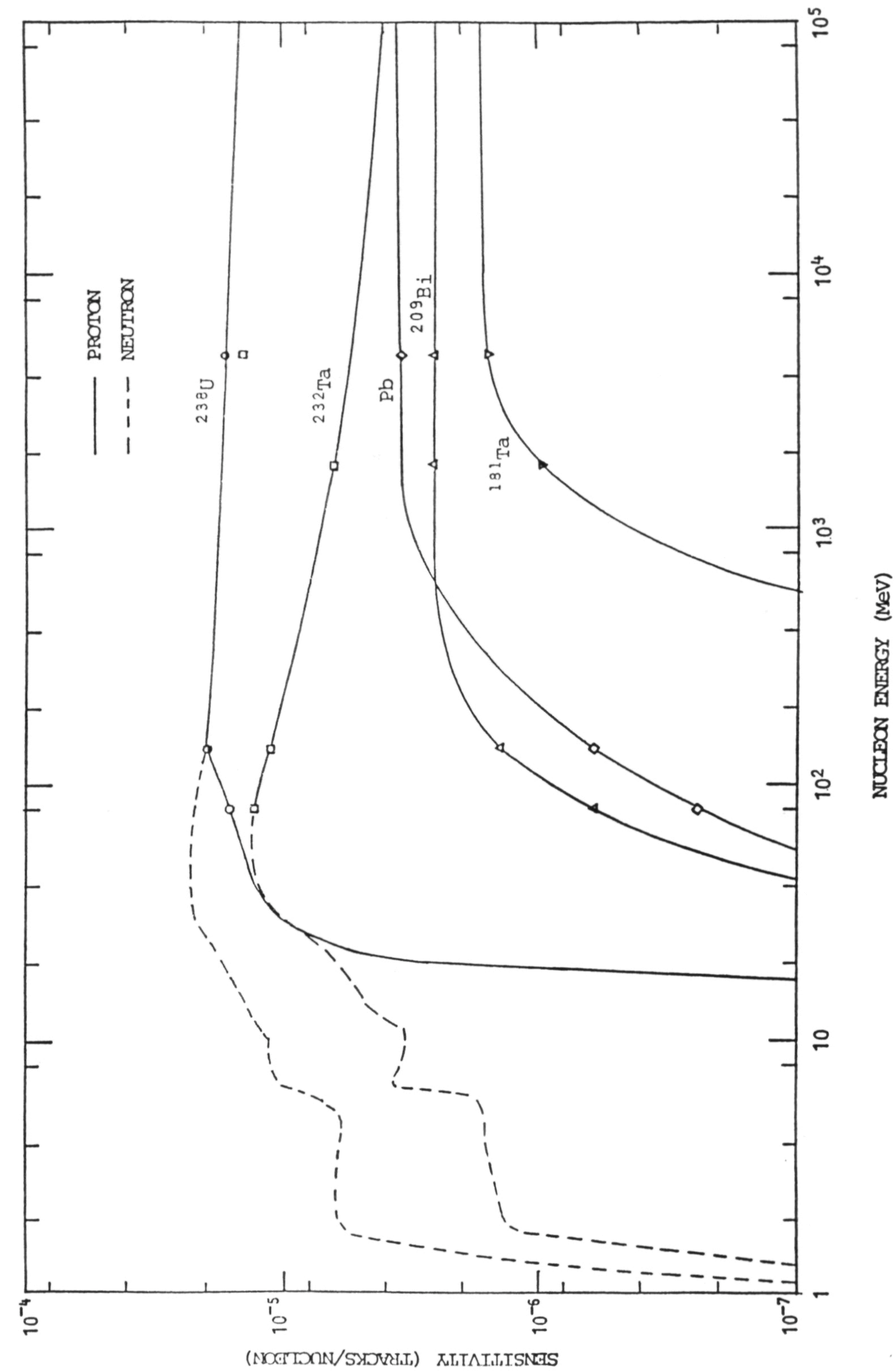

Figure 53: TLD-700 dose as a function of shielding thickness of the LDEF A0015 canister and contents. Shielding is measured vertically to the top of the canister. Minimum external shielding is the right side of the canister.

Table 13: Average Track Densities from the LDEF A0015 Fission Foil Detectors.

	Measured Track Density (cm^2)	Calculated Track Density (cm^2)
Canister #1		
^{181}Ta	131 ± 4	51.8
^{209}Bi	2340 ± 47	1030
^{232}Th	23880 ± 240	9870
^{238}U	34490 ± 500*	18800
Canister #2		
^{181}Ta	148 ± 5	49.0
^{209}Bi	2825 ± 5	2030
^{232}Th	27030 ± 315	20300
^{238}U	39490 ± 500	34600

*Corrected for spontaneous fission background and surface oxidation of foils.
Canister #1 – Earth-side
Canister #2 – Trailing Edge
The calculated track densities are based on proton and neutron spectra derived from primary/secondary particle propagation in a simple slab (one-dimensional) shield.

Canister #2 which seem to have been due mainly to shielding differences through the sides of the canisters. The larger gradients in track densities in Canister #2 would be expected near the trailing edge of LDEF and under smaller shielding.

It is of interest to note that the track density ratios between Canisters #1 and #2 change very little for the four foil types. Since the foils have different threshold energies one can conclude that the ratios of high energy to low energy nucleons are equal to within a few percent for the two FFD positions.

6.4 Calculations

Numerical integrations were carried out, as discussed above, to calculate theoretical track densities for comparison with measurements. These results are approximate since the simple

slab geometry models developed by Armstrong and Colborn[3] were used to propagate the incident particles through shielding. Secondary particles are included in the calculations.

The equation for numerical integration is

$$D_c = \sum_{E_{min}}^{E_{max}} \epsilon_p(E)N_p(E) + \sum_{E_{min}}^{E_{max}} \epsilon_n(E)N_n(E) \tag{4}$$

where ϵ_p and ϵ_n are the detector efficiencies for protons and neutrons, respectively (Figure 53), and N_p and N_n are the calculated proton and neutron spectra in the vicinity of the FFDs. An example of the proton and neutron spectra for a slab thickness of 10 g/cm^2 Al is given in Figure 54.

The calculated track densities for each of the four FFD types as functions of slab thickness are plotted in Figure 55 with the measurements. Values corresponding to the vertical shielding of the FFDs in Table 13 are given in Table 14 along with the measurements. There is better agreement between calculation and measurement for Canister #2, where the shielding is small. For thicker shielding the slab calculations fall well under the canister measurements because of the large difference in shielding from the sides.

The calculations for Canister #2 are low by 67, 28, 25 and 12% for ^{181}Ta, ^{209}Bi, ^{232}Th and ^{238}U, respectively. The higher the energy threshold, the greater the deviation. This suggests that the calculated proton and neutron energy spectra may be deficient at higher energies.

The proton absorbed doses and the neutron dose equivalents have been approximated for the FFD measurements by scaling the calculated proton and neutron track densities to the total measured values. The proton dose, in rad, is given by

$$D = 1.602 \times 10^{-8} \sum_{E_1}^{E_2} N(E)\frac{dE}{dx} \tag{5}$$

where E_1 and E_2 are 10 MeV and 100 GeV, the energy end points in this study. $N(E)$ is the differential proton spectrum in cm^{-2} MeV^{-1} and $\frac{dE}{dx}$ is the energy absorption of protons in tissue in MeV cm^2 g^{-1}.

The dose equivalent for neutrons, in rem, is given by

$$DE = 10^{-3} \sum_{E_1}^{E_2} d(E)n(E) \tag{6}$$

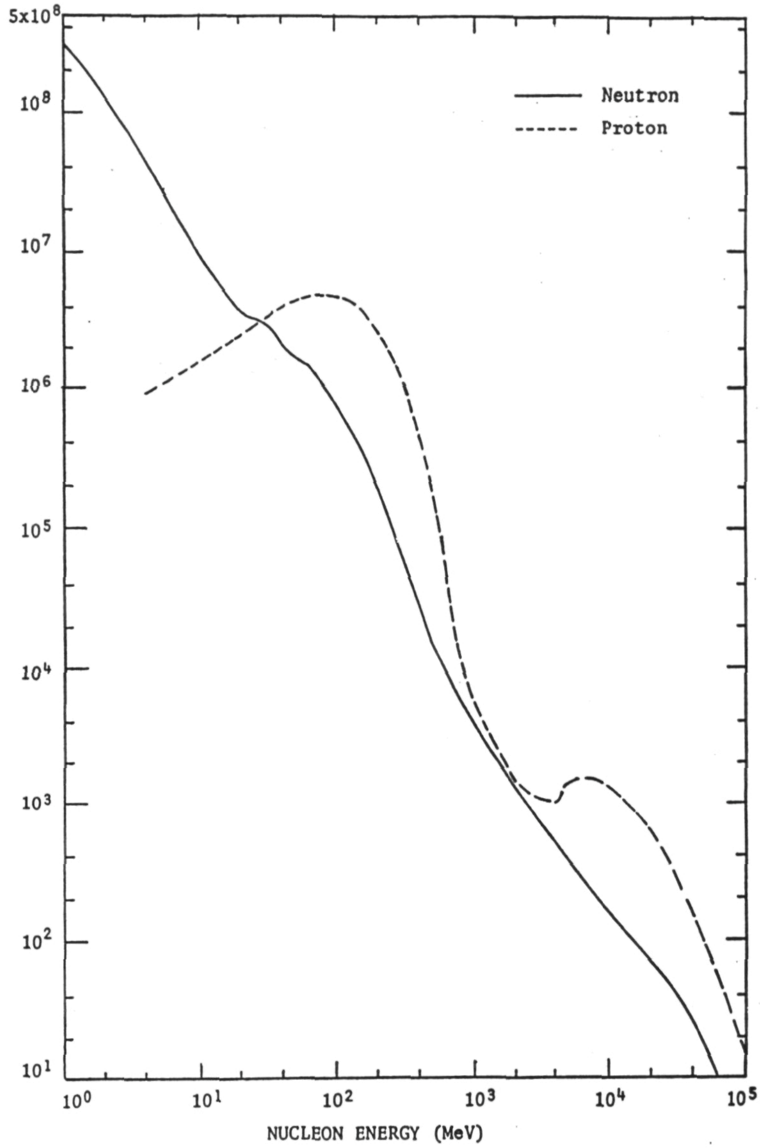

Figure 54: Differential spectra of neutrons and protons accumulated during the total LDEF mission under 10 g/cm^2 Al. From data by Armstrong and Colborn (1990). Summations and extrapolations by the authors.

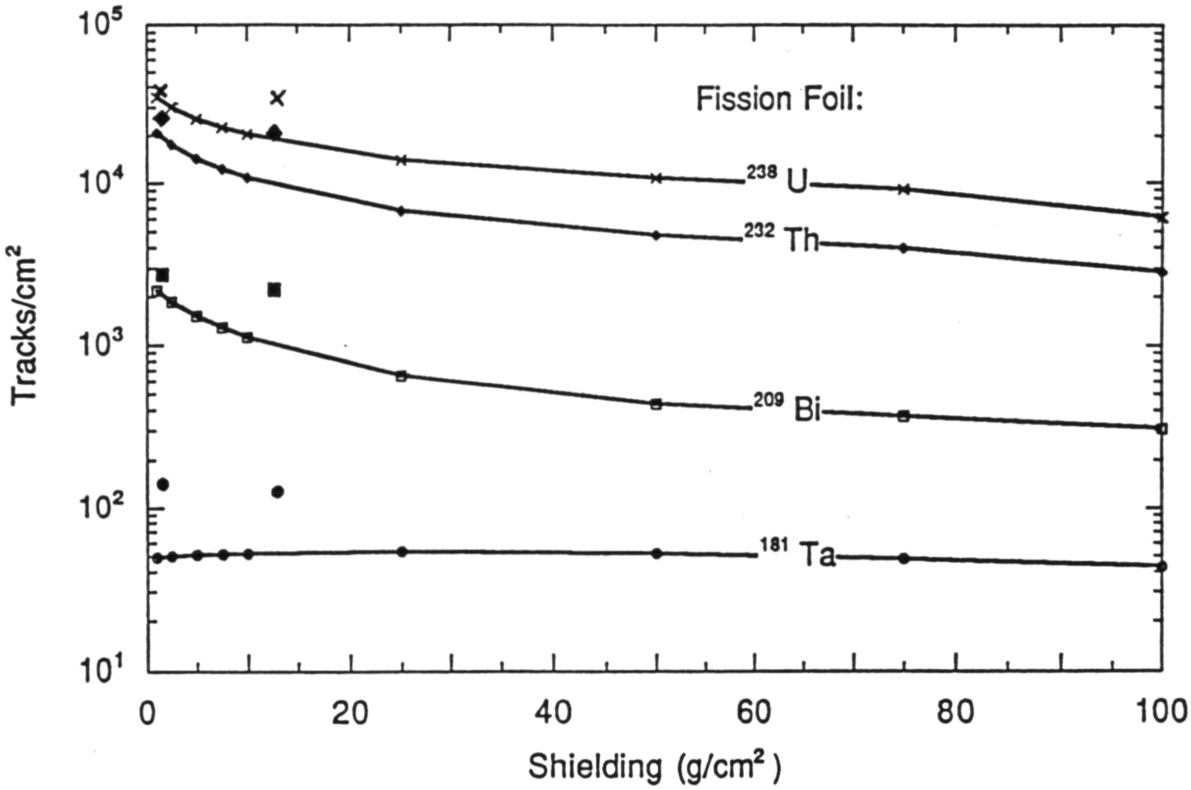

Figure 55: Calculated and measured fission fragment track densities from the combined p,f and n,f reactions in the A0015 fission foil detectors on LDEF. The calculations are based on a simple 1-D (slab) geometry (Armstrong and Colborn, 1990). The measured values lie at approximately 1 and 13 g/cm^2.

Table 14: High Energy Proton and Neutron Doses for the A0015 Fission Foil Detectors.

Canister	Position	Shielding (g/cm^2) Al Equivalent	Proton Dose (rad)	Neutron Dose (rem)	TLD Proton Dose (rad)
1	Earth-side	13.2	171	82	200
2	Trailing Edge	1.3	315	33	500

The doses were determined by scaling calculated values of proton and neutron induced track densities to total measured values.
The doses correspond to proton energies of 10 MeV to 100 GeV and neutron energies of 1 MeV to 60 GeV.

where E_1 and E_2 are 1 MeV and 60 GeV, $d(E)$ is the dose equivalent conversion factor in rem cm^2 and $n(E)$ is the differential neutron spectrum in cm^2 MeV^{-1}. The d values were taken from NCRP (1971) up to 500 MeV and extended to 60 GeV from that energy.

The doses are given in Table 14. The proton doses can be compared to measured TLD doses in the same canisters. Extrapolating from the shielding dose distribution measured with TLDs, we would expect about 225 rad in Canister #1 and 550 rad in Canister #2. About 90% of these doses would be due to protons in the energy range of the FFDs. The TLD proton doses are therefore about a factor of 1.2 higher in Canister #1 and 1.6 higher in Canister #2. Given the approximations involved in the slab calculations of proton and neutron spectra and simple scaling of track densities to get measured proton doses, these differences are within expectations.

7 High Track Densities in Polycarbonate PNTDs

7.1 Polycarbonate PNTDs in the A0015 West-side Stack

In an attempt to easily locate and measure tracks produced by ultra-heavy cosmic rays ($Z > 70$), layers of Sheffield and Tuffak PC PNTD from the LET A0015 West-side experiment were chemically processed for a short period of time (12 hours in 6.25 N NaOH at 50°C) and a layer of $\sim$2.5 μm was removed from each surface. While no ultra-heavy cosmic ray tracks were found, the short etch produced a surprising result. Analysis of Sheffield and Tuffak polycarbonate (PC) PNTD layers from the A0015 West-side stack revealed a much higher than expected track density. A track density of $> 10^7$ tracks/cm^2 was counted on the least shielded PC layer (2.0 g/cm^2). This is far higher than expected considering that the threshold for track registration in PC is usually accepted to be $\sim$250 keV/μm. By comparison, the track density measured in the CR-39 layer closest in the A0015 West-side stack (2.6 g/cm^2) was $\sim 1.1 \times 10^5$ tracks/cm^2. Track densities were counted on the front and back surfaces of each PC layer. Figure 56 shows track density in PC as a function of shielding depth. The track density can be seen to decrease with increasing shielding.

The Sheffield and Tuffak PC layers involved in this analysis were processed for only a short time and a layer of $\sim$2.5 μm thickness was removed from each surface. Most of the tracks are small and over-etched, indicating that the ranges of the particles which made them are less than 2.5 μm. Because the removed layer was so small, the resulting tracks were too small to accurately measure and only track densities were measured.

Track density profiles were measured for a number of the polycarbonate detectors in the A0015 West-side stack. Figures 57, 58, 59 and 60 show track density profiles for detector layers 2G1, 2G2, 2G9, and 2R16, respectively. Track density varies by a factor of 2 across the front of layer 2G1 under 2.06 g/cm^2. Less variation is seen in layer 2G2 under 2.09 g/cm^2 where track density varies only by a factor of 1.2. The largest concentration of tracks appears in the upper portion of the detector. Similarly in layer 2G9 under 2.30 g/cm^2, highest track density tended to be concentrated toward the top of the detector. Track density varied across the surface of 2G9 by a factor of 1.7. Higher track densities could be seen around the edges of 2R16, the Tuffak layer under 2.51 g/cm^2. Track density varied by a factor of $\sim$2. The

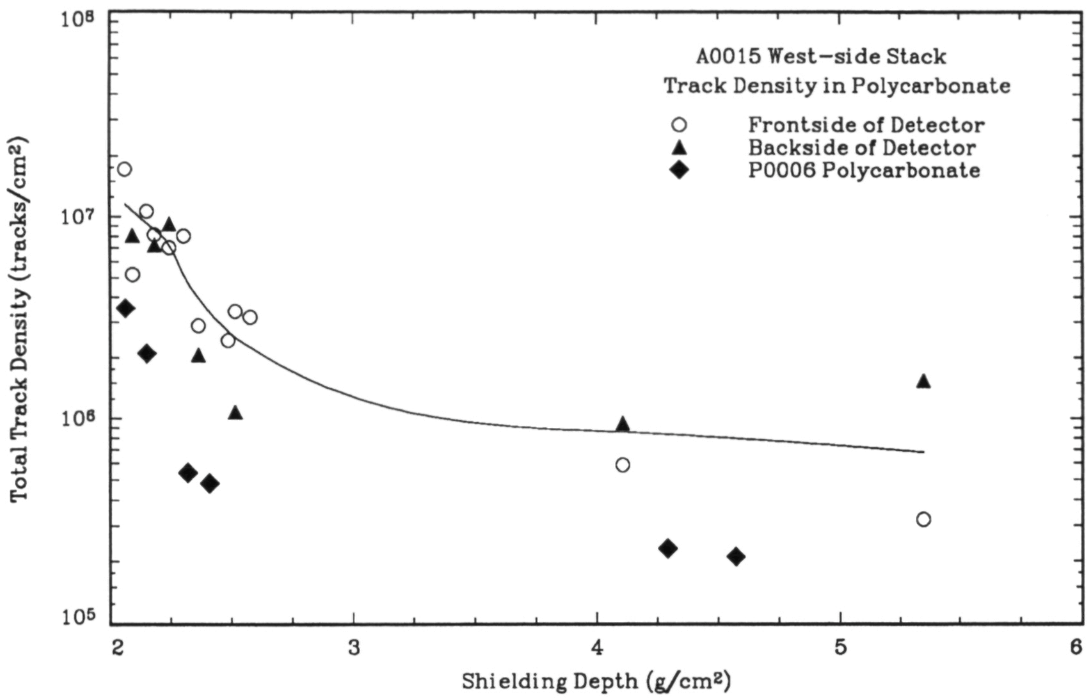

Figure 56: Track densities measured in A0015 West-side polycarbonate PNTDs as a function of shielding depth.

higher track densities along the edges of the polycarbonate detectors probably correspond to less horizontal shielding. All shielding values given are for the vertical self-shielding of the experiment stack itself.

Figures 61–66 are photomicrographs of selected layers PC PNTD from the A0015 West-side stack. All photomicrographs were taken at a magnification of 250× and have a scale of ~11 μm/cm. The highest track density can be seen in the least shielded layer, 2G1 under 2.06 g/cm^2. Figure 61 shows the tracks are overlapping, making measurement of track density difficult. The reported track density of 1.7×10^7 tracks/cm^2 is probably too low. Nearly all the tracks are over-etched which indicates the latent damage trail for track formation of these tracks is shorter than the ~2.5 μm removed by etching. Track density is seen to have attenuated rapidly in Figure 62, Sheffield layer 2G2 under 2.09 g/cm^2. The individual tracks are now distinguishable from one another. The decrease in track density is

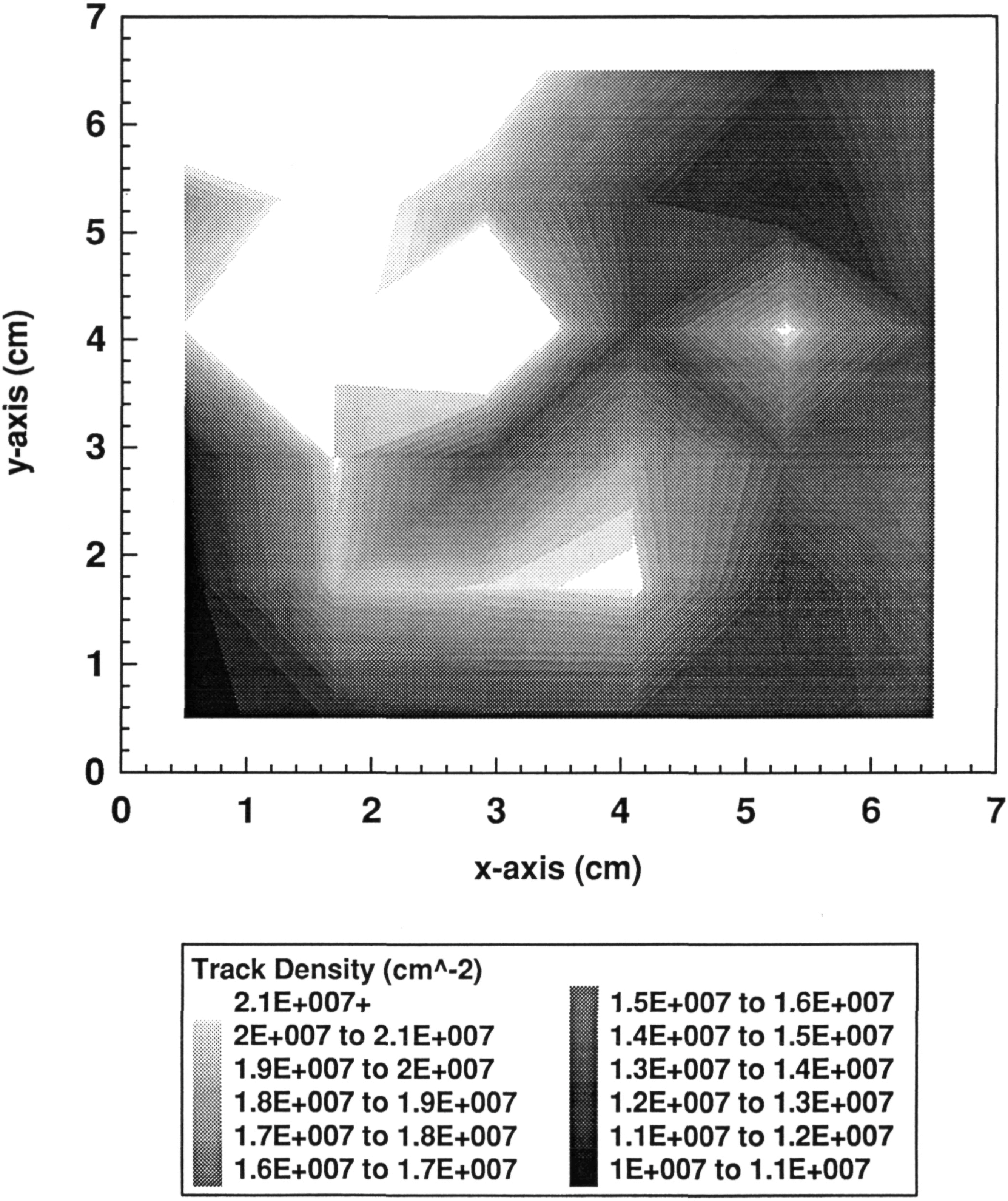

Figure 57: Track density profile measured for layer 2G1 under 2.06 g/cm^2 in the LDEF A0015 West-side stack.

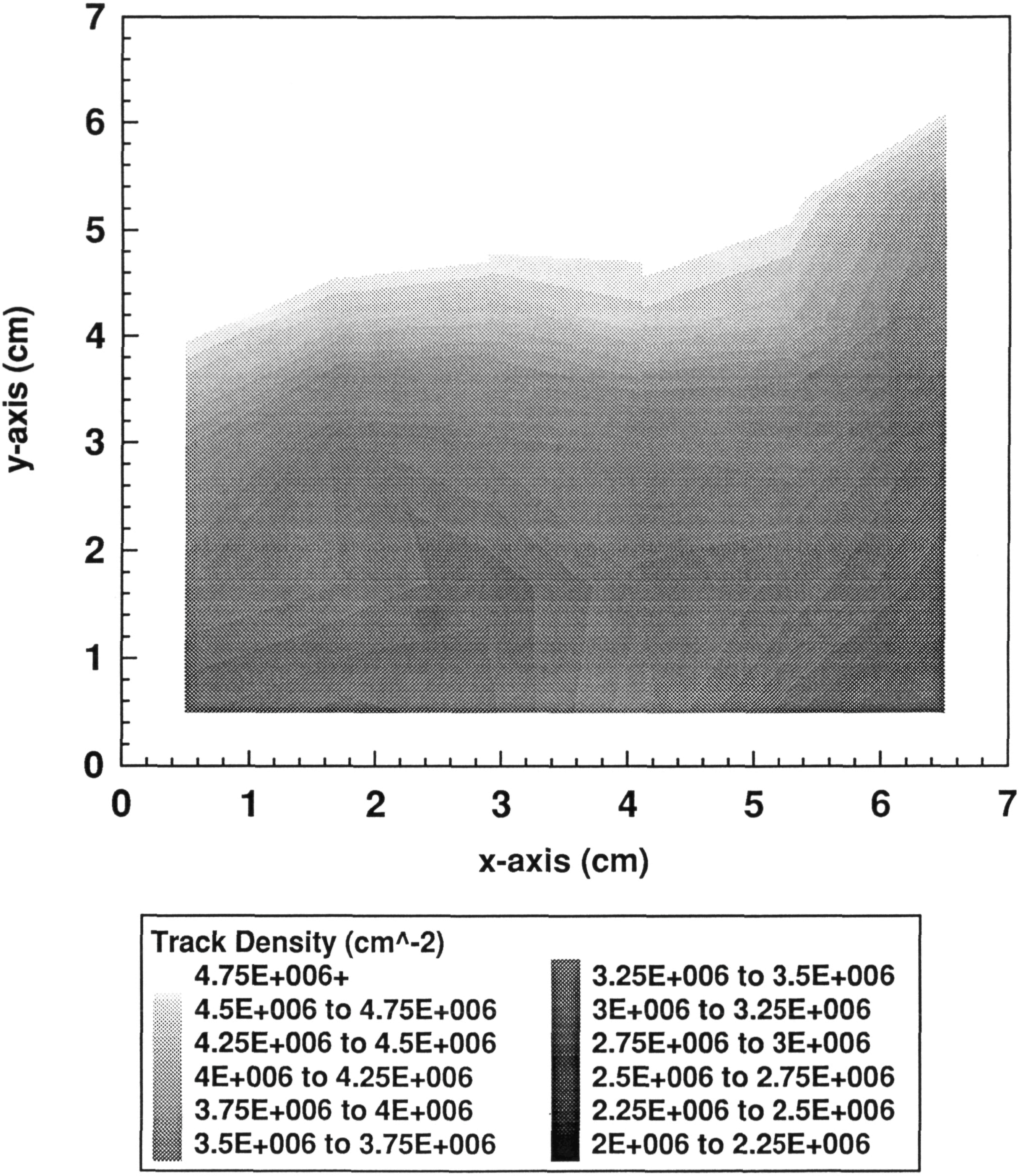

Figure 58: Track density profile measured for layer 2G2 under 2.09 g/cm^2 in the LDEF A0015 West-side stack.

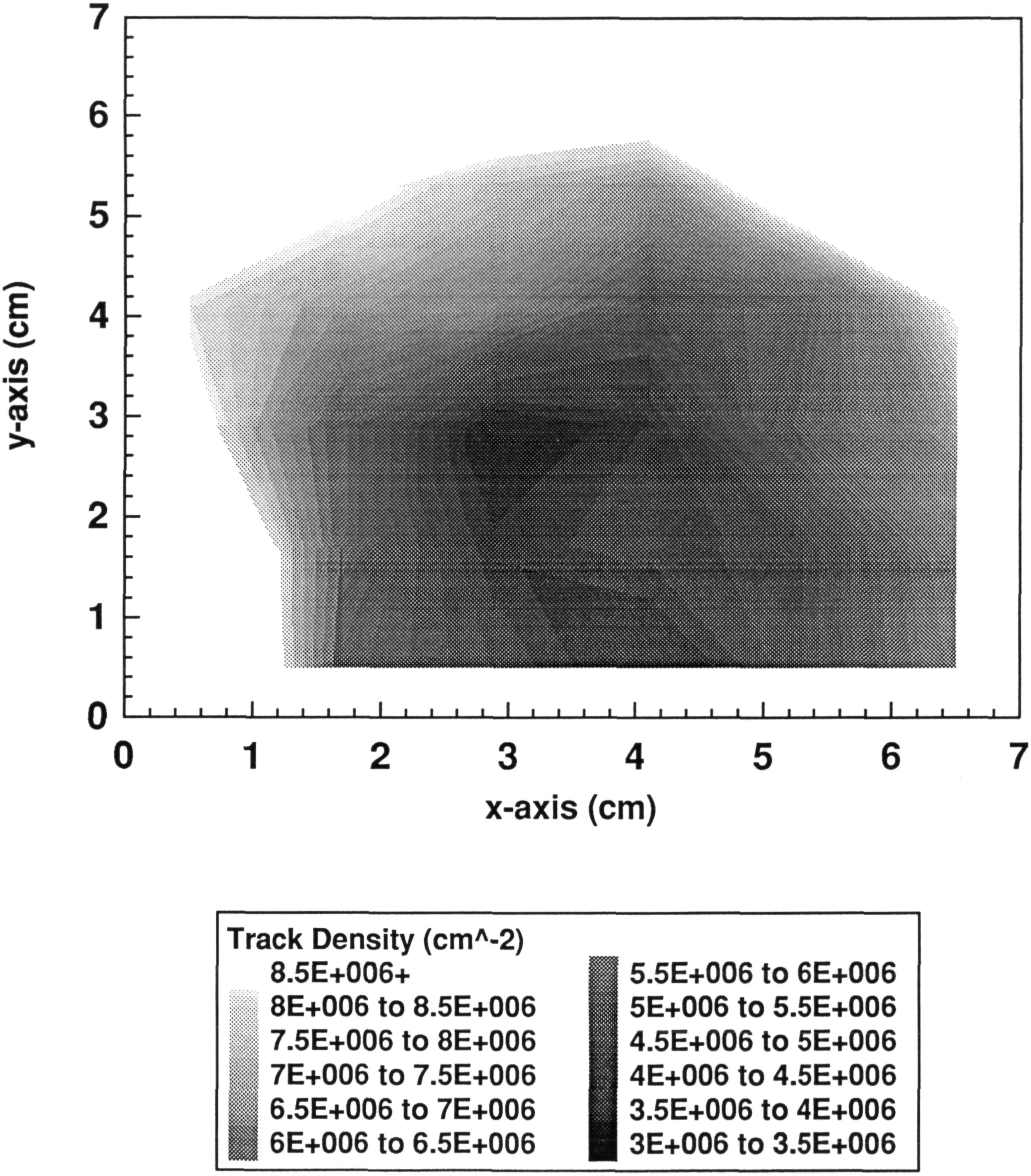

Figure 59: Track density profile measured for layer 2G9 under 2.30 g/cm^2 in the LDEF A0015 West-side stack.

C-2

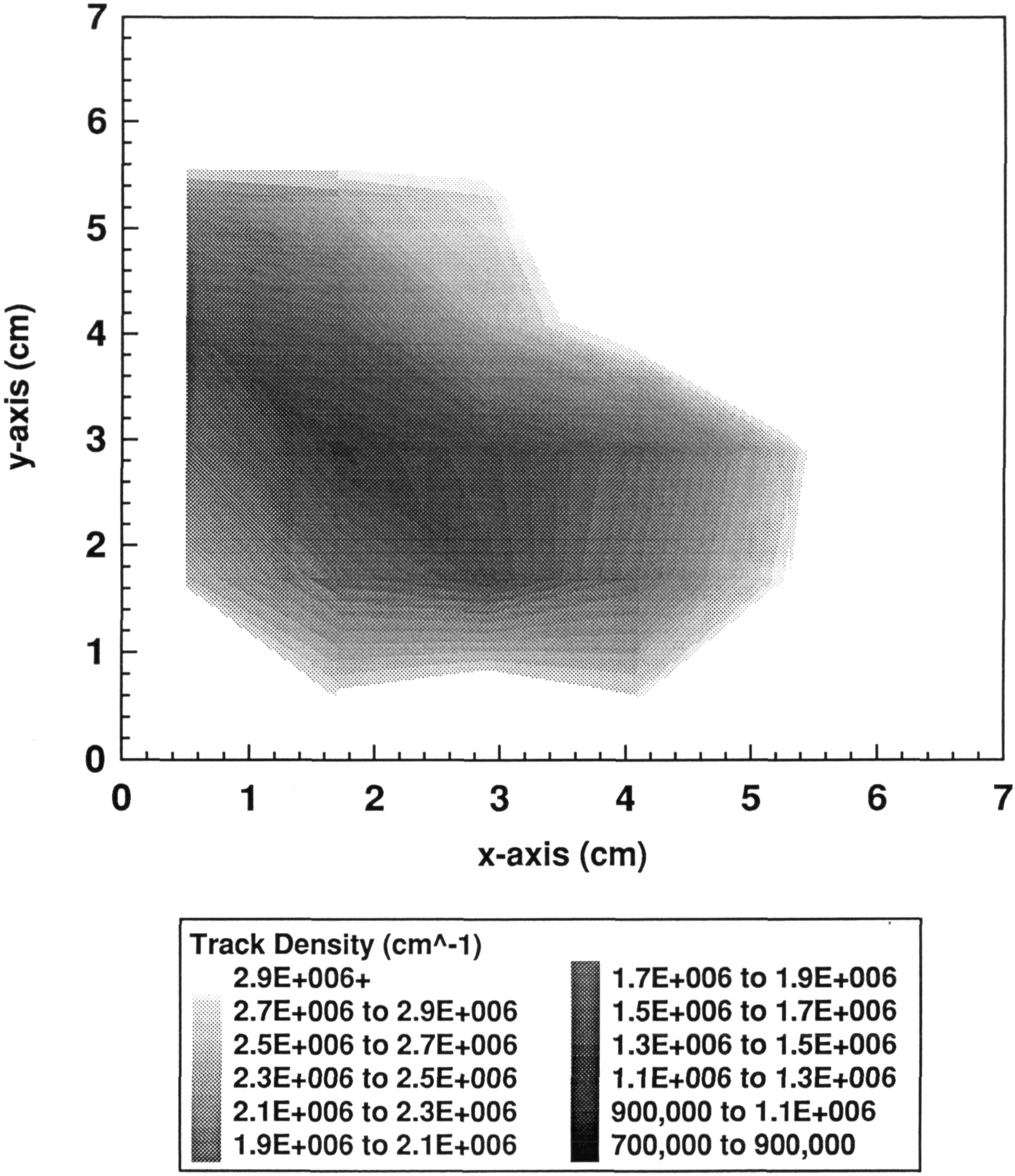

Figure 60: Track density profile measured for layer 2R16 under 2.51 g/cm^2 in the LDEF A0015 West-side stack.

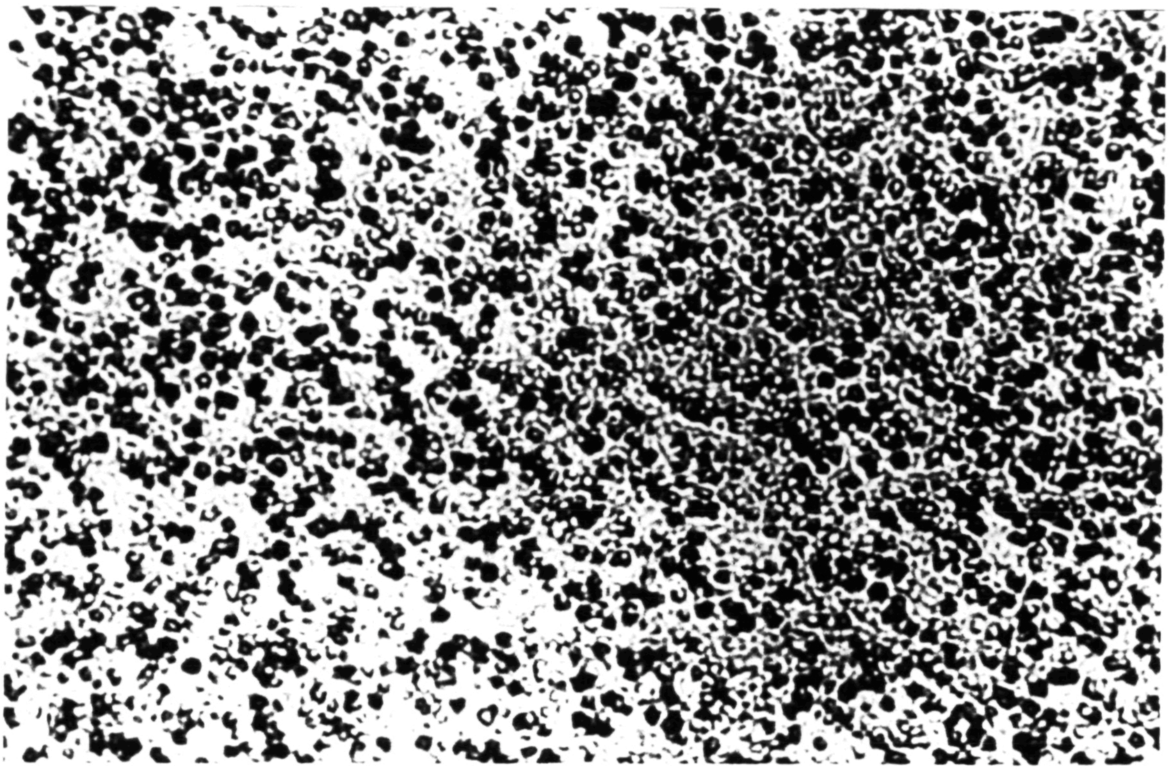

Figure 61: Photomicrograph of Sheffield layer 2G1 under 2.06 g/cm^2 in the A0015 West-side stack.

more gradual in the next two photomicrographs, Figures 63 and 64 showing layers 2G10 and 2R16 under 2.33 and 2.51 g/cm^2 shielding respectively. Layer 2R16 is Tuffak PC, while all of the previous layers have been Sheffield PC, demonstrating that the high track density is seen on more than one type of PC PNTD. Figures 65 and 66 are photomicrographs of detector layers 2G36 and 2G45 under 4.11 and 5.35 g/cm^2 shielding, respectively. Track density has decreased by nearly a factor of 10 from the previous two layers.

7.2 Polycarbonate PNTDs from other LDEF Experiments

Figure 56 also shows results from similar measurements made in the LDEF P0006 experiment during this reporting period. While absolute vales for track density in the P0006 stack are lower than in A0015, they are well above what is expected in PC. The track density in P0006 ranges from 3.5×10^6 tracks/cm^2 under 2.1 g/cm^2 to 2.5×10^5 tracks/cm^2 under 4.2 g/cm^2 showing a similar attenuation in track density with shielding as seen in the A0015 Earth-side

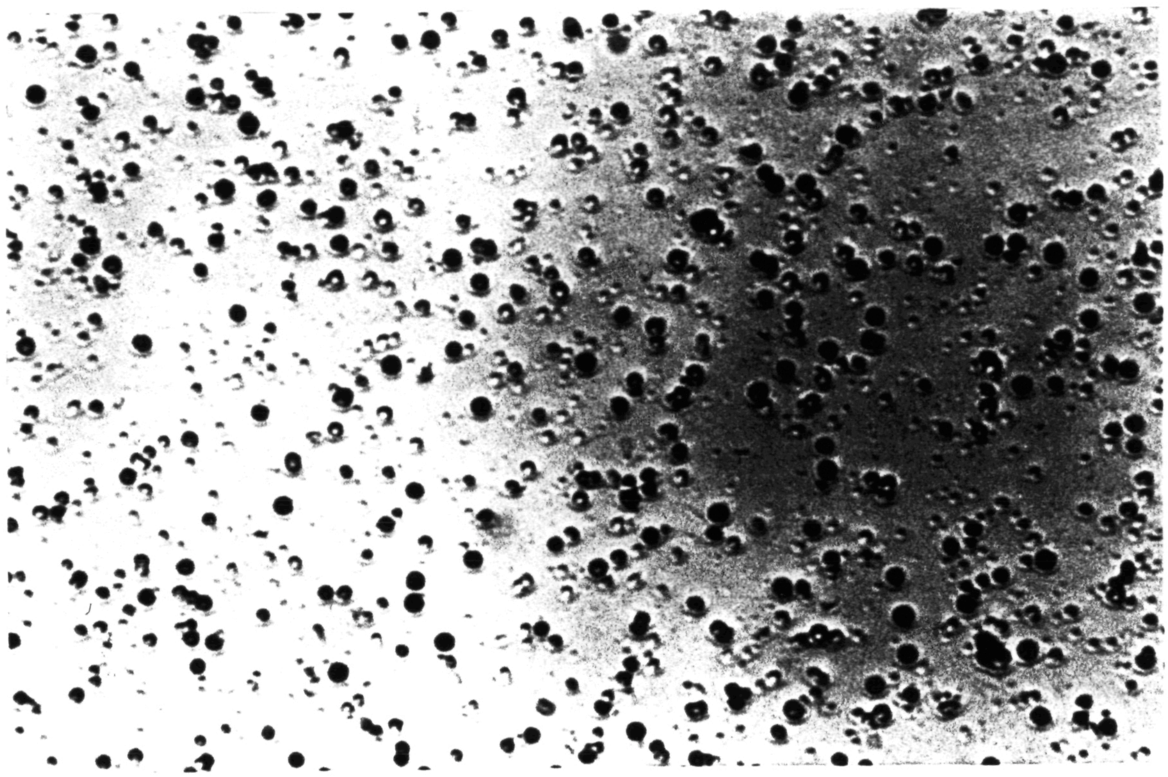

Figure 62: Photomicrograph of Sheffield layer 2G2 under 2.09 g/cm^2 in the A0015 West-side stack.

stack.

Samples of Lexan PNTD flown as part of the A0178 Ultra-heavy Cosmic-Ray Experiment and the M0001 Heavy Ions in Space experiment have been obtained and analyzed. Chemical processing of 12 hours, 6.25 N NaOH, 50°C, identical to the A0015 processing was used. Both sets of detectors exhibit the high track densities first observed in A0015. However, the quality of the tracks is somewhat different. Densities in the material from the A0178 experiment ranged from 1.22×10^7 tracks/cm^2 to 2.54×10^5 tracks/cm^2. However the quality of these tracks was much worse than in the A0015 detectors. Many of the objects assumed to be tracks appeared only as small dark pits, which may not have been tracks. This differs from the A0015 detectors wherein the objects can be positively identified as tracks. The density of objects which can be identified as well defined tracks ranges from 3.43×10^4 to 9.28×10^3 tracks/cm^2 in the A0178 experiment. Tracks in Lexan from the M0001 experiment were much more clearly defined and similar to those seen in the A0015 layers. A track density of 2.27×10^6 tracks/cm^2 was measured in the least shielded M0001 layer. The

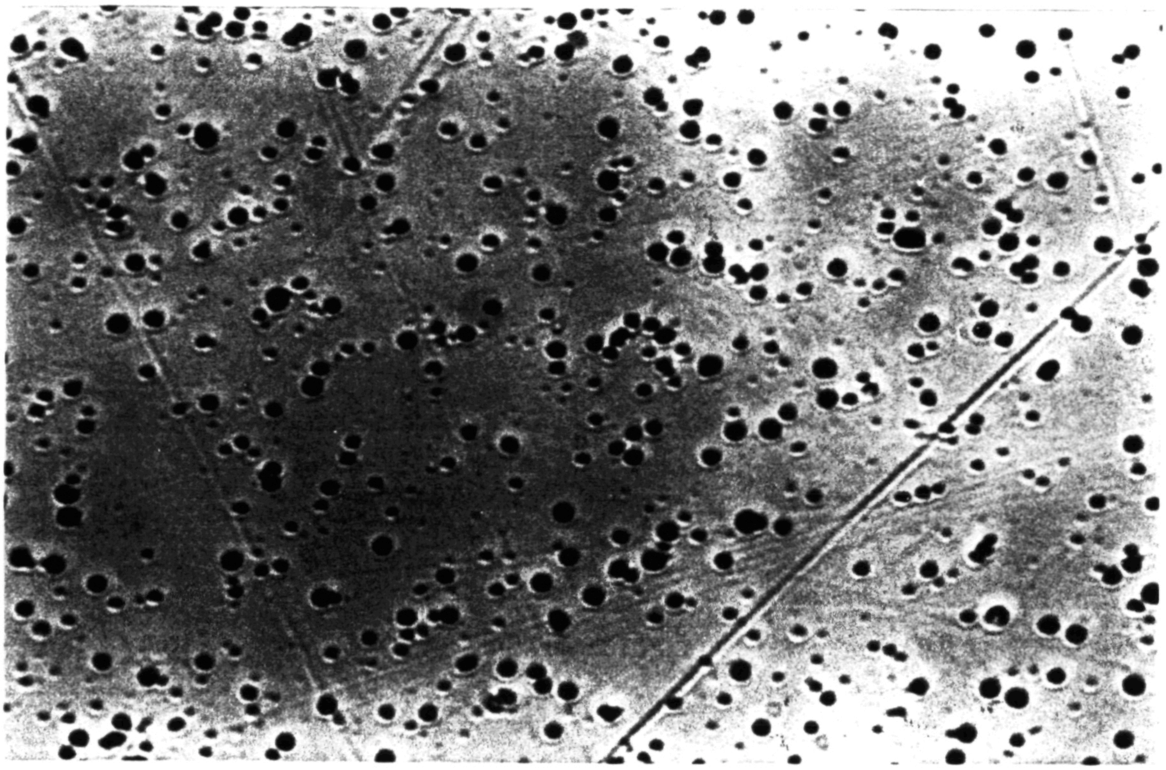

Figure 63: Photomicrograph of Sheffield layer 2G10 under 2.33 g/cm^2 in the A0015 West-side stack.

fact that high track densities are seen in nearly all LDEF experiments that contained PC PNTD material indicates that this effect is caused by some phenomena during the LDEF mission and is not local to a specific experiment. Results of track density measurements are summarized in Table 15.

Figures 67, 68 and 69 are photomicrographs of PC detectors from other LDEF experiments processed in the same way as the A0015 West-side PC layers and showing similarly high track densities. Figure 67 shows Sheffield layer 1G1 in the A0015 Earth-side stack under 10.8 g/cm^2. Figure 68 shows Sheffield layer 202G-12a from the P0006 experiment on the West-side of LDEF, under 4.29 g/cm^2. Figure 69 shows Lexan PC layer L35-2 from the LDEF A0178 experiment. Shielding for this detector is not available, but it was near the top of the detector stack, close to space, on the West side of LDEF.

Table 15: Summary of track density measurements in LDEF PC detectors. Included are results from the A0015, P0006, M0001 and A0178 experiments.

Experiment	Location	Material	Sample Name	Shielding (g/cm^2)	Bulk Etch (μm)	Track Density (cm^{-2})
A0015 West	C-2	Sheffield	2G1	2.06	2.35	1.7×10^7
			2G2	2.09	2.33	5.2×10^6
			2G4	2.15	2.35	1.1×10^7
			2G5	2.18	2.31	8.1×10^6
			2G7	2.24	2.35	7.0×10^6
			2G9	2.30	2.30	8.0×10^6
			2G11	2.36	2.29	2.9×10^6
			2G15	2.48	2.22	2.4×10^6
		Tuffak	2R16	2.51	2.27	3.4×10^6
			2R18	2.58	2.28	3.7×10^6
		Sheffield	2G36	4.11	2.99	5.9×10^5
			2G45	5.35	2.31	3.2×10^5
P0006	F2	Sheffield	223G-12a	2.06	2.88	3.6×10^6
		Tuffak	220R-12a	2.15	2.78	2.1×10^6
		Sheffield	214G-12a	2.32	2.90	5.4×10^5
		Tuffak	211R-12a	2.41	2.83	4.8×10^5
		Sheffield	202G-12a	4.29	2.76	2.3×10^5
		Sheffield	193G-12a	4.57	2.73	2.1×10^5
HIIS M0001	H-3	Lexan	LD2-1	0.89	3.23	2.3×10^6
UHCRE A0178	A-2	Lexan	L35-2-2	top	3.20	1.2×10^7
			L35-59	bottom	3.55	7.3×10^6
		Tuffak	L153-1	top	3.68	4.9×10^5
			L153-2	top	3.29	2.5×10^5
			L153-43	bottom	3.25	3.2×10^5
			L153-44	bottom	3.68	5.4×10^5

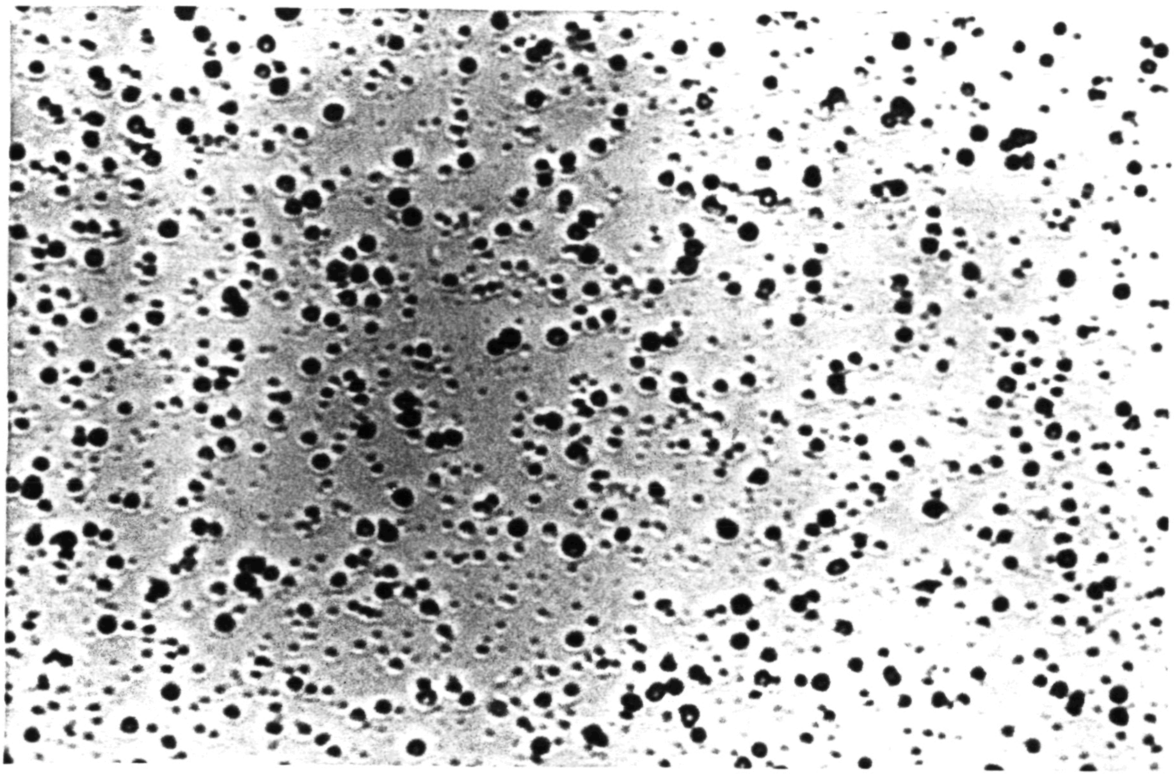

Figure 64: Photomicrograph of Tuffak layer 2R16 under 2.51 g/cm^2 in the A0015 West-side stack.

7.3 Sensitivity as a Function of Depth

Two of the A0015 West-side layers, 2G4 and 2G7, were etched repeatedly to determine whether new tracks would be uncovered with increasing depth in the detector. If the PNTD were uniformly sensitive throughout the entire thickness of the layer, new tracks would be uncovered by the chemical processing and the track density would increase. If the detector is sensitive only in the outermost region of the layer, the original tracks uncovered by the first etch will continue to get larger and eventually become spherical etch pits. No new tracks will be counted and the track density will remain constant and then decrease. This is what has been observed. Figures 70 and 71 are plots of track density as a function of removed thickness from chemical etching. Each detector was etched six times for 12 hours in 6.25 N NaOH at 50°C each time. The total removed thickness was $\sim$13 μm. For both detectors, track density is constant and then decreases indicating that the latent tracks are present only within the initial several microns removed during the first one or two etches,

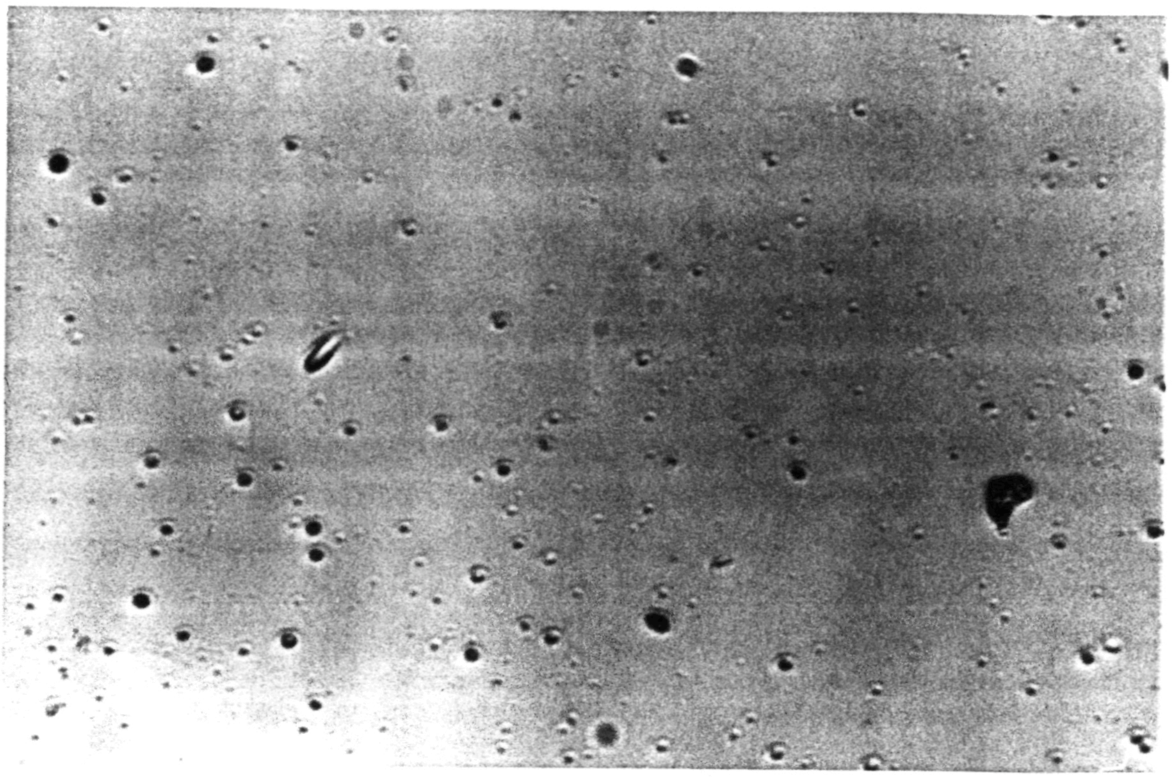

Figure 65: Photomicrograph of Sheffield layer 2G36 under 4.11 g/cm^2 in the A0015 West-side stack.

and not any deeper. The most likely explanation for this is that the sensitivity of the first $\sim$3 μm of the PC material is much greater than the >250 keV/μm LET threshold typically associated with PC. Since the track densities counted are higher than CR-39 under similar shielding, the sensitivity of this thin region in PC may be greater than the >5 keV/μm LET threshold for CR-39. Figures 72 and 73 are photomicrographs of Sheffield layers 2G4 and 2G7 after $\sim$11 μm of material has been removed by etching. The tracks can bee seen to have etched into large, overlapping, spherical pits and very few new tracks (smaller objects in the photographs) have been uncovered.

7.4 Ground-based Polycarbonate Studies

A ground-based experiment was carried out to establish the LET threshold for track registration in the outermost $\sim$2.5 μm layer of PC. Layers of Sheffield, Tuffak and Lexan PC were exposed to α-particles ranging in energy from 0.6 to 5.5 MeV and in LET from 250

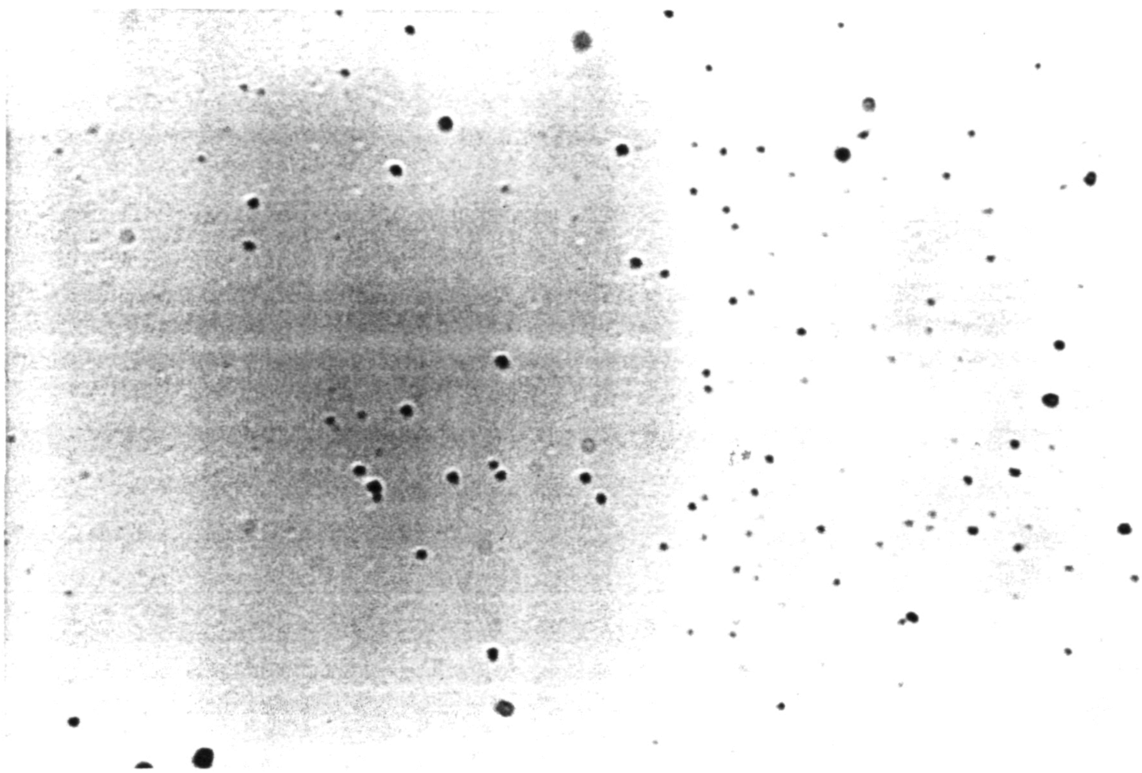

Figure 66: Photomicrograph of Sheffield layer 2G45 under 5.35 g/cm^2 in the A0015 West-side stack.

to 100 keV/μm. Each detector layer was exposed to a fluence of 3.0 $\times$ 10^7 particles/cm^2. A ^{241}Am α-particle source was used and α-particle energy was controlled by regulating the pressure in a vacuum chamber. Table 16 lists the exposures made and the results following etching in 6.25 N NaOH at 50°C for 12 hours. Removed layer thickness ranged from 2.1 to 4.5 μm. Results were similar for Sheffield, Tuffak and Lexan PC PNTDs. Figures 74 and a2pm are photomicrographs of the PC detectors exposed to 0.6 and 5.5 MeV α-particles, respectively.

In the $\sim$3 μm layer between the pre- and post-etch surfaces of the detector, the LET threshold for track registration was found to lie between 125 and 150 keV/μm. Previous experiments with polycarbonate for detector depths between 20 and 40 μm have placed the LET threshold for track registration between 250 and 300 keV/μm. This indicates a depth dependent sensitivity for track formation in PC and confirms earlier results of track formation as a function of depth in the A0015 2G4 and 2G7 detectors.

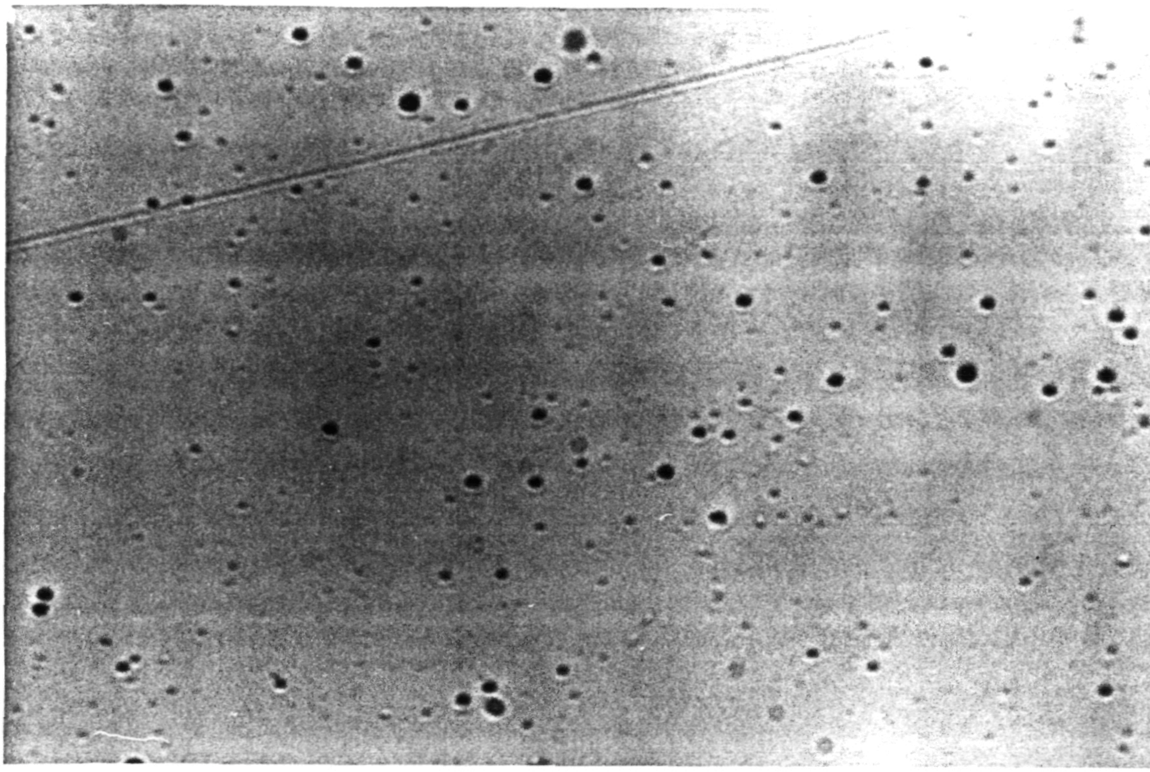

Figure 67: Photomicrograph of Sheffield layer 1G1 from the A0015 Earth-side stack. Scale is ~11 μm/cm.

Table 16: Results from α-particle exposure of polycarbonate.

α-particle Energy (MeV)	α-particle LET (keV/μm)	Vacuum Chamber Pressure (mmHg)	Visible Tracks
5.48	100	0	none
3.72	125	134	none
2.88	150	183	small
1.68	200	235	stopping
0.30	250	275	stopping

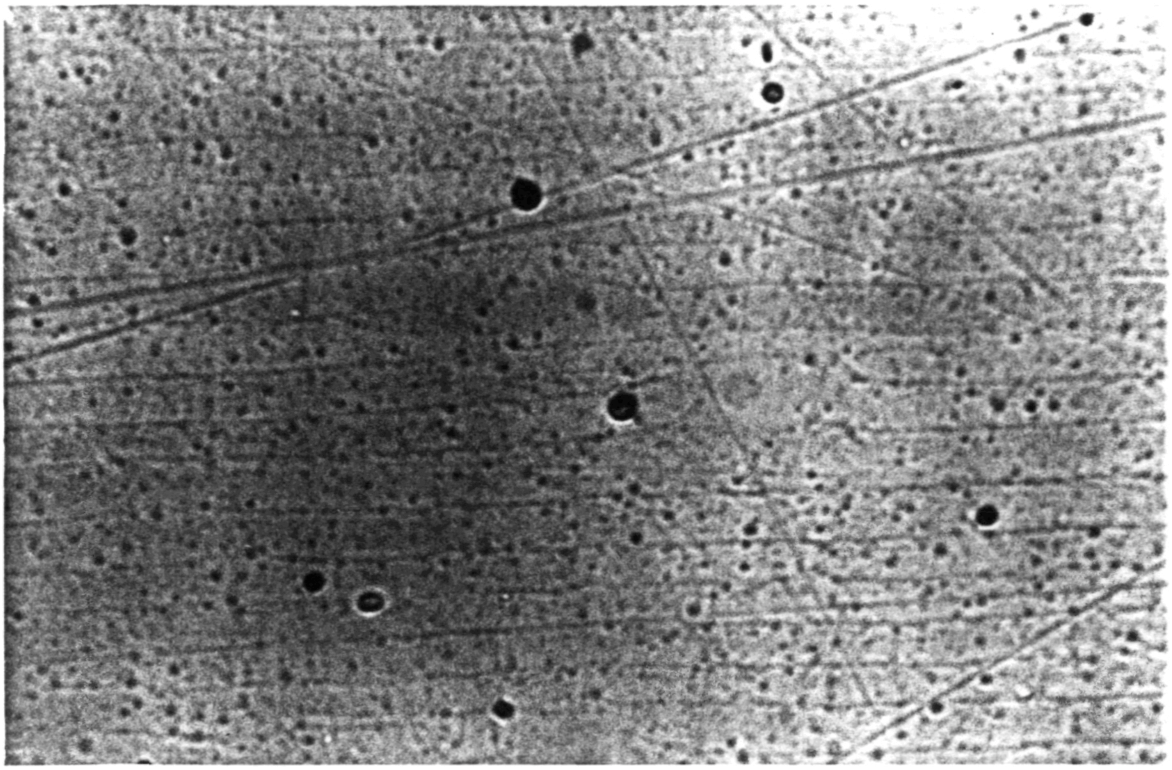

Figure 68: Photomicrograph of Sheffield layer 202G-12a from the LDEF P0006 Experiment. Scale is $\sim$11 μm/cm.

7.5 Discussion

To date, the origin of these tracks is unknown, but several possible causes have been eliminated. One possibility was that the material was irradiated at the time of manufacture. This can be discounted because high track densities are seen in both Tuffak and Sheffield PNTDs, polycarbonate made by different manufacturers. Since track density is seen to attenuate as a function of shielding depth in the stack, exposure must have taken place while the experiment was assembled. Another possibility is that what is being see are not tracks, but an effect caused be detector handling or chemical processing. This possibility has also been ruled out since these high track densities were counted in detectors which were processed separately. In addition, this effect was not seen in unexposed control detectors processed under the same conditions.

Since the detectors were near the fission foil/mica and ^{6}LiF/CR-39 neutron detectors, it was suggested that the track much be from α-particles from these sources. This possibility

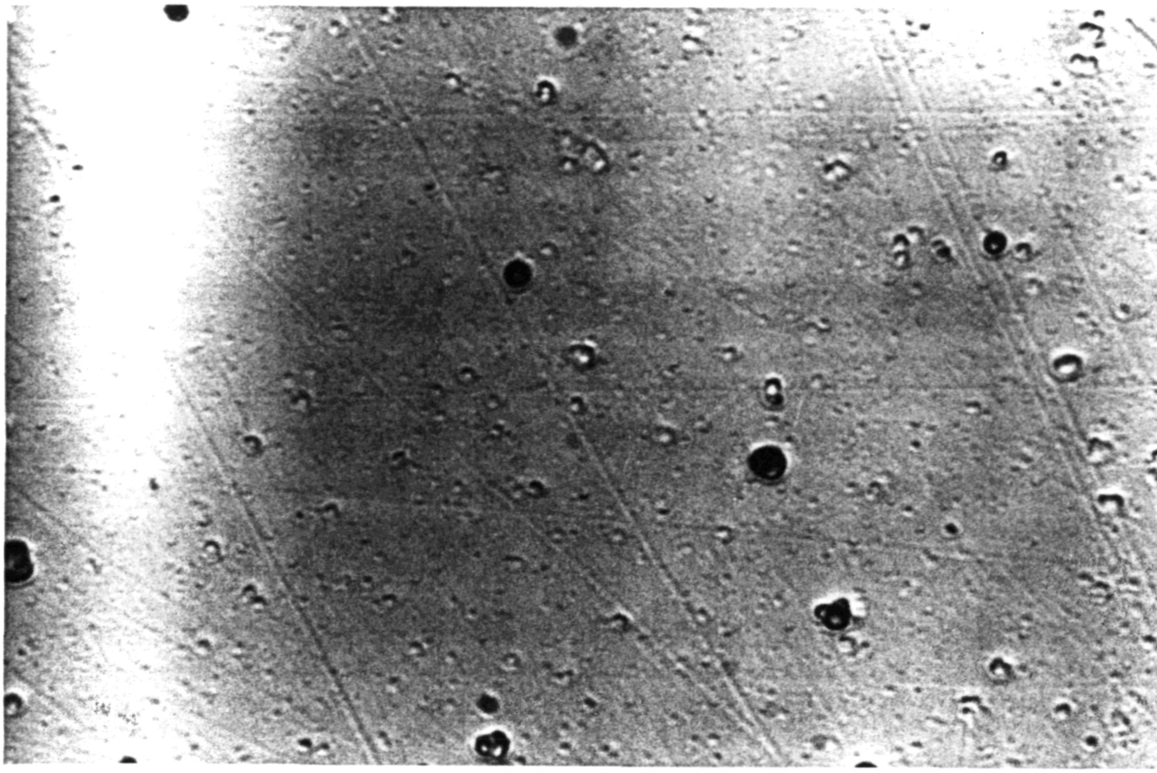

Figure 69: Photomicrograph of Lexan layer L35-2 from the LDEF A0178 Experiment. Scale is $\sim$11 μm/cm.

has been eliminated due to the fact that the range of α-particles from these sources is too short to form tracks in all the PC layers. This high track density was not seen near the activation foils contained in the A0015 Earth-side stacks. If the tracks were from ^{6}Li α-particles, a pattern of track density would be seen due to the placement of the ^{6}LiF chips in the experiment. No such pattern was seen.

It is possible that the tracks are from proton-induced secondaries. To test this hypothesis, a stack of Sheffield and Tuffak PC PNTDs was exposed to a beam of 154 MeV protons at the Harvard Cyclotron. While a small number of recoil tracks were detected, the density was far lower than the density of secondaries counted in the CR-39 PNTDs and could not account for the high track densities seen in the A0015 PC layers. Figure 76 is a photomicrograph of a layer of Sheffield PC exposed to 154 MeV protons. Several secondary tracks are visible in the image, but not on the large numbers seen in the LDEF detectors. The origin of the mottled surface is not known. In addition, if these tracks were from proton induced secondaries, a similar high track density should have been counted in the more sensitive CR-39 layers in the

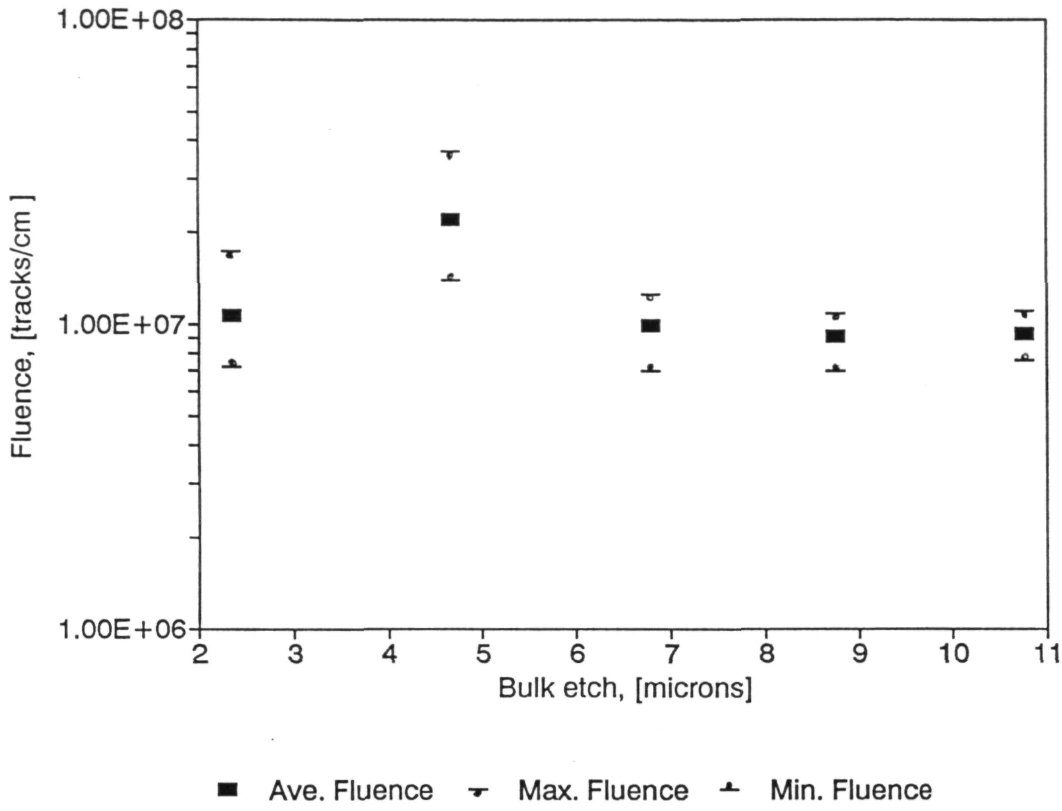

Figure 70: Sheffield layer 2G4 from the A0015 West-side stack. The layer was etched for six 12 hour periods. Tracks were found only after the first etch. Successive etches revealed no new tracks and only enlarged existing tracks.

A0015 West-side stack. A similar argument can be used to dismiss the possibility that the tracks were from stopping protons or from low energy (trapped or anomalous) α-particles.

One conclusion that can be drawn from the analysis of the A0015 West-side PC layers is that the sensitivity of the material is not constant, but varies as a function of detector thickness. Since high track densities can be counted through many layers of PC on both the front and back surfaces of the detector and since these tracks only appear in the $\sim$3 μm region directly beneath the pre-etch surface and no deeper, it can be concluded that this outer-most region of the PC layer is more sensitive that the rest of the layer. This opens

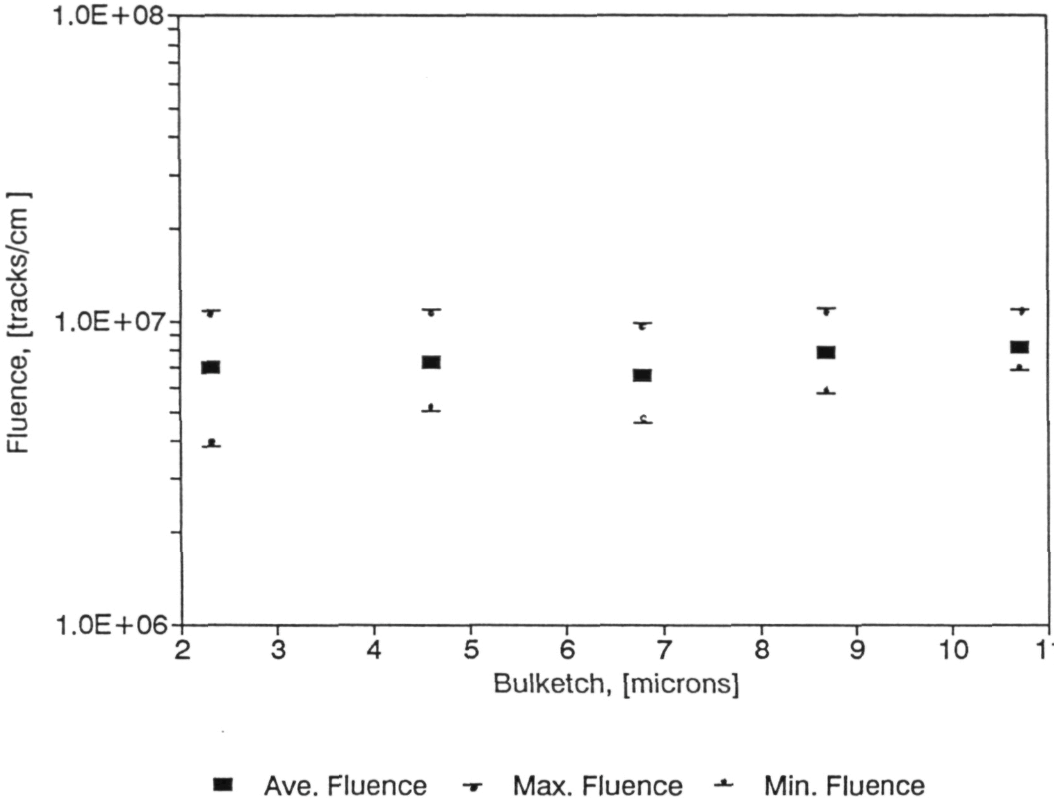

Figure 71: Sheffield layer 2G7 from the A0015 West-side stack. The layer was etched for six 12 hour periods. Tracks were found only after the first etch. Successive etches revealed no new tracks and only enlarged existing tracks.

up a number of possibilities including the possibility that this region of the detector is even more sensitive that CR-39 and that the tracks being seen are from primary protons of energy greater than 16 MeV, the highest proton energy detectable in CR-39, but lower than the 154 MeV of the Harvard Cyclotron proton exposures. Similar analysis of Tuffak, Sheffield and Lexan PC has been being carried out for other experiments containing PC on LDEF. Ground based experiments to reproduce the results seen in the A0015 West-side polycarbonate PNTDs have shown that the threshold for track registration in the outermost layers of polycarbonate, just beneath the pre-etch surface, lies somewhere between 125 and

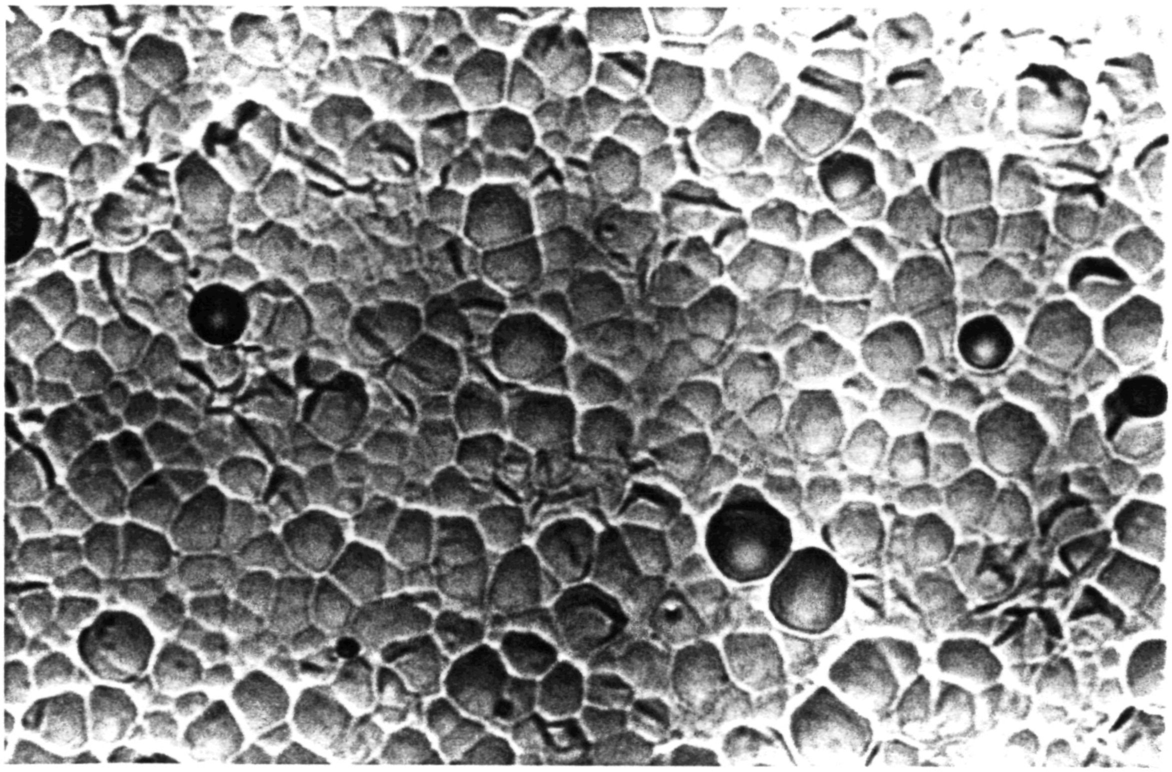

Figure 72: Photomicrograph of Sheffield layer 2G4 after ~11 μm of material have been removed by etching. Scale is ~11 μm/cm.

150 keV/μm.

There were estimated to be no particle species heavier than protons with total mission fluxes greater than the 10^7 particles/cm^2 seen in the A0015 PC. Protons reach the 150 keV/μm threshold only at the very end of their range. One possibility is that these track are produced by stopping protons. However a similar high density of track is not seen in CR-39 PNTD. The LET threshold for track registration in CR-39 is ~5 keV/μm and tracks of >150 keV/μm should be readily visible. The track density measured in CR-39 in the A0015 West-side stack under similar shielding (2.6 g/cm^2) is only 1.1 $\times$ 10^5 tracks/cm^2.

Another possibility is that the tracks are the result of elastic and inelastic collisions between primary protons and the nuclei of the constituent atoms in the polycarbonate. Estimates of total proton flux for LDEF are 10^9 protons/cm^2 and the cross section for proton-nucleon interaction is ~10^{-6} cm^{-2}[8]. This indicates the total number of secondaries should fall below that seen in the A0015 PC.

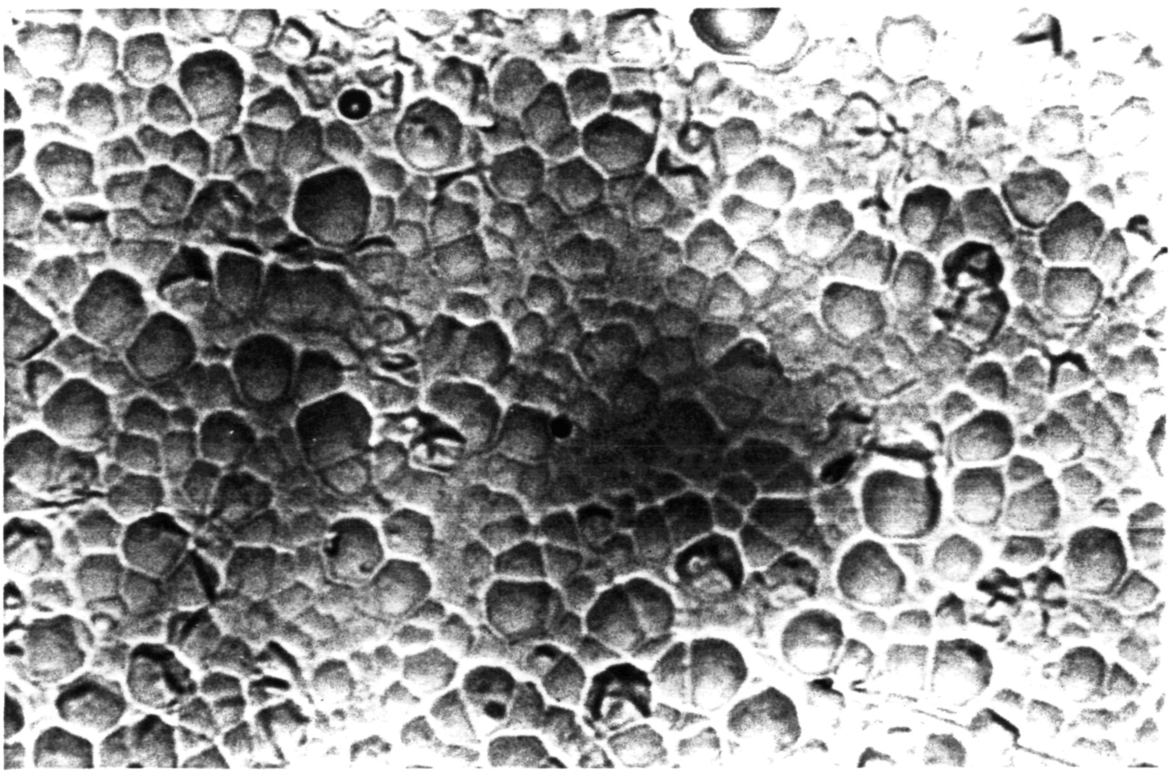

Figure 73: Photomicrograph of Sheffield layer 2G7 after ~11 μm of material have been removed by etching. Scale is ~11 μm/cm.

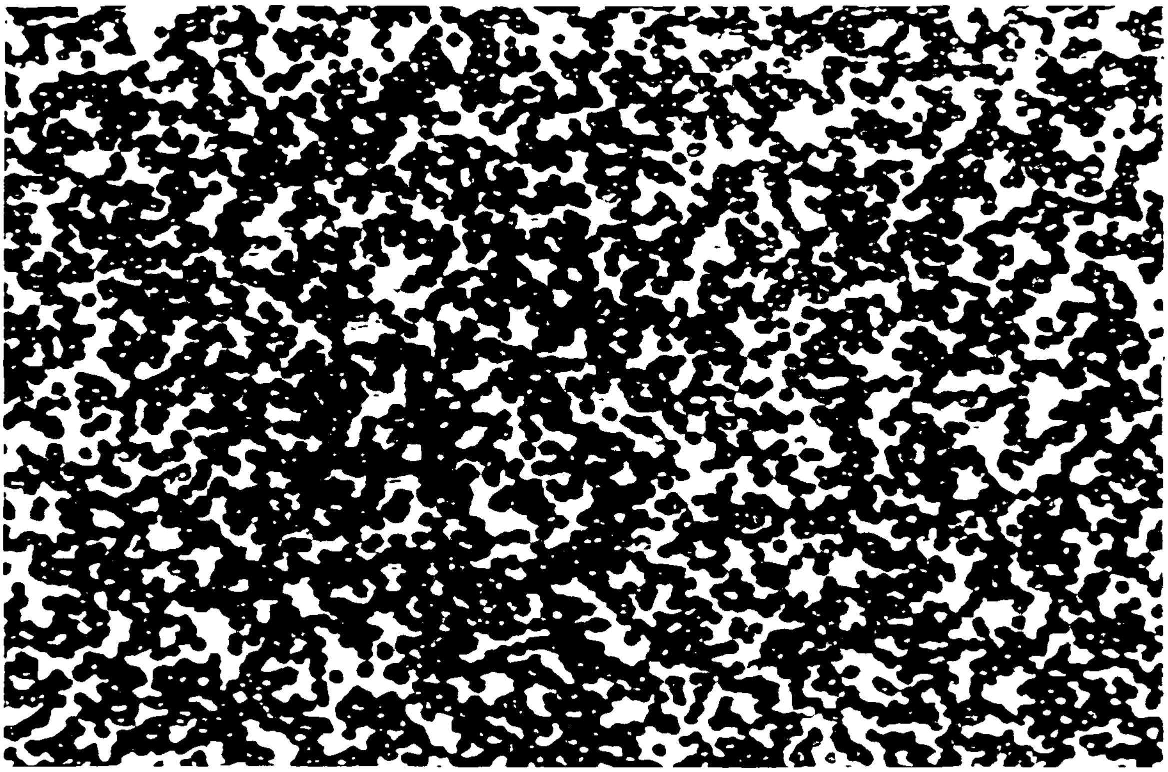

Figure 74: Photomicrograph of a Sheffield detector exposed to 0.6 MeV α-particles. Scale is $\sim$11 μm/cm.

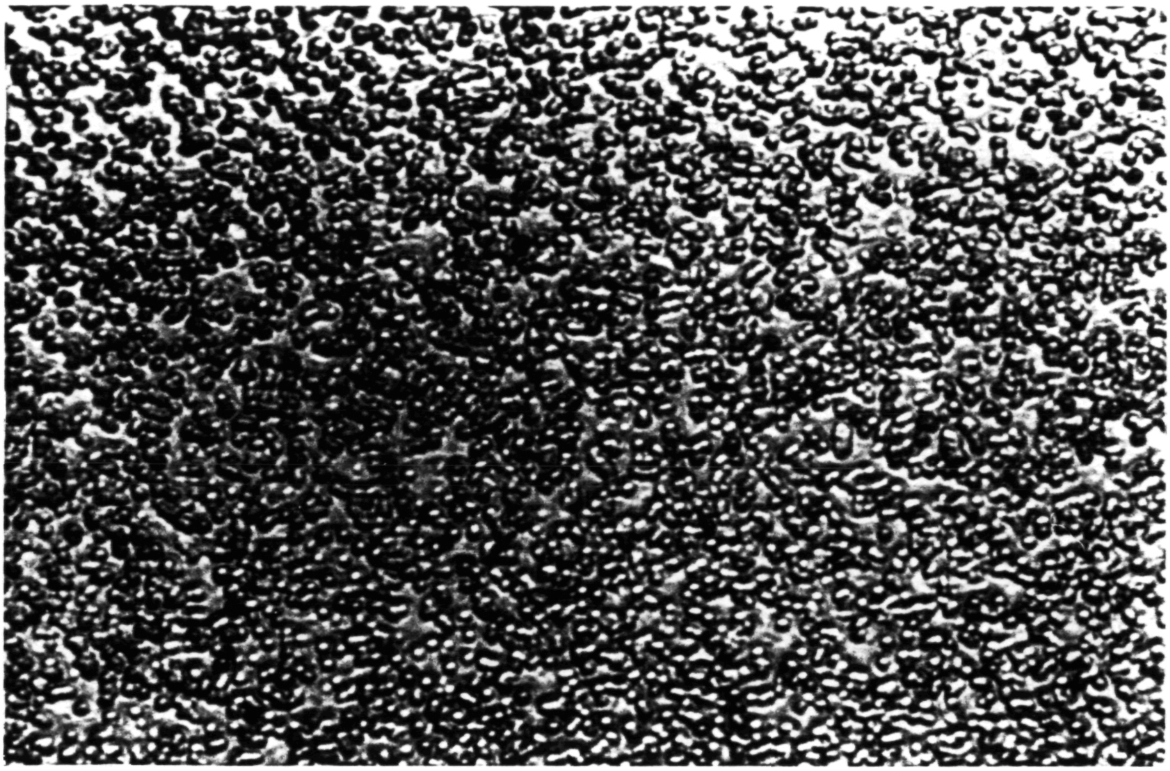

Figure 75: Photomicrograph of a Sheffield detector exposed to 5.5 MeV α-particles. Scale is $\sim$11 μm/cm.

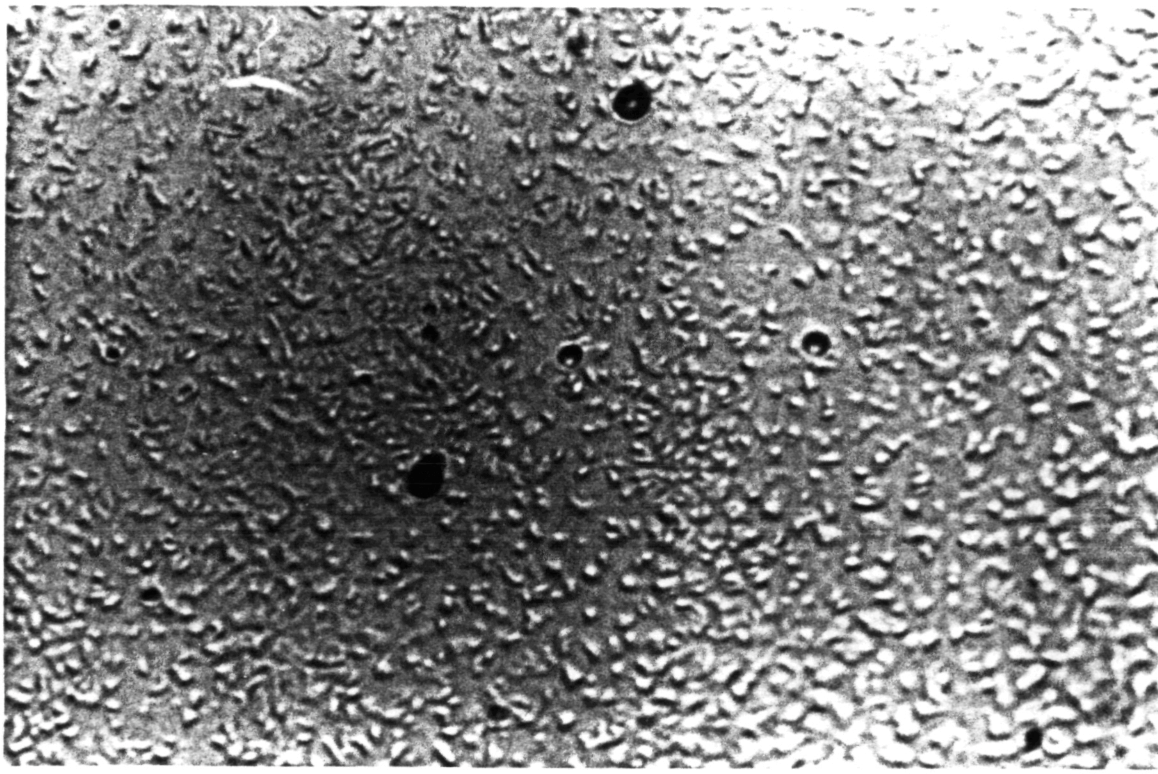

Figure 76: Photomicrograph of a Sheffield detector exposed to 154 MeV protons. Scale is $\sim$11 μm/cm.

8 Discussion and Conclusions

8.1 LET Spectra Measurements

Analysis of the A0015 CR-39 PNTDs tended to concentrate on the short-range, high-LET secondary particle component. Although this component has been previously suggested to be of radiobiological and materials-effects significance[7], it was not until the LDEF mission that comprehensive studies of secondary particles produced by trapped proton interactions with the materials of the spacecraft and its payload were undertaken. A number of conclusions can be drawn from the A0015 CR-39 PNTD results.

8.1.1 Short-range, High-LET Secondary Particles

A significant fraction of the LET spectra is made up of short-range secondary particles produced in interactions between high-energy trapped protons and the nuclei of the stopping medium. Similarities in the slopes of differential LET spectra measured in the A0015 West-side stack and in a CR-39/Al stack exposed to 154 MeV protons supports this conclusion based on the fact that all particle tracks in the 154 MeV proton detectors are from secondaries. The LET of 154 MeV primary protons is too low to form visible tracks in CR-39. In addition, the $\sim$137 keV/μm geomagnetic cut-off prohibits GCR of higher LET from being in the low inclination LDEF orbit. Measurements of LET spectra at high LETs ($>$100 keV/μm) confirmed that those particle events in the high-LET tail were short-range and not from GCR. This high-LET tail extended beyond 1000 keV/μm. The range of secondary particles in CR-39 extended from $>$16 μm as measured by the coincidence spectroscopy method to $<$2 μm measured using total event spectroscopy.

From data on cross sections for proton-induced secondary particle production([7, 6, 1] it is believed that the high-LET tail consists of heavy fragments (B, C, N, O) from inelastic collisions between incident trapped protons and the O and C nuclei of CR-39. At lower LETs ($<$100 keV/μm) the secondaries are most likely protons and α-particles from inelastic trapped proton collisions with the heavier (C and O) nuclei of the stopping medium (CR-39). The is not to say that elastic collisions (especially proton-proton) are not taking place, only that elastic secondaries produced near measurement regions have LETs too low to

contribute significantly within the measured region of the LET spectrum. Another possibility is that elastically scattered protons produced at considerable distances from the measurement regions are slowed by intermediated material and contribute in the form of measured tracks. Some additional conclusions concerning proton-induced secondaries can be drawn from the A0015 CR-39 PNTD data.

Angular Distribution: The angular distribution of secondary particles in CR-39 is anisotropic. The physics of elastic and high-energy inelastic interactions favors a scattering angle near the forward direction of travel of the incident particle. Measurements of azimuthal angle distributions in CR-39 detectors from the A0015 Earth-side stack (Figures 38 and 39 and similar azimuthal angle distributions measured in CR-39 stacks exposed at various angles to accelerator protons (Figure 40) bear out this conclusion. Peaks in azimuthal angle can be seen corresponding to the forward direction of the incident protons. At lower energies ($\sim$2 MeV), inelastic scattering is nearly isotropic[11]. However secondary ions in this energy region generally have a range below the 16 μm minimum measured using the coincidence spectroscopy technique. Azimuthal angle distributions of shorter range particles measured using the total event spectroscopy method would probably reveal this isotropy in scattering angle for low-energy inelastic secondaries.

Track Density as a Function of Shielding Depth: The cross section for the production of secondary particles increases with shielding depth as primary proton energy is attenuated. Track density profiles (Figures 21 – 25) measured in CR-39 at different shielding depths in the A0015 West-side stack show an increase in track density with increasing shielding. The mean track density under 2.6 g/cm^2 was measured to be 1.09×10^5 tracks/cm^2. This increased to a mean track density of 1.38×10^5 tracks/cm^2 under 11.9 g/cm^2. This illustrates the increase in total cross section for secondary production with decreasing primary proton energy. This result can also be seen in the two LET flux spectra measured using the total event method (Figures 33 and 34).However, in LET flux spectra measured using the coincidence method, little difference is seen in curves measured at different shielding depths. This would seem to indicate that the cross section for shorter range, lower energy inelastic secondary production

increases more rapidly with decreasing proton energy than does cross section for longer range, higher energy inelastic secondary production.

Charge Distributions of Energetic Secondaries: The charge of secondary ions in the high-LET tail ranges from 5 to 8. Figures of charge and range distribution (Figures 41 – 44) show a peak around charge 6. There is a rapid drop off after charge 8 since O is the heaviest nuclei in CR-39. These measurements only included the most energetic secondaries and neglected lower energy, lower charge, and lower LET particles. These distributions may be compared to the results from model calculations for the production of inelastic secondaries.

Modeling Proton-induced Secondary Particle Production: To date, efforts to model the contribution of secondary particles to the LDEF spectrum have been inadequate. Figure 17 includes LET spectra calculated for LDEF under 1 and 5 g/cm^2 Al shielding from the LDEF Pre-recovery Estimates[8]. The model curves fall off rapidly at $\sim$137 keV/μm, the geomagnetic cut-off of Fe, and do not included to high-LET tail component from short-range secondaries measured in the LDEF CR-39 detectors. Measurements of the high-LET tail on LDEF, and the secondary particle contribution to the LDEF LET spectra in general, can aid in the development and refinement of calculational models of the space radiation environment in LEO and its transport through the material of the spacecraft. Additional LET measurements made in CR-39 stacks exposed to monoenergetic protons at ground-based accelerators can also be of use in the development and validation of such models. Efforts are currently underway by Armstrong (*et al.*)[1] using results from LDEF to include the secondary particle component to calculational models.

8.1.2 East/West Trapped Proton Anisotropy

The presence of the East/West trapped proton anisotropy in the SAA was confirmed through LET flux spectra measurements of secondary particles made on the East and West-sides of LDEF (Figure 17). The LET spectra measured in the M0004 experiment on the East (leading-edge) side of LDEF falls below the A0015 LET spectra measurement made on the West (trailing edge) side under similar shielding by more than a factor of 2. The smaller

overall flux of trapped protons entering the spacecraft from the East leads to a smaller number of secondary particles compared to the larger flux of trapped protons from the West and the correspondingly larger number of secondaries. This result is consistent with TLD measurements of absorbed dose which showed a comparable factor of 2 difference between the East and West sides of LDEF.

8.1.3 Galactic Cosmic Radiation

Galactic cosmic radiation makes a relatively modest contribution to the LET spectra in the 28.5°, ~450 km LDEF orbit, especially when compared to the contribution form secondary particles. This is largely due to the low inclination of the orbit and the geomagnetic cut-off imposed on galactic cosmic Fe particles. This result can be seen in Figures 13 – 18, LET flux spectra measured under various shielding depths and at different locations around LDEF.

8.2 Total Absorbed Dose Measurements

Total absorbed dose measurements were made using TLDs in the three A0015 locations on LDEF. Results are tabulated in Table 4. TLD measurements in A0015 Experiment and the other three LDEF experiments have yielded absorbed dose as a function of shielding thickness near the leading and trailing edges and at the Earth side of the LDEF vehicle. A consistent set of dose values is produced which defines much of the LDEF radiation environment and provides comparisons for dose calculations using advanced trapped proton predictions and transport codes.

Figure 77 is a comparison of A0015 and M0004 dose measurements and calculations. The smaller measured doses of M0004 as compared with the A0015 West-side show the effect of the East/West trapped proton anisotropy. The largest difference can be seen at ~4.5 g/cm^2 Al equivalent shielding, where the West-side dose measurement exceeds that of the East-side by a factor of ~2.

The comparisons of measured and calculated absorbed doses clearly show that the trapped proton (Ap8) environmental model needs revision. Not only are absolute magnitudes of calculated values (in general) too low, but neglecting directionality of the protons leads to

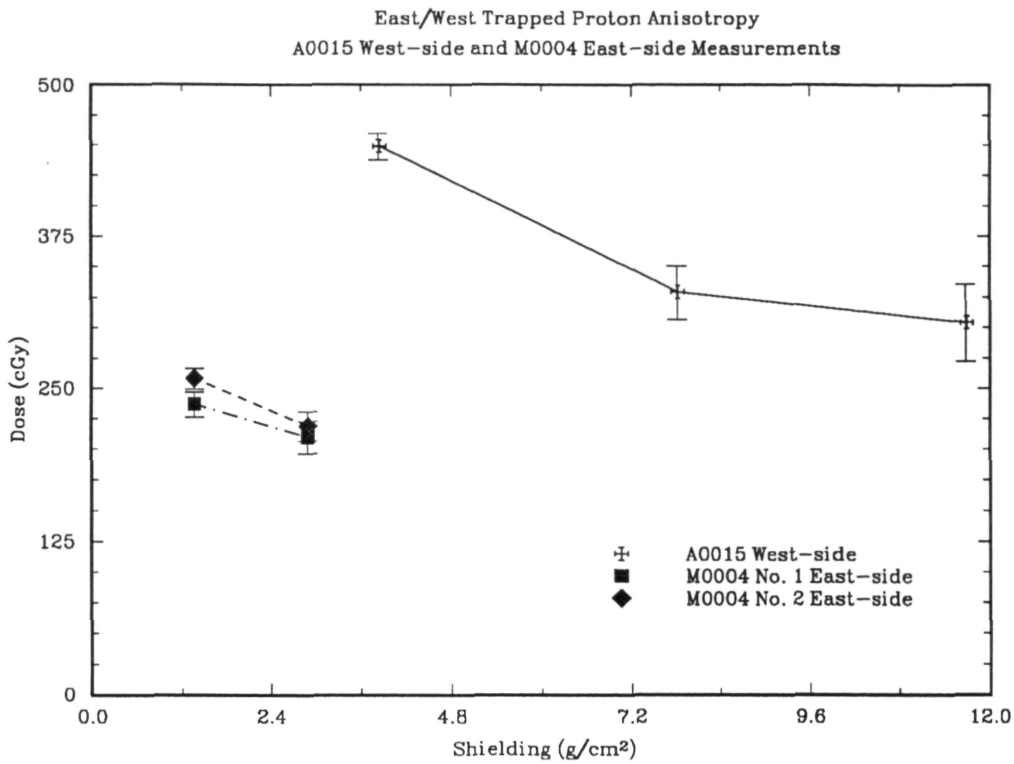

Figure 77: Comparison of A0015 and M0004 dose calculations and measurements as a function of shielding, demonstration the effect of the East/West trapped proton anisotropy.

substantial errors in calculations involving any complex shielding geometry.

8.3 Thermal and Resonance Neutron Measurements

Thermal and resonance neutron dose equivalents were measured using ^{6}LiF/CR-39 detectors and the results are reported in Table 11. In comparing neutron measurements made at Earth-side and the Trailing Edge of LDEF, we must keep in mind that the incident charged particle fluence was greater at the Trailing Edge while the shielding was greater at Earth-side. The differences in neutron production and moderation make comparisons difficult to interpret. The thermal neutron fluence was 27% greater at the Trailing Edge while the resonance fluence was 44% greater at Earth-side. This implies that shielding depth is more important in increasing resonance fluences than for thermal neutrons. These results can be compared with P0006 measurements at the Trailing Edge under 15 g/cm^2 Al equivalent shielding. The P0006 dose equivalent measurements were 3.4 times higher (0.34 mrem d^{-1}) than the A0015 average. The P0006 canister contents were more massive (~3 times more weight) than the A0015. The added mass for charged particle interactions and neutron production

and, subsequently, for neutron moderation are a major source of the differences seen.

The LDEF measurements can also be compared with measurements made on previous STS missions by the University of San Francisco. The average of 11 flights (from a variety of altitudes and inclinations) is 0.26 mrem d^{-1} with a σ of 0.12 mrem d^{-1}. This is a factor of 2.7 higher than the average A0015 dose equivalents and 24% lower than the P0006 dose equivalent. Thus the A0015 measurements are at the lower end of the range for previous measurements while the P0006 measurement is slightly above mid-range.

In A0015 the low energy neutron dose equivalent represented a small fraction of total dose equivalent. TLDs in the vicinity of the ^{6}LiF/CR-39 detectors measured absorbed doses which averaged a factor of 1670 higher than the low energy neutron dose equivalents. On P0006 this factor was 438. The spacing of the detector canisters on LDEF resulted in a limited mass about the detectors for the build-up of thermal and resonance neutrons.

8.4 High-Energy Neutron Measurements

High-Energy neutron dose equivalents were measured using fission foil/CR-39 detectors. Results of high-energy neutron dose equivalent and proton dose are tabulated in Table 14. A comparison has been made between fission foil detector measurements (track densities) induced by proton/neutron fluences encountered on LDEF and predicted track densities based on calculated proton and neutron spectra. The calculations employed a simple slab geometry[3]. The predicted track densities on the detectors were less than measurements by ~25% at 1 g/cm^2 shielding (trailing edge) and more than a factor of 2 at 13 g/cm^2 (Earth-side). The differences are primarily due to the slab geometry approximation of actual spaceflight conditions. Future calculations based on a geometrical model of the A0015 experiment are needed for a more accurate test for the radiation modeling code.

The proton doses derived by combining measurements and calculations were 16% and 37% less than TLD doses measured in the flight canisters, when extrapolated to equivalent shielding. The differences can be explained by the approximations involved in the calculations.

In Table 17 the A0015 neutron dose equivalent rates are compared with measurements

Table 17: Spaceflight High Energy (>1 MeV) Neutron Measured Comparisons.

Space flight	Experiment	Shielding	Altitude (km)	Inclination	Dose Equiv. Rate (mrem/d)
LDEF	A0015	1 g/cm^2	478	28.5°	16
	A0015	13 g/cm^2			39
	P0006	17 g/cm^2			33
STS-9(SL-1)	VFI	Pallet	241	57°	4.2
STS-51F(SL-2)	VFI	Pallet	322/304	49.5°	4.0
STS-3		Locker	280	40.3°	0.95
STS-4		Locker	297	28.5°	1.3
STS-5		Locker	284	28.5°	2.2
STS-6		Locker	293	25.5°	1.3
Cosmos 936	Inside Spacecraft		419/224	62.8°	6.8
Cosmos 1129	Inside Spacecraft		394/226	62.8°	6.8
Cosmos 2044	Outside Spacecraft		294/216	82.3°	3.3

Due to approximations made in separating neutron and proton contributions to the fission foil detector measurements, the accuracy of neutron dose equivalents is estimated to be within a factor of 3.

from other spaceflights. The LDEF rates are seen to be higher than all other measurements, by factors of approximately 6 to 40. The primary reason for the large differences are in the greater LDEF flight altitude, with higher primary proton and secondary neutron fluxes. Shielding differences may also play a significant role. This is opposite to the thermal/resonance neutron measurements which were low to mid-range when compared to measurements from other LEO flights. This implies that most neutrons are produced in the high energy (>1 MeV) range and that the thermal/resonance fluxes are more dependent on amount and type of shielding surrounding the detectors.

8.5 High Track Densities in Polycarbonate PNTDs

Measurements of track density in polycarbonate PNTDs in the A0015 West-side experiment revealed a much higher than expected track density ($> 10^7$ tracks/cm^2 under 2 g/cm^2 shielding). Similar results have been measured in other LDEF experiments containing PC PNTDs. To date no adequate explanation has been found to account for the high track density in LDEF polycarbonate. Anomalies in the manufacture, exposure and processing of the material have been eliminated. The sensitivity of the material appears to change with detector depth. The total track density is seen to attenuate as a function of shielding depth.

A possibility is that the tracks being counted are from primary protons. There were estimated to be no particle species heavier than protons with total mission fluxes greater than the 10^7 particles/cm^2 seen in the A0015 PC. Protons reach the 150 keV/μm threshold only at the very end of their range. It might be possible that these tracks are produced by stopping protons. However a similar high density of tracks is not seen in CR-39 PNTD. The LET threshold for track registration in CR-39 is $\sim$5 keV/μm and tracks of $>$100 keV/μm should be readily visible. The track density measured in CR-39 in the A0015 West-side stack under similar shielding (2.6 g/cm^2) is only 1.1×10^5 tracks/cm^2.

Another possibility is that the tracks are the result of elastic and inelastic collisions between primary protons and the nuclei of the constituent atoms in the polycarbonate. Estimates of total proton flux for LDEF are 10^9 protons/cm^2 and the cross section for proton-nucleon interaction is $\sim 10^{-6}$ cm^{-2}[8]. Thus the total number of secondaries should fall below that seen in the A0015 polycarbonate.

Acknowledgements

We are grateful to the many dedicated individuals who made the LDEF mission and the subsequent analysis of flight experiments possible. In particular, we thank Bill Kinard, Jim Jones, and Arlene Levine of the LDEF Project Office at NASA Langley Research Center, VA, and Drs. Tom Parnell, John Watts and Jim Derrickson of NASA Marshall Space Flight Center, AL, for their support of our efforts in analyzing the radiation detectors flown in the A0015 experiment. We thank Dr. Tony Armstrong of SAIC, TN, for his help in interpreting our results. We thank Dr. Denis O'Sullivan of the Dublin Institute of Advanced Studies,

Ireland, and Drs. Jim Adams, Alan Tylka, Lorrain Beahm and Thomas Kleis of the Naval Research Laboratory, Washington DC, for providing polycarbonate detectors from the A0178 and M0001 experiments. We'd especially like to thank Dr. Gunther Reitz and Prof. Horst Bücker of DLR, Germany, for inviting us to participate in the A0015 experiment.

References

[1] T. W. Armstrong. Preliminary nuclear recoil calculations. private communication.

[2] T. W. Armstrong and B. L. Colborn. Radiation model predictions and validation using LDEF data. In *LDEF–69 Months in Space: Second Post-Retrieval Symposium*, pages 207–220, Washington DC, 1993.

[3] T. W. Armstrong and B. L. Colborn. *Scoping Estimates of the LDEF Satellite Induced Radioactivity.* Technical Report 90/1462, SAIC, 1990.

[4] W. Atwell, G. D. Badhwar, A. C. Hardy, and M. D. Weyland. Space radiation doses for the Long Duration Exposure Facility. unpublished paper.

[5] E. V. Benton, R. M. Cassou, A. L. Frank, R. P. Henke, and D. D. Peterson. Space radiation on board Cosmos 936: U. S. portion of experiment K-206. In S. N. Rosenzweig and K. A. Souza, editors, *Final Reports of U. S. Plant and Radiation Experiments Flown on the Soviet Satellite Cosmos 936*, NASA, Ames Research Center, 1978.

[6] E. V. Benton, M. R. Cruty, and R. P. Henke. *Proton-Induced High-LET Fragments.* Technical Report TR-32, University of San Francisco, 1974.

[7] E. V. Benton, S. B. Curtis, R. P. Henke, and C. A. Tobias. Comparison of measured and calculated high-let nuclear recoil particle exposure on Biosatellite III. *Health Physics*, 23:149–157, 1972.

[8] E. V. Benton, W. Heinrich, T. A. Parnell, T. W. Armstrong, J. H. Derrickson, G. J. Fishman, A. L. Frank, J. W. Watts, and B. Wiegel. Ionizing radiation exposure on LDEF: pre-recovery estimates. *Nuclear Tracks and Radiation Measurements*, 20(1):75–100, 1992.

[9] E. V. Benton, R. P. Henke, A. L. Frank, R. M. Cassou, C. S. Johnson, and M. T. Tran. *Final Dosimetry Reports for STS-3, STS-4, STS-5, STS-6, TR-54, -56, -57, -57.* Technical Report TR-, University of San Francisco, 1982-83.

[10] E. V. Benton, R. P. Henke, A. L. Frank, C. S. Johnson, R. M. Cassou, M. T. Tran, and E. Etter. Space radiation dosimetry aboard Cosmos 1129: U. S. portion of experiment K-309. In M. A. Heinrich and K. A. Souza, editors, *Final Reports of U. S. Plant and Radiation Experiments Flown on the Soviet Satellite Cosmos 1129*, NASA, Ames Research Center, 1981.

[11] F. E. Bertrand and R. W. Peelle. Complete hydrogen and helium particle spectra from 30- to 60-mev proton bombardment of nuclei with A=12 to 209 and comparison with the intranuclear cascade model. *Physical Review C*, 8(3):1045–1064, 1973.

[12] M. O. Burrell. *The Calculation of Proton Penetration and Dose Rates.* Technical Report NASA TM X-53063, George C. Marshall Space Flight Center, Huntsville, AL, August 1964.

[13] B. L. Colborn and T. W. Armstrong. Development and application of a 3-d geometry/mass model for LDEF satellite ionizing radiation assessments. In *LDEF–69 Months in Space: Second Post-Retrieval Symposium*, pages 195–206, Washington DC, 1993.

[14] P. N. Dobson, Jr. and A. A. Midkiff. Explanation of supralinearity in thermoluminesence of LiF in terms of an interacting track model. *Health Physics*, 18:571–573, 1970.

[15] V.E. Dudkin, Yu.V. Potapov, A.B. Akopova, L.V. Melkumyan, Sh.B. Rshtuni, E.V. Benton, and A.L. Frank. Neutron fluences and energy spectra in the Cosmos-2044 biosatellite orbit. *Nuclear Tracks and Radiation Measurements*, 20(1):139–141, 1992.

[16] A. L. Frank, E. V. Benton, E. R. Benton, V. E. Dudkin, and A. M. Marenny. *Radiation experiments on Cosmos 2044: K-7-41, Parts A,B,C,D,E.* Technical Report TR-76, University of San Francisco, 1990.

[17] A. L. Frank, D. Yang, T. Atallah, and E. V. Benton. *Review of Radiation Measurements on Selected STS Missions and Environmental Effects in PNTDs.* Technical Report TR-78, University of San Francisco, 1990.

[18] R. P. Henke and E. V. Benton. On geometry of tracks in dielectric nuclear track detectors. *Nuclear Instruments and Methods*, 97:483–489, 1972.

[19] J. W. Kern. A note on vector flux models for radiation dose calculations. *Nuclear Tracks and Radiation Measurements*, 23(1):43–48, 1994.

[20] M. F. Lomanov, C. G. Shimchuk, and R. M. Yakovlev. Solid state detectors of fission fragments for the rem-dose measurement of mixed proton and neutron radiation. *Health Physics*, 37:667–686, 1979.

[21] National Council on Radiation Protection and Measurements. *Guidance on Radiation Received in Space Activities.* National Council on Radiation Protection and Measurements, 1989.

[22] S. Pretre, E. Tochilin, and N. Goldstein. A standardized method for making neutron fluence measurements by fission fragment tracks in plastics. In *Proceedings of the 1st International Congress on Radiation Protection*, Rome, 1968.

[23] G. Reitz. Preliminary doses on LDEF. In *Proceedings of the XXVIII Pleneary Cospar Meeting*, The Hague, 1990.

[24] D. W. Sawyer and J. I. Vette. *AP-8 Trapped Proton Environment Model for Solar Maximum and Solar Minimum.* Technical Report NSSDC/WDC-A-R&S 76-06, National Space Science Data Center, Goddard Space Flight Center, December 1976.

[25] J. F. Stehn, M. D. Goldberg, R. Weiner-Chasmon, S. F. Mughabghab, B. A. Magurno, and V. M. May. *Neutron Cross Sections, Volume III.* Brookhaven National Laboratory, 1965.

[26] J. W. Watts, T. W. Armstrong, and B. L. Colborn. Revised prediction of LDEF exposure to trapped protons. In *LDEF–69 Months in Space: Second Post-Retrieval Symposium*, pages 137–146, Washington DC, 1993.

[27] H. A. Wollenberg and A. R. Smith. *Energy and Flux Determinations of High-Energy Nucleons.* Technical Report 19364, UCRL, 1969.